8-2013

Hybrid Nanostructured Textile Bioelectrode for Unobtrusive Health Monitoring

Pratyush Rai
University of Arkansas, Fayetteville

Hybrid Nanostructured Textile Bioelectrode for Unobtrusive Health Monitoring

Hybrid Nanostructured Textile Bioelectrode for Unobtrusive Health Monitoring

A dissertation submitted in partial fulfillment
of the requirements for the degree of
Doctor of Philosophy in Biological Engineering

by

Pratyush Rai
Indian Institute of Technology Madras
Bachelor Technology in Biotechnology, 2006
University of Arkansas
Master of Science in Biomedical Engineering, 2008

August 2013
University of Arkansas

This dissertation is approved for recommendation to Graduate Council.

Dr. Vijay K. Varadan
Dissertation Director

Dr. Thomas A. Costello
Committee Member

Dr. Randy L. Brown
Committee Member

Dr. David Zaharoff
Committee Member

ABSTRACT

Coronary heart disease, cardiovascular diseases and strokes are the leading causes of mortality in United States of America. Timely point-of-care health diagnostics and therapeutics for person suffering from these diseases can save thousands of lives. However, lack of accessible minimally intrusive health monitoring systems makes timely diagnosis difficult and sometimes impossible. To remedy this problem, a textile based nano-bio-sensor was developed and evaluated in this research. The sensor was made of novel array of vertically standing nanostructures that are conductive nano-fibers projecting from a conductive fabric. These sensor electrodes were tested for the quality of electrical contact that they made with the skin based on the fundamental skin impedance model and electromagnetic theory. The hybrid nanostructured dry electrodes provided large surface area and better contact with skin that improved electrode sensitivity and reduced the effect of changing skin properties, which are the problems usually faced by conventional dry textile electrodes. The dry electrodes can only register strong physiological signals because of high background noise levels, thus limiting the use of existing dry electrodes to heart rate measurement and respiration. Therefore, dry electrode systems cannot be used for recording complete ECG waveform, EEG or measurement of bioimpedance. Because of their improved sensitivity these hybrid nanostructured dry electrodes can be applied to measurement of ECG and bioimpedance with very low baseline noise. These textile based electrodes can be seamlessly integrated into garments of daily use such as vests and bra. In combination with embedded wireless network device that can communicate with smart phone, laptop or GPRS, they can function as wearable wireless health diagnostic systems.

ACKNOWLEDGEMENTS

I would like to thank my faculty advisor Dr Vijay K. Varadan for teaching about smart materials and their place in this world. I would like to thank Dr Gyanesh N. Mathur for his guidance and support in my research work and industrial liaison. I would like to thank Dr Linfeng Chen and Dr. Mourad Benamara for spending many morning hours to help me with my SEM scans. My colleagues Dr Sechang Oh, Prashanth Shyamkumar, Hyeokjun Kwon and Mouli Ramasamy have been a great source of encouragement and source of knowledge during my research work. I would like to thank Mr. Jeff Haggard (Ms Hills Inc.) and Shri. Nirmal Jhajahria (Ms Shri Lakshmi Cotsyn Ltd.) for providing valuable input and materials for perfecting my fabrication processes. I would like to thank Dr. David Zaharoff and Dr. Jeff Wolchok for allowing me access to lab facilities.

I would like to thank my wife for her support and patience during our all night dissertation writing sessions. I would like thank my parents and grandparents for constantly encouraging me to finish my PhD thesis.

This dissertation is based on my research which has been enriched by the scrutiny from my critiques and facilitators alike

DEDICATION

I wish to dedicate this dissertation to my family. The high academic standards established by them have been a source of inspiration for me. Their unconditional support was a fundamental force in completion of this doctoral dissertation.

TABLE OF CONTENTS

LIST OF FIGURES

LIST OF TABLES

1. Introduction

Unobtrusive health monitoring is highly beneficial for maintaining health and independence of high risk and chronic disease patients. It is an extension/expansion of healthcare service outside of the hospitals for monitoring over extended periods of time. Intelligent wearable sensor systems with simple installation, minimal maintenance and user involvement can be the best method for ubiquitous health monitoring. Wearable sensor systems in form of smart clothing can contribute tremendously to self-defined and autonomous (at home) living with improved quality of life. They are cost effective and provide lightweight simple technical infrastructure. Long term real-time health monitoring is useful in chronic diseases for event detection, onset of critical episodes, and disease management through diagnostics and therapeutics. Unobtrusive health monitoring is found to be effective in prevention and early diagnosis of cardiovascular disease by non-invasively monitoring person's vital signs and physiological data [1].

1.1 Epidemiology of cardiovascular diseases

Coronary heart disease, cardiovascular diseases and strokes are the leading causes of mortality in United States of America as well as around the world. According to 2005-2010 statistics by Centers of Disease Control and Prevention (CDC), cardio-vascular or cerebro-vascular disease was the most prominent cause of death in United States of America. It was the cause of death in more cases than cancer, accidental injury, diabetes and infectious diseases [2]. Hence, an average American is more likely to die of heart attack or stroke than cancer, accidental injury, diabetes or deadly infections such as HIV.

Since the beginning of industrial revolution, there has been an increasing emphasis on individuals to be physically active and productive to meet the full potential of this explosion of technological advancements. During this period, individuals have changed their lifestyle to adapt to these demands. Some of these changes have been found to be stressors in long term.

Stressors such as excess alcohol consumption, fatigue, cigarettes, consumption of large amounts of caffeine, high cholesterol diet, infectious diseases, myocardial diseases and pulmonary diseases result in ectopic beats in the atria [3]. Most of aforementioned stressors can be associated with the modern industrial society. These stressors can cause abnormalities in heart's function, such as, atrial arrhythmia. Though heart's Atrioventricular (AV) node prevents these atrial arrhythmias from causing ventricular arrhythmias by their pace making activity, this presents a serious risk in case of AV node dysfunction. In addition to that, irregular heart beat due to premature contraction of atria or ventricles can lead to abnormal cardiac function and cardiac arrest [4]. Toxicity and infectious diseases can trigger cardiomyopathy and inflammatory heart diseases such as myocarditis [5].

Hypertension is another residual effect of modern society. It is the most common cause for damage to blood vessel lining (endothelium) exposing the underlying collagen where platelets accumulate to initiate repair. In case of imperfect repair, it becomes a site for plaque formation i.e. atherosclerosis. Sustained hypertension makes the blood vessels narrow, stiff, even stenotic and more susceptible to blood pressure fluctuation [4]. Artery blockage in coronary arteries, which provide blood to cardiac muscles, can lead to ischemia and/or infarction. High prevalence of cardiovascular diseases has encouraged development of prevention, early diagnosis and treatment strategies.

1.2 Point-of-care health diagnostics and therapeutics for cardiovascular disease patients

Timely point-of-care health diagnostics and therapeutics for patients suffering from these diseases can save thousands of lives. This cannot be fully accomplished with the existing medical infrastructure e.g. hospitals and office based physician. Institutional point of care approach offers intermittent treatments that are brief and expensive supervised episodes. Because of this, new methods are required to provide continuous and ubiquitous healthcare in an affordable way. However, lack of accessible minimally intrusive remote health monitoring systems makes timely diagnosis difficult and sometimes impossible. As a result, thousands of deaths occur due to delayed treatment that would have been possible if the associated physician was alerted on time [6,7].

The point of care techniques suitable for ambulatory or out of hospital monitoring are non-invasive electrophysiological techniques: electrocardiogram (ECG) and electrical impedance tomography (EIT). Both the techniques measure electrical activity and properties of cardiovascular system for long periods of time to detect abnormality. In current medical practice, they are considered preliminary testing techniques. Any abnormalities detect in these tests are confirmed by in-hospital techniques: Echocardiogram, Cardiac Catheterization, Computed Tomography (CT) scan, Magnetic Resonance Imaging (MRI).

In present form, ECG and EIT techniques use bulky instrumentation and constrictive conductive gel electrode based sensor systems that are not suitable for very long monitoring. Smart textile technology incorporates textile based dry and glueless sensor system in textile of daily use such as vest, brassier and under garments. Nanostructured surface of dry textile electrodes, developed in this study, improve sensor contact with the skin to match the performance of conductive gel based sensor system. In point-of-care system of the future, ECG

and EIT will serve as reliable diagnostic and monitoring tools for detection of cardiovascular event towards preventive medication and disease management. In combination with state of the art wireless technology, they will be able to establish a remote communication link between patient and doctor for telemedicine prescription and/or quick medical intervention in case of emergency [8].

1.2.1 Electrocardiogram

The Electrocardiogram (ECG) is the fundamental and non-invasive method of monitoring heart activity, by measuring the electrical signal generated by the heart, by placing electrode(s) on the skin. ECG provides multiple perspectives of heart's electrical activity simultaneously [9]. Each perspective is represented by electrode pair that forms a plane of measurement of the electric field vector generated due to electrical current circulating in the heart. ECG complex has 5 types of waveforms: P, Q, R, S and T waves (Figure 1). The P wave is generated at the time of electrical pulse transmission through the SA node and corresponds to atrial contraction. The Q, R and S wave form a QRS complex that corresponds to ventricular contraction or depolarization. The T wave corresponds to ventricular relaxation or repolarization [9]. The electrodes can be placed on the body to provide different perspectives or Leads to assess the quality, intensity and direction of flow of hearts electrical activity.

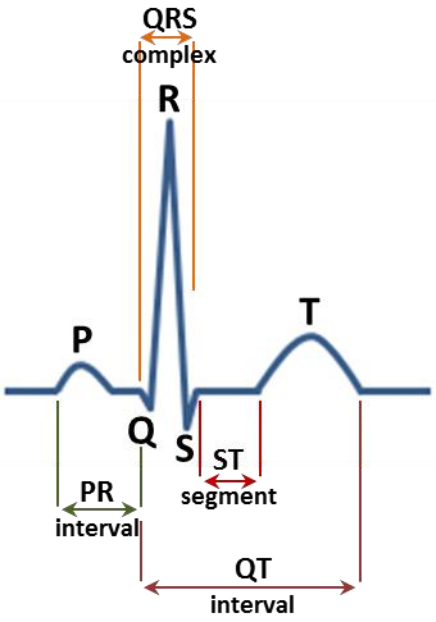

Figure 1: The ECG complex and salient features significant to medical diagnosis [9]

The setup can be a 3 lead system (Figure 2), which uses 3 electrodes positive, negative and ground that are placed at the extremities of the limbs (right arm, left arm and left leg). They provide a limited view of electrical cardiac activity, but the polarity of these leads is useful for determining the direction of propagation of depolarizing pulse through the cardiac tissue a.k.a. electrical axis. The setup can also be a 12 lead system (Figure 2), which uses 10 electrodes 4 of them placed at the extremities of the limbs (arms and legs) and 6 of them are placed on the chest. The 6 chest electrodes are called precordial leads that give perspective of electrical cardiac activity in a horizontal plane that is orthogonal to the electrical axis [10].

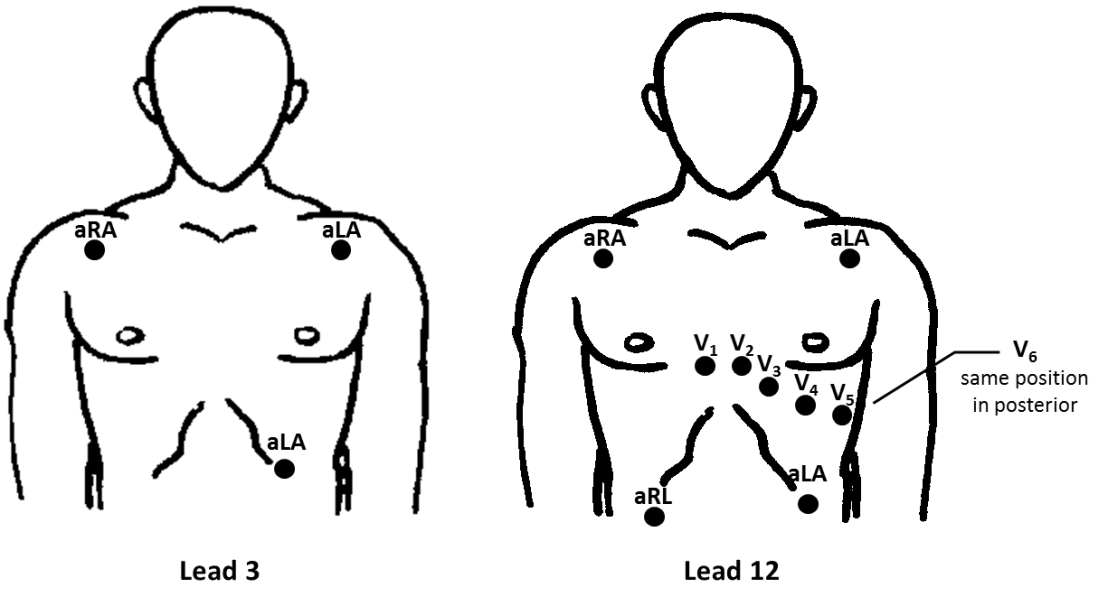

Figure 2: Electrode placements for 3-lead and 12-lead ECG [9].

The ECG leads involve placement of electrodes at the extremities of the limbs and so many electrodes with wires that the movement of the patient is restricted. It is fine for bed ridden patients but not for chronic disease management, out of hospital rehabilitation and diagnostics such as event detection require full time ECG recording on moving patients. In these cases augmented limb leads are used, in which the electrodes are placed corners of the upper section of body that can be considered as boundary points for the cardiac activity domain. The augmented right leg lead is considered as reference and the other 3 augmented (Figure 2) leads form an imaginary triangle a.k.a. Einthoven's Triangle [10]. In a similar fashion, the 12 lead ECG setup can be simplified to 5 electrode system and mathematical calculations to derive the 12 lead ECG a.k.a. EASI system. These 5 electrodes are on the upper part of body along the sternum and midaxial region [11]. Hence, ECG panel can be used as an image of the cardiac activity for non-invasive medical diagnosis.

ECG is the most commonly used test for detection of arrhythmias [12]. The P wave abnormality in the ECG complex is a marker for atrial enlargement, which is a precursor to arrhythmia [13]. In addition to this, abnormality in the QRS complex is associated with blockage in conduction of pace making electric pulse from AV node to the cardiac muscles and injury to cardiac tissue due to ischemic event. Cardiac events such as myocardial infarction result in damaged/scared tissue that becomes cause of future cardiac event or chronic condition such as Right/Left Bundle Branch Block. This interferes with the entire depolarization-repolarization cycle of the heart that shows up on ECG. Similarly, coronary heart disease has signatures in the ECG panel (leads). The elevation of S-T segment (between S and T wave) is observed in patient suffering from coronary heart blockage or myocardial infarction. Whereas, S-T segment depression and T wave abnormalities can be related ischemia due to lack of supply of oxygen to cardiac muscles, electrolyte imbalance, exercise or even pulmonary embolism. In addition to this, Q-T interval that denotes the time between beginning of depolarization and ending of repolarization can help in diagnosis congenital and acquired heart conditions [14].

1.2.1.1 Types of ECG monitoring and recording systems

All ECG monitoring systems in market are mostly defined by the type of signal acquisition and storage system they use. Recording and acquisition of ECG signals can be done by a multichannel desktop recording, display and monitoring system (Figure 3(a)), or it's handheld version, or portable data logging device aka Holter monitor (Figure 3(b)). A majority of systems can be classified into these two categories. Modern multichannel desktop recording systems can connect to the physician’s office from a remote place with the help of Ethernet connectivity or by wireless network to a nearby workstation for easier workflow. Further advancement has allowed inclusion of automatic triggers that can alert the nursing staff in the

hospital but it is still confined to the hospital bed. The Holter monitoring system is the only commercially available multiple lead ambulatory ECG measurement system and it performs just data logging (Figure 4(a)).

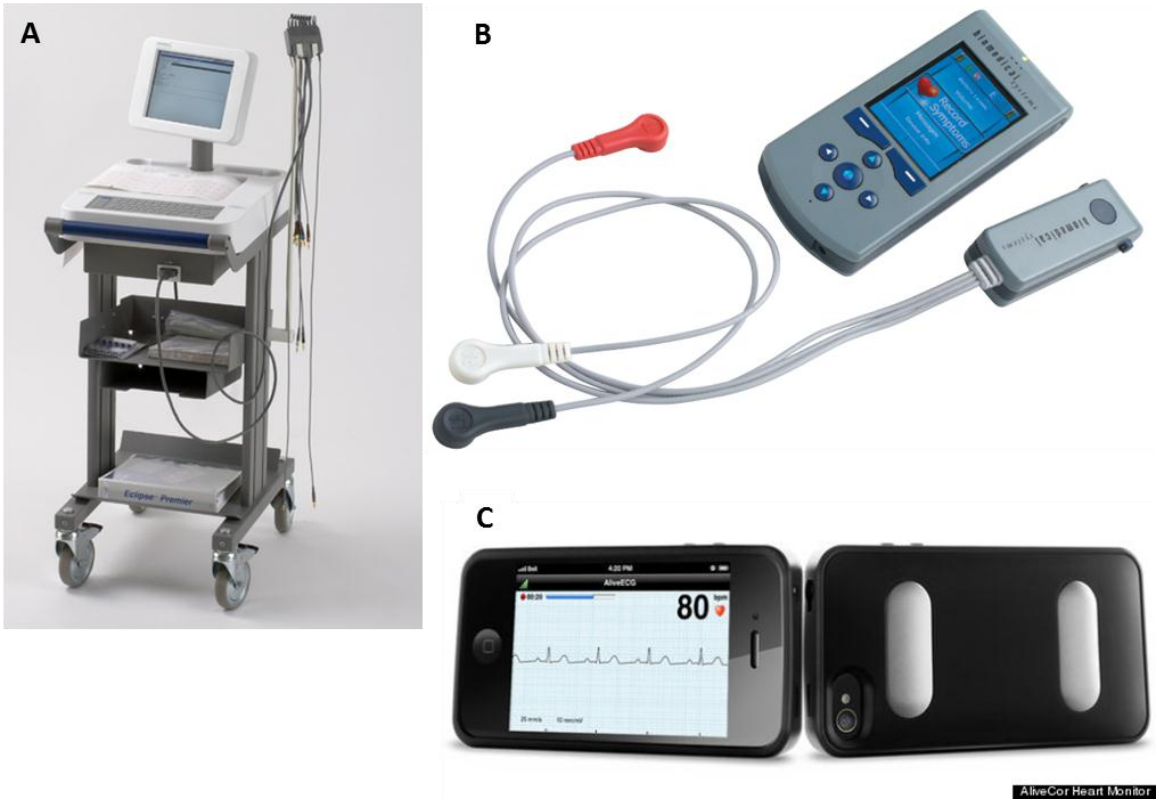

Figure 3: Electrocardiogram monitoring system: A. Desktop 12-lead ECG monitoring system equipped with ECG interpretation algorithms and wireless internet access or an ECG strip print out for diagnostics, B. Patient worn system that transmits wirelessly to handheld device for interpretation, recording and transmission, C. Cellular Smartphones for recording and transmission

In recent years, these monitors have been equipped with event recording functionality that allows for automatic or manual logging of the time of the event onset, while continuously

recording the ECG signals. In addition to this, the Holter can be interfaced with wireless electronics to achieve ambulatory monitoring (Figure 4(b)). This measure has challenges such as shorter battery life and large data volume for transmission.

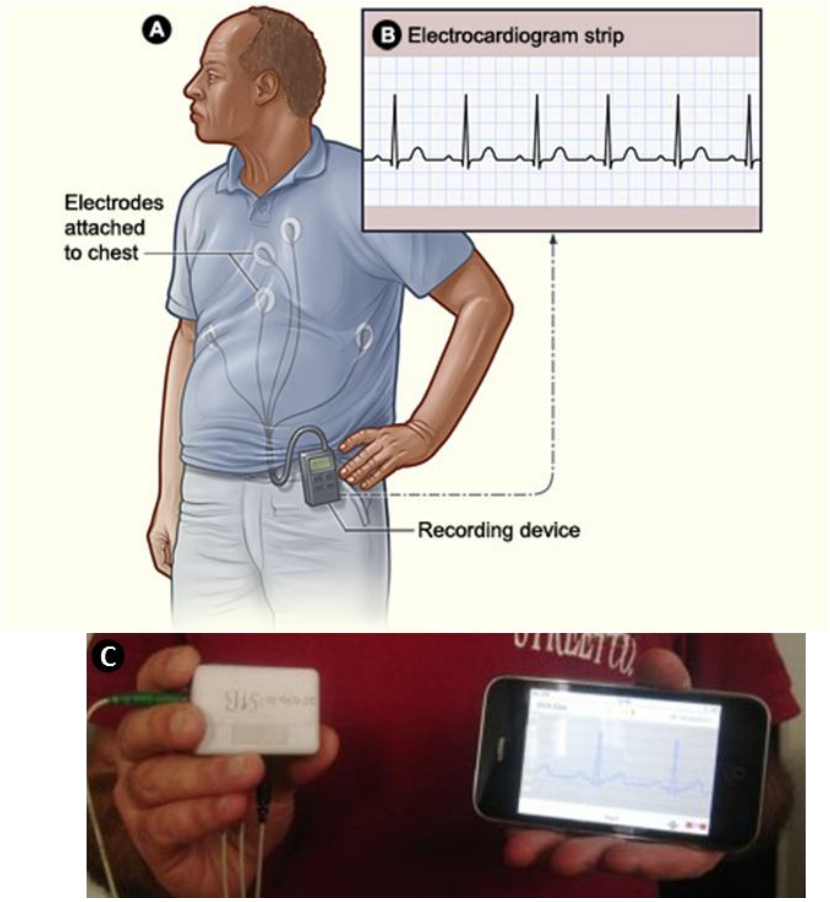

Figure 4: **(A)** Classic set up of ambulatory Electrocardiogram recording system a.k.a. Holter monitor, **(B)** ECG signal as recorded by the system, **(C)** A multi-lead module that interfaces with Smartphone for recording and transmission.

1.2.1.2 Types of ECG electrodes

Different types of electrodes are used by ECG systems based on the duration and type of scan to be done. Pre-screening of patients are of short duration and do not require hospitalization. Conductive sodium chloride-potassium chloride hydrogel filled chest lead suction cups (Figure 5A) and limb lead clamps (Figure 5B) are commonly used for these tests. They can be easily put on and can be used repeatedly. But they do not make sturdy physical contacts and do not function properly in long term testing or testing that involves upright position and movement. For long term and ambulatory testing the ECG recording systems use silver-silver chloride electrode that uses conductive sodium chloride-potassium chloride hydrogel to make electrical contact with the skin (Figure 5C). The performance of these electrodes is affected by drying of gel or glue and sweating. This leads to signal attenuation and causes allergic reaction or skin irritation during prolonged use for more than a couple of days. Patients with sensitive skin, such as babies and old people, develop rashes that interfere with further testing.

Dry electrodes are used as alternative to gel based electrodes. Dry electrodes such as non-contact capacitive electrodes (Figure 5D), silver/silver chloride Mylar strip electrodes (Figure 5E) and conductive rubber based electrodes (Figure 5F) have been commercialized. Although the problem of gel drying up is eliminated, they require adhesive strip to hold them against the skin. Like their gel based counterparts they can be used only once, which means the patients are not allowed to expose to water, i.e., take bath or shower during the period of health monitoring, with exception of non-contact capacitive electrodes. They are held in place by elastic straps. As compared to gel based electrodes, dry electrodes are affected by the change in skin properties such as moisture and texture. They introduce parasitic impedance into the

electrical contact between electrode and skin. This leads to signal attenuation and increase in baseline noise. Therefore the performance varies from individual to individual.

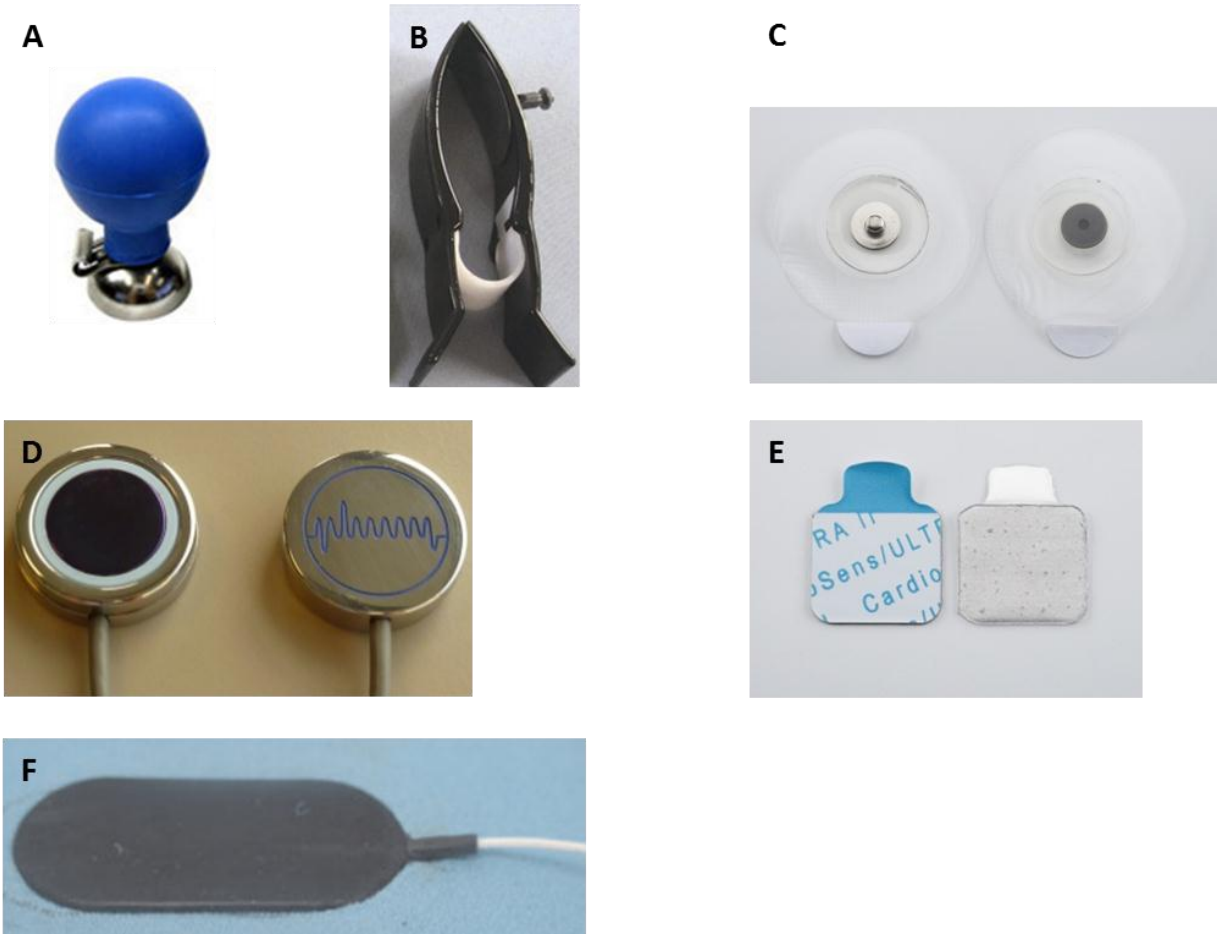

Figure 5: Types of ECG electrodes: A. Suction cup, B. Clamp for limb leads, C. Silver/Silver Chloride electrode, D. Non-contact capacitive electrode, E. Silver/Silver Chloride coated mylar strips, F. Conductive rubber based dry electrode

Current technologies make ambulatory ECG monitoring an added chore rather than an unobtrusive monitoring of heart function during day to day work. The electrodes need to be replaced after the conductive gel dries up or prolonged exposure to sweat. Putting these electrodes requires help of a clinical technician and dry electrodes require mechanical

appendage such as strap-ons to keep them in place. In addition to this, ECG systems have wire-outs from the electrodes to the recording equipment. Unless tucked and taped as is the case of Holter monitor, the wires limit the movement of patient.

1.2.2 Trans Thoracic Impedance

Trans Thoracic Impedance (TTI) is a technique used to measure the change in impedance across the thoracic cavity. It is a type of Electrical Impedance Tomography (ETI) technique. It is very important for monitoring pulmonary function, trans-myocardial current, cardiac output and over all fluid retention of the thoracic cavity. The latter is a significant in monitoring hypertensive patients.

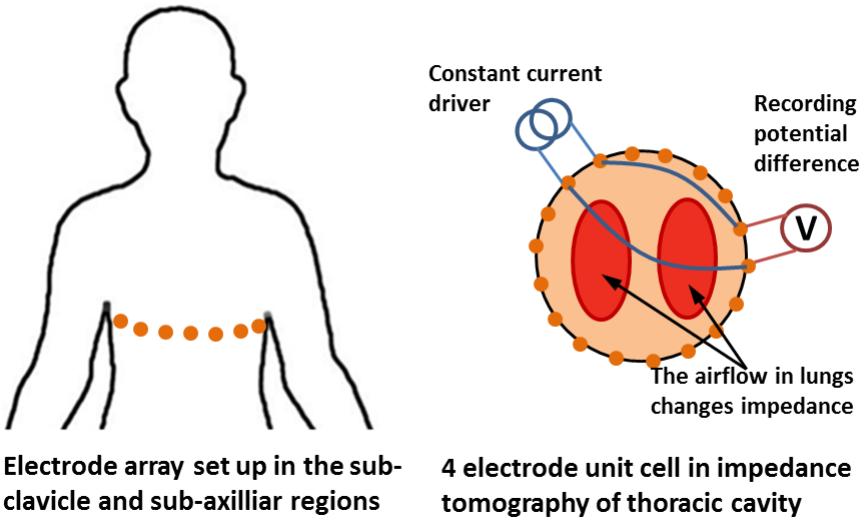

Figure 6: Electrical Impedance Tomography (EIT) of thoracic cavity to lung function

The set up uses 4 electrodes placed in the sub-clavicle, sub-axilliar, anterior or posterior positions (Figure 6). A constant current is applied to 2 electrodes and resulting voltage is recorded across the other 2 electrodes. The electrode pairs are placed across the thoracic cavity from each other to capture change in conductivity due to ventilation of lungs or cardiac function. This system is capable of acquiring impedance image of the thoracic region by using

electrode array (16 electrodes or more) placed all around the thoracic cavity. Each set of 4 electrodes acts as a perspective (angle) for scanning the bioimpedance.

The 4 electrode system includes the electrodes, a current driver (source), a voltage recording unit and a phase-sensitive demodulator. The phase demodulator records voltage values while in phase with the current source and at a phase delay of 90° to extract resistance and reactance values of the bioimpedance. Applied current is $1/10^{th}$ of the current threshold for causing any sensation on the skin. Input current frequency is kept around 50kHz. At this frequency, impedance characteristics of the tissue are similar to those at d.c. That is, the current travels in extracellular space but the electrode-skin impedance is much lower than that at d.c. Hence, there is less instrumentation error due to baseline noise and impedance mismatch. However, measurements taken across a frequency spectrum can help in rectifying any phase effects [15].

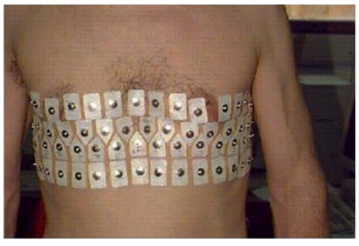

Ag|AgCl electrodes for thoracic impedance tomography
(Wikimedia Creative Commons)

Scheffield MK 3.5
(Maltron International Ltd. Essex U.K.)

Figure 7: Commercial EIT system: Electrode setup and Scheffield MK 3.5

Early systems such as the Sheffield Mark 1 (Figure 7), used a single impedance measurement circuit and a multiplexer to link with the array of electrodes. More recent systems use devoted circuits for each electrodes set. While former is portable but slow, the latter is fast

but bulky. Two types of electrodes are commonly used for this system silver-silver chloride gel electrodes and the conductive gel filled gold cup electrode.

In theory, EIT system should be free of impedance at electrode-skin interface. In practice, skin preparation (abrasion) is used for reducing impedance at electrode-skin interface. Still, the system experiences change in impedance at the interface. During thoracic impedance monitoring for longer periods of time, the conductive gel may dry up and increase electrode-skin impedance. Dry flexible electrodes are not applied because of the high electrode –skin impedance observed in their case. If the impedance is reduced, they can be a good alternative to gel based electrodes for long term monitoring.

1.3 Smart textile for health monitoring

The current technologies for measuring and recording ECG and EIT are suitable for bedside monitoring, with the exception of Holter monitor. The point of care diagnostics and therapeutics require ambulatory and/or remote monitoring techniques. Such techniques will allow the patients and high risk individuals to stay in their homes and follow their routine, while continuous monitoring of their cardiac functions. The key to successful adoption of remote health care is invisibility, i.e. sensors that intertwine with the day to day normal activities of the individual and at the same time efficiently monitor parameters critical to cardiac health such as heart rate, ECG and Trans Thoracic EIT.

Textile based sensor systems are flexible sensors that are made of textile or have texture and flexibility to be able to embed or integrate into textile of daily use. The resultant textile is called E-textile or smart textile. They are distinct from wearable computing systems because they emphasize on seamless integration of textile with sensors and sensor electronics.

Textiles act as flexible base material for medical health monitoring techniques and most natural material to use close to human body. They facilitate unobtrusive observation, where it simply senses and records physiological signals of the subject without any kind of interaction with the subject.

In the case of ECG and Trans Thoracic EIT, the textile based sensors are conductive fabric. It acts as dry electrode and it can be stitched to or woven in to the base textile. The textile based sensor systems can be integrated with compact textile integrated wireless electronics, with the help of woven or printed connections, for remote wireless health diagnostics (Figure 8) [16]. It eliminates the use of stick on glue based electrodes and can be worn without the help of medical personnel, therefore, making it a very desirable diagnostic system in hospital as well as remote location.

Like any other dry electrode, it experiences high impedance at electrode-skin interface because improper and small area of contact. Changes in skin property lead to increase in contact impedance at the skin-electrode interface. This makes it a bad electrical contact, which leads to decrease in signal strength and high susceptibility to motion of the skin or electrode. This effect is more profound in dry electrodes because they do not have conductive gel medium. The high variance in skin-electrode contact impedance due to skin properties leads to different contact impedances at different electrode sites i.e. the input leads to the differential amplifier electronics of the system. Normally differential amplifiers counter this with high common mode rejection ratio (CMRR). But if this impedance unbalance increases it results in perception of common modes noises as a part of differential input. The noise gets amplified and ECG signal quality drops down significantly.

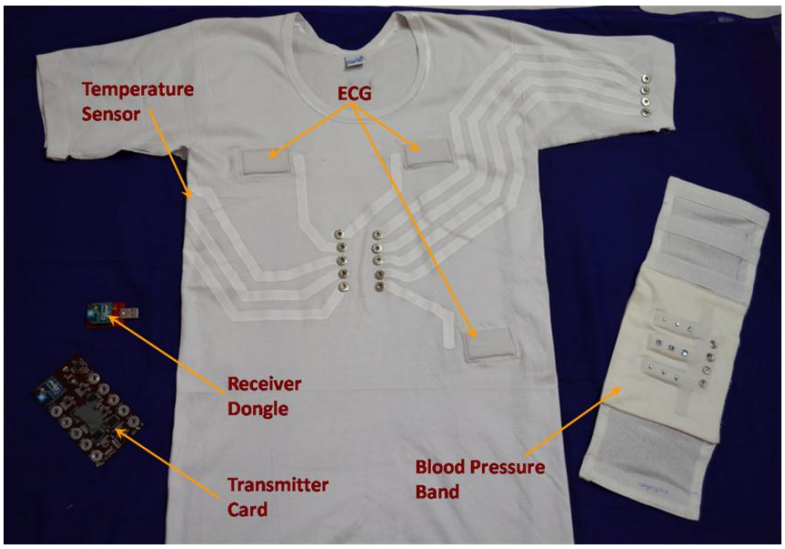

Figure 8: Textile based sensors connected to wireless electronics with printed tracts

Like any other dry electrode, it experiences high impedance at electrode-skin interface because improper and small area of contact. Changes in skin property lead to increase in contact impedance at the skin-electrode interface. This makes it a bad electrical contact, which leads to decrease in signal strength and high susceptibility to motion of the skin or electrode. This effect is more profound in dry electrodes because they do not have conductive gel medium. The high variance in skin-electrode contact impedance due to skin properties leads to different contact impedances at different electrode sites i.e. the input leads to the differential amplifier electronics of the system. Normally differential amplifiers counter this with high common mode rejection ratio (CMRR). But if this impedance unbalance increases it results in perception of common modes noises as a part of differential input. The noise gets amplified and ECG signal quality drops down significantly.

To remove the dependency of electrode performance on skin properties and reduce overall electrode-skin impedance, large contact area between electrode and skin is required. Flexible substrates with specially grown nanostructures on them have large effective surface

area. Therefore nanostructured electrode surfaces will make good electrical contact with the skin and diminish the effect of skin properties. To meet this goal, we have developed flexible nano-bio-textile sensors with vertically aligned hybrid conductive nanostructures on textile substrate. The system incorporates flexible textile based wireless sensors in the garment of daily use e.g. a vest or brassiere. The sensor can combine with wireless health diagnostic system made of embedded wireless networking device which can communicate with a smart phone. This enables the connection of nanosensors to cloud computing, via smart phone, to fundamentally advance remote cyber-enabled health care.

This thesis focusses on the science behind sensing of electrophysiological signals in human body. It is a study and implementation of the theory of electrical conduction at the interface between nano structured dry textile electrodes and skin through experimental techniques and mathematical simulations. Section 2 is a survey of literature on work done in previous studies on textile sensor systems for remote health monitoring, nanostructured textile bioelectrode sensors for bio-potential and bio-impedance measurement, and tools for evaluation of conductivity of interface between nanostructured dry electrodes and skin. This is followed by section about materials and methodology of this study. Section 3 discusses the design components and techniques used for fabrication of the nanostructured electrode sensor system. Section 4 explains in detail the theory used for modeling of electrical conduction for electrode-skin interface and its extension to nanoscale geometries. Section 5 is a compilation of the results and discussion, along with the presentation of a case study highlighting the implementation of the nanostructured dry electrodes for biomedical application. Section 6 presents the conclusion of this study and future scope of work.

2. Review of Literature

Doctors and emergency medical professional, who treat patients and high risk individuals of cardiovascular diseases, are mainly concerned with early detection of onset of critical event such as ischemia and underlying conditions such as arrhythmia, and coronary or pulmonary embolism. It saves time involved in medical intervention by a trained personnel or community intervention by friends, bystanders or coworkers [17,18]. This improves prognosis for the patient i.e. decreases mortality and permanent damage to heart. Continuous health monitoring for long duration of time can ensure event (onset) detection and early diagnosis by individual specific understanding of cardiac functioning.

Textile based unobtrusive health monitoring can be effective in providing continuous monitoring of heart function in patients and high risk individuals. This section discusses the existing textile based systems for remote health monitoring and major challenges to their successful application in medical practice. It is followed by introduction to nanotextured-textile based bio electrodes, which are the basic idea explored in this thesis as the solution to the existing challenges. Further, basic concepts of skin anatomy and current flow through electrode-skin have been discussed to lay ground work for the fundamental research towards establishing the merits of nanotextured textile based bio electrodes as sensors for detection of ECG and bioimpedance in EIT.

2.1 Smart textile for remote health monitoring

In past few decades, there has been a tremendous growth in technology for gathering information and means to distribute it over a world wide web. It can be seen as a degree of connectivity, of which, previous generations of engineers could only dream [19]. With

perfection of sophisticated information and communication technologies, together with microelectronics and systems development provide an opportunity for integration of functional electronics with textiles which radically transforms the norms of computing and embedded systems into soft textile interface. Textiles hold a unique and universal place in our lives. Across societies and cultures it is the material which forms the interface between the body and potentially hostile environment. Through a multi-disciplinary approach of nano-bio-infotech, new possibilities for enhanced functionalities and capabilities within textile are now achievable. New fiber structures, composite materials and coating at the nano and micro levels can be developed towards integration of wearable electronic assemblies in clothing to make them smart textiles.

2.1.1 Textile platform for sensors

Smart textile has been a focus of attention for space exploration, biomedical and consumer electronics communities for their potential to significantly augment the Body Area Network (BAN) [20,21]. Xiaoming Tao describes Smart Textile as a subclass of smart materials and structures that sense and react to environmental conditions or stimuli [22]. They are divided into three subcategories [23]. Passive smart textiles can only sense environmental conditions and stimuli. Active smart textiles can sense and react to environmental conditions and stimuli. Very smart textiles can sense, react and adapt to environmental conditions and stimuli. Peijs adds to this classification by describing intelligent textiles that cause predictable effect or phenomena by interacting with the environment and the wearer [24].

Smart textile (fabric) can be made from traditional cotton, polyester, nylon to advanced Kevlar, with integrated functionalities. Keeping the scope of this study in mind, the fabrics with

electrical conductivity will be of interest for making textile based sensors and electronics. There are two kinds of smart textile (fabric) products that have been developed and studied for health monitoring: fabric with textile based sensor electronics [25-29] and fabric that envelopes traditional sensor electronics [30,31]. Pioneering research work, done by Jayaraman and co-workers, showed that weaving can be used to incorporate electrically conductive yarn into the fabric to obtain textile that can be used as a "Wearable Motherboard". It can connect multiple sensors on body, such as wet gel ECG electrodes, to the signal acquisition electronics [25,26]. Later researchers have shown that conductive yarns can be instrumental in fabrication of textile based sensors made of fabric [27,28] or metallic meshes [29] coated with silver or conductive metal cores woven into the fabric [30].

2.1.2 Systems integration in textile

In ascending order of the degree of integration, the combination of electronics and textiles can be divided into embedded electronics, textronics and fiberonics. Embedded electronics uses textile as a platform for building in existing off-the-shelf electronics for example, Phillips illuminative LED shirts and Lifeshirt by VivoMetrics [32]. In such smart textiles, the electronics have to be disconnected prior to washing because they cannot endure washing. Their advantage is in the fact that the devices are off the shelf electronics available in market. This means the wearable health care systems can be readily made. The disadvantage is in lack of flexibility, washability, dimensions and weight of electronics that causes discomfort to the users.

Textronics uses electronic components manufactured by using textile materials and textile production techniques. Mazz et.al. and Rossi et.al. have developed textronics based suits

for monitoring rehabilitation, studying ergonomics, virtual reality and ambulatory monitoring [33,34]. They used textile based electronics for ECG measurement and strain gauges for the measurement of posture, movement and respiration. The materials of choice were polypyrrole (PPy) on Lycra and carbon filled rubber. They could be printed on to the fabric or wires drawn out and woven. Textronics offer the advantage of easy seamless integration but are limited by the types of components that can be built this way. Complex electronic components such as microprocessors, cannot be fabricated by textronics technology and should still be embedded in textiles. Research work done by Clemens et.al. [35] is attempting to integrate basic electronic building blocks, such as semiconductor electronics, in yarns for fabrication of transistors on textile. This fiberonics technology can help in full inclusion of microprocessors in future textiles.

Importance of textronic technology is in the potential for textiles manufacturers to create new attributes for their product, which means added value and capabilities. Whereas in the case of embedded electronics, anyone can build them by putting existing electronic components in textile materials. For textronic technology, knowledge of and access to textile production is necessary. There are many textile production techniques that can be used to build electronic components. A very commonly used concept for making textile based sensors and electronics is weaving or knitting conductive thread into the garment fabric. Jacquard loop weaving can weave conductive yarn into specific patterns for making conductive tracks, contacts and antennas [36]. Plain and circular knitting, warp knitting or crocheting can be used for knitting of conductive yarns into making textile electrodes and strain sensors. Embroidery of conductive yarns into textiles can be useful in making wearable keyboards [37] and antennas [38].

2.1.3 Smart textile systems for detection of electrophysiological signals

Smart textile can serve as a platform for electrophysiological sensors that require being in contact with the body. The sensor systems, seamlessly integrated in the textile fabric, can perform their health monitoring function and have the benefit of being unobtrusive. Smart textiles have beneficial properties of textile: light weight, flexible, comfort and reusability. Since they are regular pieces of clothing with sensors at fixed places, they do not require cumbersome preparations before usage and no special training to use them. The sensor systems used for detection of electrophysiological signals are electrodes that can be textile based. Studies have shown that the textile based sensor electrodes are as reliable as the conventional silver-silver chloride gel based electrodes for detection of ECG signals [39-41].

The materials of choice for making textile based sensor electrodes are conductive threads. The conductive threads are made of synthetic fiber nylon or polyester that are ideal for metal coating, because of their smooth surface, for electrical conductivity [42,43]. Fibers woven into fabric have been used as electrode pairs that can measure heart rate by recording R peaks of the ECG waveform and transfer them to a smartphone, (e.g. GOW trainer [44], Numatrex by Adidas [43]) An improvement on this system has been achieved by using layer of conductive gel transferred on to the textile electrodes for reliable ECG monitoring (e.g. Wearable Wellness System from Smartex s.r.l. Pissa Italy [45]). Thus making it a textile based wet gel electrode that has to be recharged with conductive gel layer before every use.

Contrary to wet gel silver-silver chloride electrodes used for monitoring cardiac health, the proposed textile based nanosensor electrodes are dry and have desirable properties such as high sensitivity, and without the hassle of drying gel or glue. They have consistent electrical

properties and do not lead to any allergic reaction or skin irritation during prolonged use for more than a couple of days. They can be used multiple number of time as a part of apparel items, therefore, the patients can take bath or shower during the period of health monitoring. Wearable sensors are easy to put on without help of a clinical technician. These characteristics are crucial to insure unobtrusive and long term health monitoring.

2.2 Hybrid nanostructured textile bioelectrode sensors for bio-potential and bio-impedance measurement

The existing dry textile based electrodes, made of metalized fabric, faces the issue of high impedance at electrode-skin interface and is affected by changes in skin conditions. The signals are affected by high noise level and only strong physiological signals are discernible, thus limiting the use of dry electrodes to heart rate measurement and respiration. Therefore, dry electrode systems cannot be used for recording complete ECG waveform or measurement of bioimpedance. This hinders development of sensor systems that can perform comprehensive cardio-vascular health monitoring e.g. heart rate, conventional and derived Electrocardiogram (ECG), and Trans-Thoracic Impedance Plethysmography (TTIP).

2.2.1 Nanostructured textile

Smallest units of the textile are fibres or filaments. Innumerable combinations of these units can result in many textile materials with varying length, cross-section area and shape, and surface roughness. The intelligent functionality can be introduced into textile at different levels. At fibre level, a coating can be applied or threads can be added to make a composite textile. Fibres of different types can be arranged at random or strictly organized way in yarns or fabric

to form even 3D structures. These structures can be metallized to fabricate a conductive textile electrode with micro or nanorod array.

2.2.1.1 Nanotextured textiles as electronic sensors

Textile as a substrate can support nanostructures grown on it [46], embedded as composite [47], embedded/mounted as nanomaterials based devices [48-50] or nanomaterials based coating and dyes [51,52]. Conductive fabrics can be obtained by weaving conductive yarn in to fabric [53,54], coating conductive layers on fabric surface by chemical processes such as polymerization [55], electroless plating [56,57] electroplating [58], or physical processes such as vacuum sputter deposition [59,60]. Incorporation of nanofibers in the textile is also possible by drawing out nano-filaments using electrospining technique [61]. Alternatively, pre-extruded nanofibers can be deposited with the help of electrodeposition. In either case, the nanofibers form a mat or a web that renders the textile substrate as nanotextured. These textile surfaces have large surface area and surface to volume ratio. The large surface area improves absorption or adsorption property of the textile substrate to make them useful as sensor layer for gas sensors [62], biological sensors [63], chemical sensor [64], biomedical textile [65], water purifier [66] and electrodes for biopotential measurement [67].

Free standing aligned nanostructures have the potential to improve performance of textile substrate as sensor surfaces because of increase in bio-sensing surface area and surface energy. The sensor aims at improving the textile based sensor electronics. The surface of sensor electrodes can have nanoscale and mesoscale free standing conductive structures. This contributes to increasing the effective surface area of the electrodes and high aspect ratio nano/mesoscale structures can overcome the obstruction due to rough skin surface and body

hair. Electrode surface area, which is in contact with the skin, is important for the signal quality. The biopotential signals are electrical potential measured across the load resistance between the two electrodes that can be associated with impedance due to body bulk, skin and electrodes. Large electrode surface area results in low skin-electrode contact resistance. Thus, it helps in increasing the sensitivity of sensor electrodes. This has been shown through impedance analysis with gold nanowires on flexible polyimide substrate (Figure 9) [68]. Similar conclusion was drawn by Oh et.al.(2012) from assessment of their nanotextured textile electrode [67].

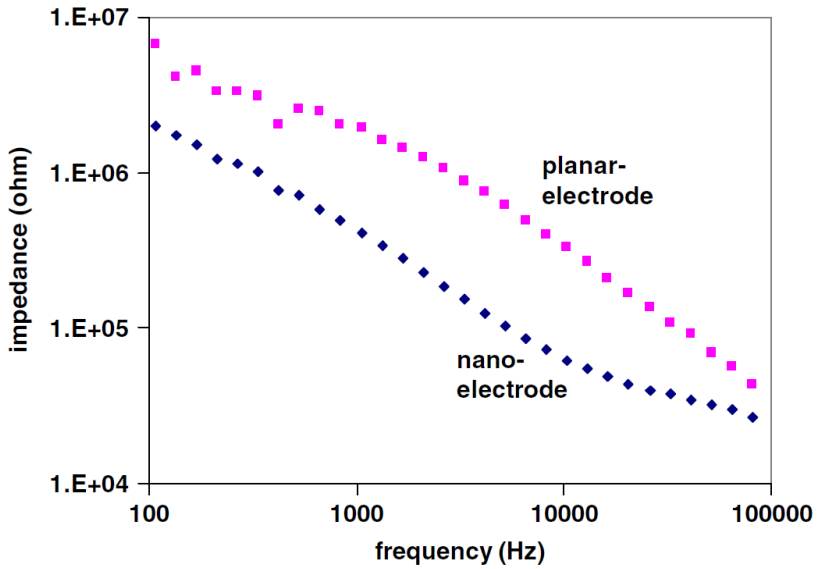

Figure 9: Comparison of impedance spectroscopy on gold electrodes with planar surface and nanowire bundles measured in PBS buffer at 5 mV AC and 0 V DC potential versus an Ag/AgCl reference electrode.

2.2.1.2 Nanometer scale filament and fibers

To obtain free standing nanostructures on the textile, it is important to determine the smallest dimension achievable on the textile. In the beginning of this section, it was mentioned that the smallest units of textile are fibers and filaments. Different kinds of fiber have been in

use. The natural fibers have their diameters fixed by the nature, such as cotton (12-20 µm), wool (20 µm), jute (20 µm) and silk (10 µm) [69]. Regenerated natural fibers are obtained by reducing the natural material to pulp and redrawing (solvent spinning) them into fibers, such as cellulose based viscose (18-20 µm) and lyocell (50 µm), protein based aralac or milk wool (15-30 µm) and soybean fiber (14-27 µm), alginate (10-20 µm), chitosan (15 µm) [69]. Artificial fibers such as fiber glass (15-20 µm), carbon fiber (5-10 µm) and ceramic fiber (10 µm) are commercially available [70]. These fibers cannot be used for obtaining free standing nanostructures on the fabric that can be functionalized to form nanowire electrodes.

Synthetic long chain polymers such as polyester, nylon, polyimide and polyaramid are melt blown or solution blown and spun into fibers on spinneret. The techniques for drawing out the fibers can be modified to obtain fibers with diameter in the order of nanometers. Electrospining is method of producing fibers with diameters between 40 and 2000 nm. In this process, the tensile force is generated by the interaction of applied electric field with the electrical charge carrier i.e. polymer precursor solution. The free charges or ions move under the influence of displacement force of the electric field. This acts as the driving force for the polymer rather than spindles and reels in conventional spinning. This process can obtain fibers that are only as wide as the single layer crystal made of polymer chains [70].

The conventional synthetic polymer fiber spinning technology has been improved to produce composite fiber. A mixture of two polymers, that are mutually immiscible, is drawn in to fibers by extrusion. Such that, one polymer forms long fibers in a matrix of the other. A cross-section of such a fiber shows that 60-1500 islands of one polymer fibers are distributed in a sea of the other polymer, thus giving the impression of islands in sea [71]. The fibers can be

woven or knitted by using conventional techniques and the sea polymer can be dissolved away to give the finished textile a suede like texture.

2.2.1.3 Textile based vertically free standing (flocked) conductive nanostructures

Textiles with vertically free standing nanometer scale filaments or fibers can be obtained by using the traditional technique of flocking. It uses electric field or pneumatic force to drive down millions of individual fibers that have a static charge on them. The electric field, in particular, aligns the charge fibers vertically and static charge insures that they are apart from each other. The vertically aligned fibers are driven down on to a flexible surface, such as textile or polymer substrate, pretreated with adhesive for the fibers to get planted. A schematic of this process is shown in Figure 10.

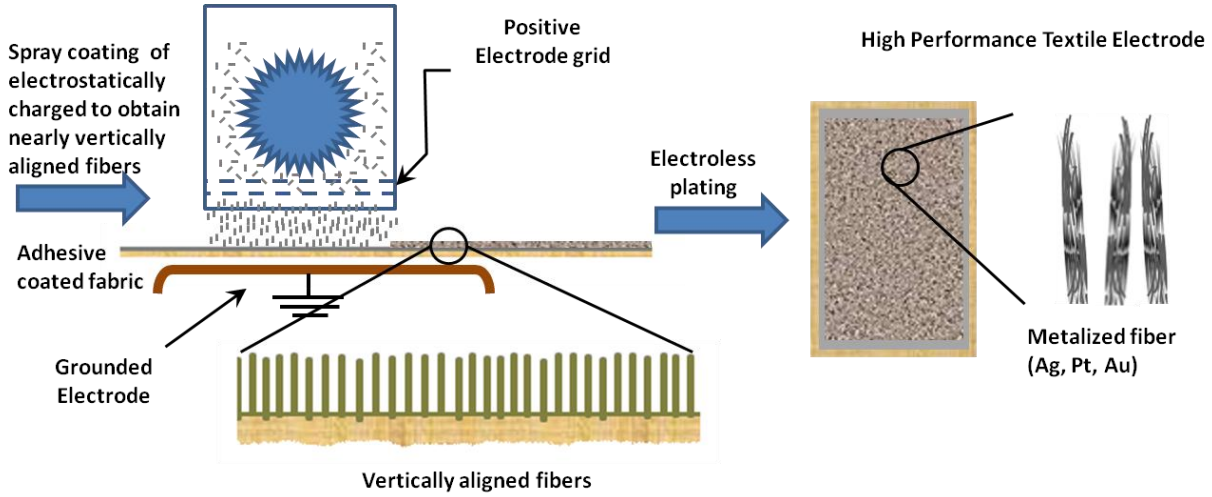

Figure 10: Electrode fabrication technique: Flock application by electrostatic method and then Electroless plating

Electrospun nano-fibers are free range filaments that get entangled during production. In addition to that, the process is very slow (less than 1m/sec of fiber) [70]. This makes it incompatible for mass production. The fibers need to be cut in to small lengths of <100 µm for

flocking. These fibers are slender and very light. They will require a high intrinsic static electrical charge and very strong applied electric field to achieve optimum flocking. Nano-fibers will also have problem in penetrating the meniscus of the adhesive on the substrate. To solve these problems, an innovative approach has been devised. Islands in sea fibers provide the option of textile fabrication followed by dissolving of the sea polymer to expose the nanofibers. The fibers can be cut and flocked like normal micrometer scale fibers and a subsequent dissolving step can release the nanofibers. This shall result in vertically free standing nanostructures on the textile.

Fabric functionalized with silver conformal coat, nanoparticles and nanoparticle composites have been researched for applications ranging from anti-microbial textile and electronic textile to fashionable accessories [72]. These processes are classified as electroless plating process, which means plating without any electrolytic cell. The methods for producing silver nanoparticles include physical processes like atomization or milling, chemical synthesis methods like chemical reduction, biological irradiation, water in oil micro emulsions and green synthesis [73-77]. One of the green synthesis methods is Tollen's procedure, which involves synthesis of silver nanoparticles by reduction of diamine silver (I) ion $[Ag(NH_3)_2]^+$ in an aqueous solution (Tollen's reagent) by aldehydes in presence of ammonia [77].

Electroless plating electrically functionalizes the nanostructures by enmeshing/decorating them with conformal conductive thin film of silver. The electroless plating process used self-nucleation of the silver nanoparticles directly on the surface of the nanofibers. This approach is a modified Tollen's reagent process that involves following reactions:

$$2AgCH_3CO_2 + 2NH_4OH \xrightarrow{H_2O} Ag_2O + 2NH_4CH_3CO_2 + H_2O$$
$$Ag_2O + 4NH_3 + 2NH_4CH_3CO_2 + H_2O \xrightarrow{NH_3/H_2O} 2Ag(NH_3)_2CH_3CO_2 + 2NH_4OH$$

The final solution contains diamminesilver (I) cations, acetate ions and formate ions. This acts as a silver ink that can be used to coat the nanostructures on the textile. Upon drying this ink, labile ammonia ligands evaporate allowing the silver cations to be reduced to elemental silver by formate and acetate ions [78]. In this way, electrically conductive nanowire electrode can be fabricated that are suitable for sensor applications similar to that of the aforementioned gold nanowire electrodes [68]. The evaluation of this design can be done by measuring electrical impedance of the sensor electrode-skin interface. It is expected that the nanostructured electrode surface will improve electrical impedance characteristics of the electrode [79-81].

2.2.2 Modeling electrode-skin interface

2.2.2.1 Skin anatomy

Skin tissue is made of three principle layers that form a protective barrier around the body to protect it from the environment and act as an interface (Figure 11). The outermost layer or the epidermis is the most important and a dynamic layer. The cells in this layer grow and divide at the bottom. The newly formed cells push the older cells outwards. As they move outward they begin to die and lose nuclear material. Further, they degenerate into flat keratinous material that forms a horny layer of dead material on skin's surface that is called stratum corneum. It constantly wears off and is replaced by the newer materials from below. Layer below the epidermis have a network of blood vessels, nerves and sweat ducts [82].

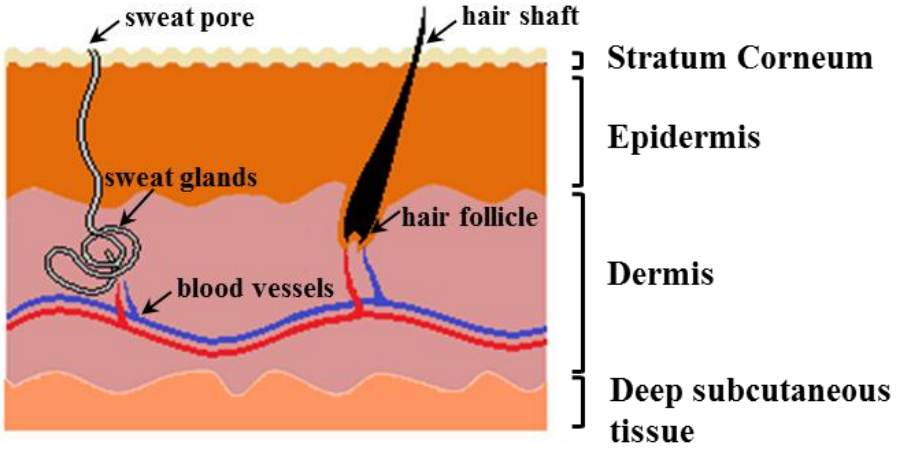

Figure 11: Basic human skin anatomy

The conduction of electricity through skin tissue is by virtue of the movement of endogenous ions through it. Hence, the conductivity of the skin or it's permittivity to ions is a measure of the ease of movement of endogenous ions through the least conductive (permeable) layer. This means our layer of interest is the semi-permeable stratum corneum. The experimentation techniques for measurement of skin electrical conductivity have been present for close to 100 years. Over this period of time, they have contributed to a lot of literature in the fields of electrical engineering, psychology and dermatology.

2.2.2.2 Skin impedance and equivalent electrical circuit

Over the past century, characterization of skin by measurements of its electrical properties has been a popular tool among researchers. Non-invasive electrical experiments are much easier compared to skin penetration experiments. Studies based on measurement of conduction of direct (d.c.) and alternating (a.c.) current through the skin can be found in various fields of research ranging from electrical engineering to psychological journals [83]. The following description summarizes these studies and provides structural and theoretical basis of the electrical behavior to be observed.

In a unique way human skin cell surface behaves like a good dielectric material. That is, it has electrical capacity that is independent of frequency and resistance is close to infinity. Intracellular and extracellular media act as resistances. All combined, the impedance of the tissue varies with frequency. However, it was observed by Fricke (1932) [84] that the phase angle of this variable resistance-capacitance combination remains a constant. This is similar to the phenomena of polarization capacity as found at metal electrolyte interfaces. Polarization impedance Z_P is given by the equivalent circuit shown in Figure 12, where P is the constant phase element, f is the frequency and ϕ is the phase angle of the input signal (current).

$$Z_P = kf^{m-1}$$

$$\phi = (1-m)\frac{\pi}{2}$$

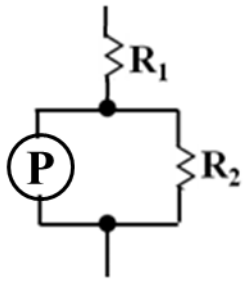

Figure 12: Polarization impedance element as a part of R-[RC] circuit

Different approaches have been taken for modeling the electrode-skin interface. Model equivalent circuits assume the electrode to have a lead resistance and a parallel RC circuit at the contact. In absence of any conductive gel, the dry textile electrodes possess strong capacitive impedance [85]. The interface between electrode and epidermis skin layers is supposed to have a resistive element and a polarizable capacitive element, and the transient phase between electrode and skin as well as the deeper subcutaneous skin tissues to be purely resistive [82,85,86,87].

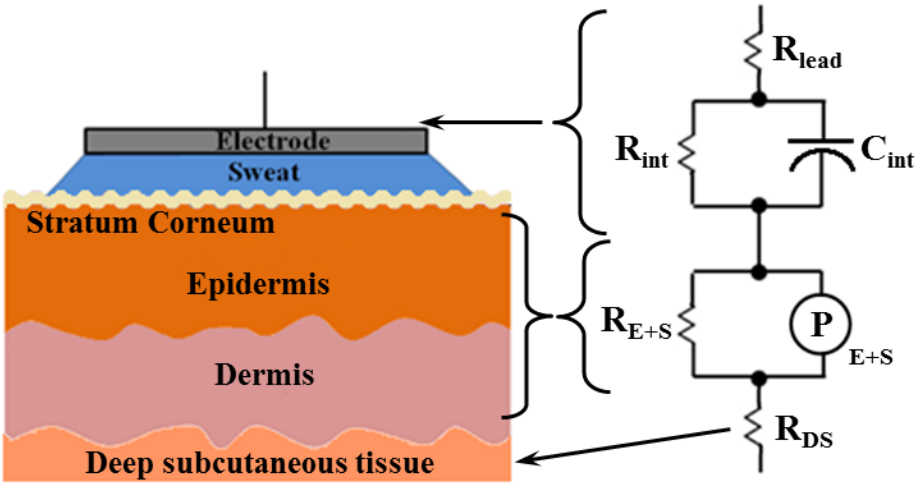

Figure 13: Model of electrode-skin interface for dry electrode and equivalent electrical circuit.

Equivalent circuit shown in Figure 13 incorporates all these concepts. The impedance for the electrode can be broken down into lead resistance R_{lead} and R_{int} C_{int} combination for the contact. The impedance of skin-electrode interface includes resistance R_{E+S} due to skin moisture/interstitial fluids and polarization capacitance P_{E+S} for intracellular fluid of the stratum corneum and epidermis. The deep subcutaneous tissue resistance can be included as R_{DS} in series. The values of resistances and capacitances can be determined by least mean square error minimization algorithm. The data can be generated through impedance measurement by using input voltage with frequency varying from 0.1Hz to 1MHz [85,87,88].

2.2.2.3 Impedance measurement techniques

The most common electrical experiment involves passage of current between two electrodes applied to skin surface. The current flows in at one area of skin, through undefined internal tissue and out again at the other skin area. The resistance across the skin-electrode interface can be measured by a 2 electrode configuration as shown in Figure 14 [89]. The current passed between two electrodes applied to the skin surface. The current flows through

one area of the skin, through undefined intervening (deep subcutaneous) tissue, and out again through another area of the skin. One of the electrodes requires skin preparation (*Prepared Surface*) like alcohol swab and a little skin abrasion to remove dead skin, so that impedance measurement is characteristic of the electrode-skin interface of the other electrode.

To compute the impedance of skin-electrode interface, it is necessary to know the e.m.f. across an individual skin area. In the 2-electrode configuration, one skin-electrode interface can be prepared such that the voltage drop across it is negligible. In that case for d.c. or low frequency a.c. (<1kHz), nearly all the voltage drop is across the other skin-electrode interface and not the deep tissue [90]. This can be done by making one electrode very large and dampening the skin with which it is in contact; conductive jelly can be used.

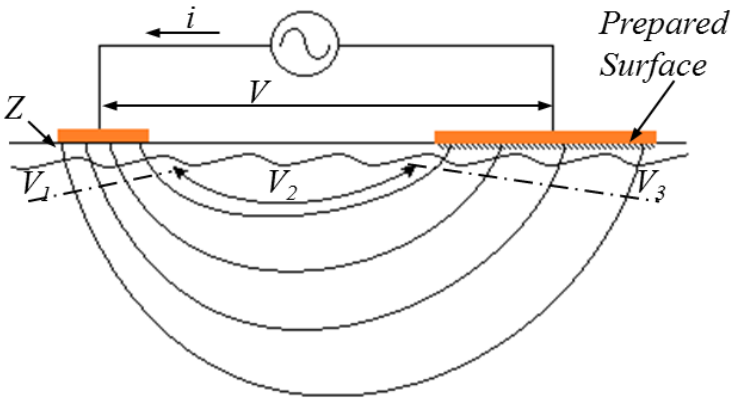

Figure 14: 2-electrode configuration for recording skin-electrode impedance (Z) such that Z = V/i because $V_1 >> V_2, V_3$.

For high frequency (>1kHz) a.c., the skin impedance is reduced. In this case, the above approximation is no longer valid. The voltage drop across the skin is separated from that of the whole system by introducing a third non-current carrying electrode as shown in Figure 15.

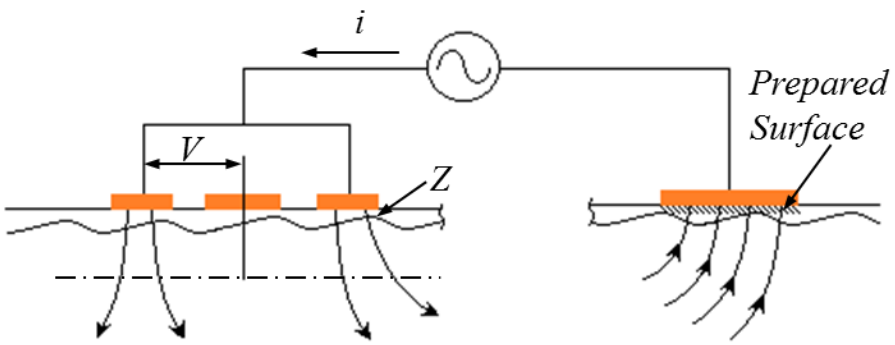

Figure 15: 3-electrode configuration with a non-current carrying electrode to isolate the voltage drop across the skin from that of the whole system.

The dry electrode (metal plate or metalized textile) in contact with the skin or agar gel phantom has high initial impedance. The impedance falls rapidly if contact is maintained and reaches a steady value after a few minutes [89]. Impedance measured after several minutes of electrode-skin contact, without any current flow, is called quasi-steady impedance. It is an important parameter in almost all skin-electrode electrical models.

The skin impedance at low frequencies is predominantly resistive, influenced by electrode-skin contact area and skin moisture content. The impedance is also affected by fringe effect that allows for conduction of electricity through the skin around the electrode edges. Impedance drops and phase angle rises as the frequencies increases. This is due to increase in reactance (capacitance) of the skin. The frequency, at which, the phase angle rises above 45° is called the turnover frequency. At this time capacitive current is dominating. At frequencies in excess of the turnover frequency, the phase angle reaches a value that varies little with further increase in frequency e.g. for human skin the angle is between 65-75° over the frequency range

of 1-15 kHz. Therefore, the electronic circuit equivalent model of the skin-electrode contact uses a constant phase element (Figure 13) for the epidermis [89].

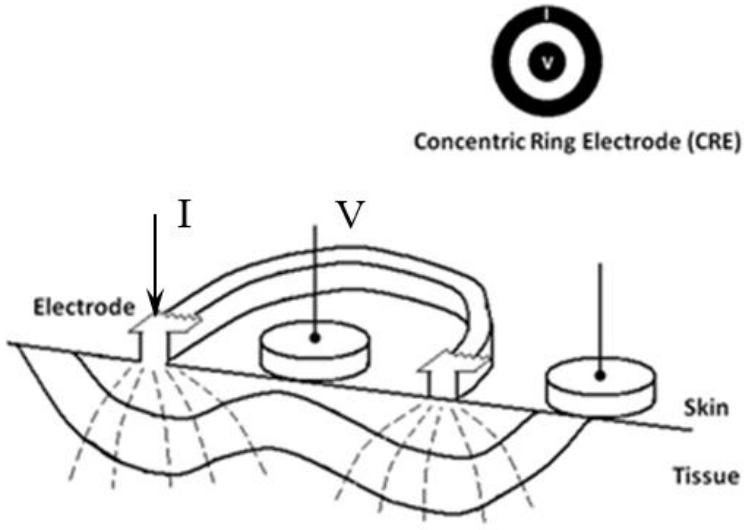

Figure 16: Concentric Ring Electrode: working (current) electrode as annular conductive ring and a voltage taping (non-current carrying) electrode as conductive disc in the center

The 3-electrode system can be emulated by using the electrode pair shown in Figure 16 with a Concentric Ringed Electrodes (CREs) and a remote electrode. A CRE has a working (current) electrode in form of annular conductive ring and a voltage taping (non-current carrying) electrode in form of a conductive disc in the center. This electrode (CRE) is useful for skin impedance measurements as well as Bioimpedance Spectroscopy in a 4-electrode configuration.

2.3 Effect of Hybrid nanostructure on the sensor signal flow at electrode-skin interface

The evaluation of nanostructured textile electrodes can be done through impedance characterization of the contact made by the electrode surface to the skin. For analyzing the

effect of hybrid nanostructure geometry and distribution, models are required that explain the dominant effects of electrode-skin contact impedance such as fringe (edge) effects [91,92]. Finite Element Method (FEM) has been an effective tool for studying electrical field distribution within electrode-skin interface [91,92] It estimates the surface electric current and voltage to obtain the image of impedance distribution on electrode-skin interface. The model follows Maxwell's equations that form the electromagnetic theory for the ECG electrodes [92]. For a nonmagnetic material such as biological tissue, the Maxwell's equations and equation of continuity can be written as

$$\vec{\nabla} \times \vec{H} = \vec{J} + \frac{\partial \vec{D}}{\partial t} \tag{1}$$

$$\vec{\nabla} \cdot \vec{B} = 0 \tag{2}$$

$$\vec{\nabla} \times \vec{E} = -\frac{\partial \vec{B}}{\partial t} \tag{3}$$

$$\vec{\nabla} \cdot \vec{D} = \chi(\vec{r}, t) \tag{4}$$

$$\frac{\partial \chi}{\partial t} + \vec{\nabla} \cdot \vec{J} = 0 \tag{5}$$

Where $\chi(\vec{r}, t)$ is the charge density, $\vec{J}$ is the current density, $\vec{E}$ is the electric field, $\vec{D} = \varepsilon \vec{E}$ is the electric displacement with ε the electric permittivity, $\vec{B}$ is the magnetic field and $\vec{H} = \vec{B}/\mu$ is the magnetic intensity with μ the magnetic permeability. For modeling the electrodes for biopotential acquisition, following assumptions are made to simplify the problem:

i. External $\vec{B}$ field is negligible i.e., there is no electromagnetic interference [92].

ii. Quasi-static state $\left(\frac{\partial \vec{D}}{\partial t} = 0\right)$, which holds as long as the sampling rate is low enough to neglect the electromagnetic wave propagation delay $\left(t_{delay} = Size\,of\ human\,body / speed\,of\ light\right)$ [93]. In addition to that, displacement current is negligible in comparison to the conduction current [94].

Under these assumptions and an externally applied current $\vec{J}^{external}$, time harmonic form of Maxwell's equations state that

$$\vec{\nabla} \times \vec{H} = j\omega\varepsilon\vec{E} + \vec{J} = 0 \tag{6}$$

And

$$\vec{J} = \frac{\vec{E}}{\rho} + \vec{J}^{external} \tag{7}$$

Therefore, continuity or charge accumulation equation (5) can be written as

$$\begin{aligned} &\vec{\nabla} \cdot \vec{J} = \vec{\nabla} \cdot \left(\frac{\vec{E}}{\rho} + \vec{J}^{external}\right) = -j\omega\varepsilon\vec{\nabla} \cdot \vec{E} \\ &i.e. -\vec{\nabla} \cdot \left(\left(\frac{1}{\rho} + j\omega\varepsilon\right)\vec{\nabla}\phi - \vec{J}^{external}\right) = 0 \qquad as\ \vec{E} = \vec{\nabla}\phi \end{aligned} \tag{8}$$

And external boundary conditions are set as

$$\hat{n} \cdot \vec{J} = 0 \tag{9}$$

This is based on the assumption that the fringe current density vector component of the nano-bio electrode along the skin surface is negligible.

Current density $\vec{J}$ and electrical potential ϕ satisfy the above Poisson equation, where current density $\vec{J}$ is a function of resistivity ρ, permittivity ε, carrier frequency $f = \omega/2\pi$ and electrical potential ϕ [92]. The models, applicable for a pair of electrodes, divide the skin into a

two dimensional mesh and the electrode-skin interface into a one dimensional mesh (Figure 17) [95]. Equation (8) will be applicable in the electrode-skin interface. The electrode can be modeled as Concentric Ring Electrode (CRE) (Figure 18). On the CRE, outer concentric ring is used for input current I_{input} and the center disc is used for measuring electrode potential [96].

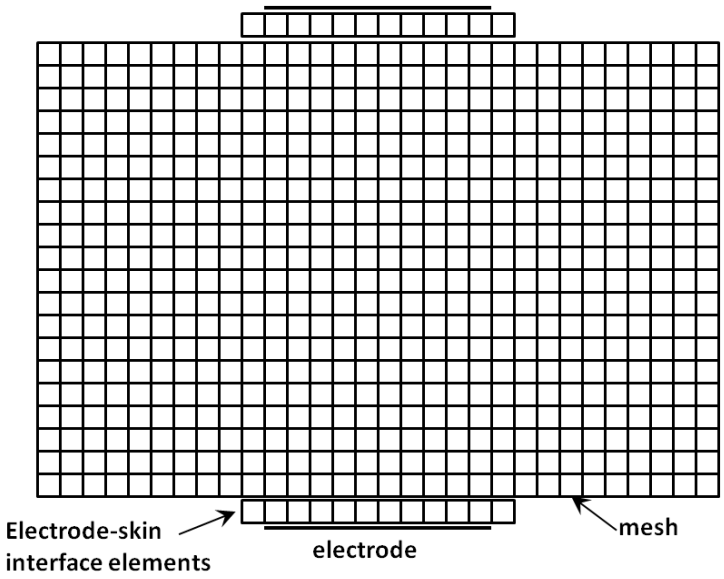

Figure17: The testing mesh and the electrode-skin interface for a two electrode system

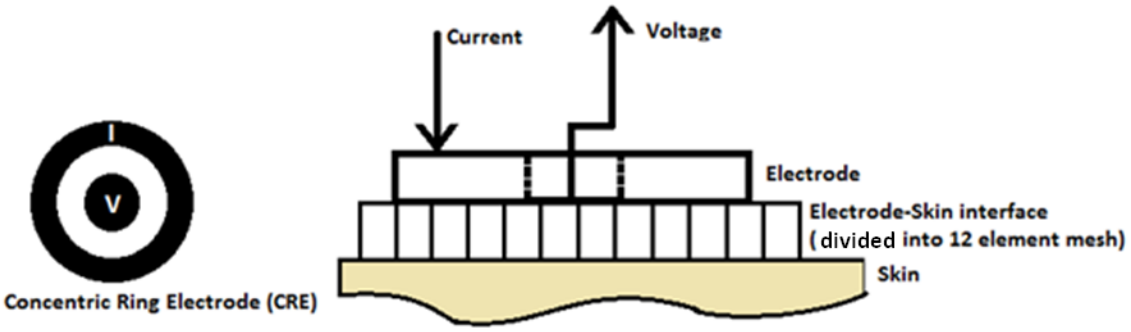

Figure 18: Concentric Ring Electrode (CRE) for the experiment and implementation of the testing mesh to the CRE

Boundary condition given by equation (9) is applicable to all points except at the current injection and current absorption electrodes. They follow boundary conditions

$$\int \frac{\phi}{Area} = Z_{E/S} \cdot I_{input} \text{ and } \phi = 0 \quad (10)$$

are applicable respectively. Continuity (internal boundary condition) between two adjacent cells p and q will be given $\hat{n} \cdot \left(\vec{J}_p - \vec{J}_q\right) = 0$. The accordance of net $Z_{E/S}$ from simulation result with the experimental value will validate this assumption.

This FEM model can be solved for electrical potential ϕ at each node. These values can be used to derive current density, which can be plotted on the electrode surface and each node can be assigned an equivalent impedance element. This model is applicable in different skin conditions: dry, normal, moist and sweating, as well as for different electrode structures: plane, microstructured and nanostructured. It is not applicable to skin-electrode contacts during body motion because of the uncertainty in contact area under this condition.

3. Research Methodology

The objective of this research was to study the novel hybrid nanostructured textile bioelectrode and validate the hypothesis, **"Nano-Bio Textile electrode improves bio-potential sensing."** The governing hypothesis was validated by finding answers to the following queries:

1. Is it possible to fabricate chemically and mechanically sturdy conductive textile based nanostructures on fabric?
2. Are size and distribution of hybrid nanostructures on the fabric causal to overall conductivity of the nano-bio sensor electrode?
3. How vertically free standing nanostructures on textile electrode contribute to signal flow at the electrode-skin contact interface?
4. Is the performance of hybrid nanostructured textile based bioelectrode better than silver-silver chloride electrode under variation in skin condition?

To answer these questions following goals were set:

Goal 1: Design and fabricate nano-bio textile sensors with vertically free standing textile based nanostructures.

Goal 2: Testing the electrical properties of nano-bio textile sensors under conditions: abrasion and washing.

Goal 3: Impedance mapping of nano-bio textile based sensors to study effects of conductive hybrid textile based nanostructures on signal flow through electrode-skin interface.

Goal 4: Nano-bio textile sensor performance in measurement of electrocardiogram (ECG) signals and electrode-skin interface electrical impedance under varying skin conditions.

To summarize, hybrid nanostructured textile bioelectrode sensors with different nanostructure sizes and distributions will be tested for sturdiness of their silver coating, ECG signal quality, electrode-skin interface impedance with varying skin condition and motion, and impedance distribution. This data will be used to validate the above mentioned hypothesis.

3.1. GOAL 1 - Design and fabricate nano-bio textile sensors with vertically free standing textile based nanostructures

This aimed at design and development of dry electrodes for biopotential and bio impedance sensing with high sensitivity and fidelity. The textile based electrodes were developed as electrically functionalized piece of fabric with novel hybrid nanostructures. They were packaged as sensors mounted on garment fabric for detection of potentiometric electrophysiological signals.

3.1.1 Fabrication process

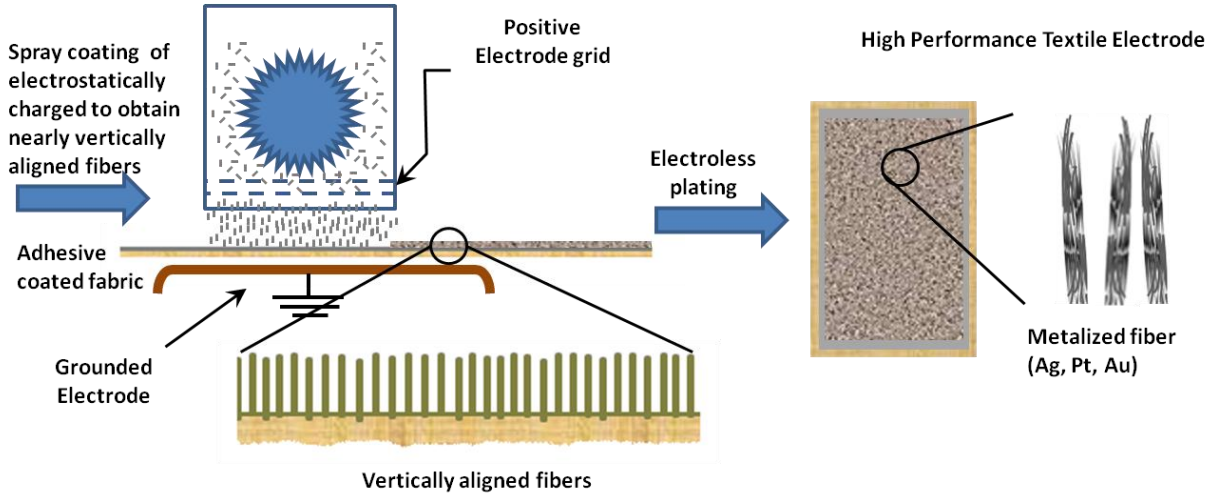

Figure 19: Electrode fabrication technique: Flock application by electrostatic method and then Electroless plating

Nanostructures were realized on textile by deposition of finely cut fibers by flocking technique (Figure 19). These fibers were high aspect ratio structures, i.e. length of 200-250microns nylon fibers10-12micrometer in diameter or 200 nanometers in diameter [polypropylene island in polylactic acid sea] nanocomposite yarn (Hills Inc., Melbourne, FL). The fibers were chemically treated to impart electrostatic charge, a.k.a. activation. The flock fibers were prepared for the activation process by washing with hot water followed by washing with cold water. The flock fibers were dried before further treatment. Dry 1 gram of flock fibers are added to a bath of 30mL of distilled water with constant stirring at 150-200 rpm. The bath was heated with the stirring. When temperature of the bath reached 40°C, 15mg of aluminum sulfate (Sigma Aldrich, St. Louis MO) was added and pH of the solution was lowered to 4.5 with acetic acid (Sigma Aldrich, St. Louis MO). When the bath temperature reached 50°C, 15mg of tannic acid (Sigma Aldrich, St. Louis MO) was added. At 60°C, 10mg of aluminum sulfate (Sigma Aldrich, St. Louis MO) was futher added. This solution was maintained at 60°C for 30 minutes with stirring. The solution is drained out and the fibers were retained by filtration and washed with DI water 2-3 times. The fibers were re-suspended in 30mL of DI water. The temperature was raised under constant stirring. At 40°C, 160mg ammonium sulfate (Sigma Aldrich, St. Louis MO) was again added and the pH was brought to 5.5 with acetic acid (Sigma Aldrich, St. Louis MO). When the bath temperature reached 50°C, 15mg cationic softener (Star Chem., Wellford SC) was added. The bath temperature was brought up to 60°C and maintained for 30 minutes with constant stirring. The solution is drained out and the fibers were retained by filtration. The fibers were dried at room temperature till only 6-8% of moisture was left. This was done for electrostatic activation of the fibers. The fibers were sifted to remove long fibers.

Thus prepared fibers can be applied to a fabric such that they are free standing because of mutual repulsion.

The flocking process used high strength electrostatic field of 3kV/cm for deposition of electrostatically charged fibers. The fibers move at a high velocity under the influence of electric field applied perpendicular to the substrate (adhesive coated fabric) and were attached vertically on it. This resulted in vertically aligned microstructured or nanostructure arrays.

The flocked fabric was electrically functionalized with the help of electroless plating by enmeshing/decorating the nanostructures with conformal conductive thin film of silver. The electroless plating process used self-nucleation of the silver nanoparticles directly on the surface of the fibers. The process had four steps: 1) pretreatment by soaking in mild detergent solution followed by deionized water rinse, 2) a 20 minutes long sensitization by adsorption of stannous (Sn^{2+}) colloids on fiber surface, 3) plating by using a mix of silver salt and reducing agent by soaking the flocked fabric in the mix for 1 hour followed by drying the fabric in nitrogen environment and annealing at temperature in excess of 100°C, and 4) post treatment by rinsing with deionized water to remove any unreacted precursors.

The stannous (Sn^{2+}) colloid was made from 16mM $SnCl_2.2H_2O$ (Alfa Aesar, Ward Hill, MA) and 0.35% v/v HCL (36.5%-38%, J.T. Baker, Phillipsburg, NJ) in DI water [97]. The silver salt and reducing agent mix was made by dissolving silver acetate (Sigma Aldrich, St. Louis, MO) 0.4g/mL in aqueous ammonium hydroxide (28%-30% NH3, Sigma Aldrich, St. Louis, MO) at room temperature followed by titration of formic acid (95% pure, Sigma Aldrich, St. Louis, MO) at 0.08mL per mL of aqueous ammonium hydroxide. This approach is a modified Tollen's reagent process that involves following reactions:

$$2AgCH_3CO_2 + 2NH_4OH \xrightarrow{H_2O} Ag_2O + 2NH_4CH_3CO_2 + H_2O$$

$$Ag_2O + 4NH_3 + 2NH_4CH_3CO_2 + H_2O \xrightarrow{NH_3/H_2O} 2Ag(NH_3)_2CH_3CO_2 + 2NH_4OH$$

The final solution contains diamminesilver (I) cations, acetate ions and formate ions. Upon drying this solution, labile ammonia ligands evaporate allowing the silver cations to be reduced to elemental silver by formate and acetate ions [98].

3.1.2 Fabrication process optimization

The electrode fabrication process was optimized by assessing the effect of process parameters on the electrical functionality of the electrodes. The process parameters have been listed in TABLE 1. The variables have been listed in TABLE 2. The level of variation for each parameter is given by the experiment design shown in TABLE 3.

TABLE 1: Process parameters for electroless silver coating of flocked electrodes

Parameters	**Remarks**
(P1) Temperature for reduction of silver	Temperature at which the diamminesilver (I) solution is dried and ammonia ligand is allowed to evaporate
(P2) Annealing temperature	The process of heating silver coating to induce homogeneity and improve grain size for better conductivity
(P3) Annealing time	Longer treatments increase the effect of annealing

TABLE 2: Variables of electrical conductivity

Variables of Silver coating	**Remarks**
(V1) Electrical conductivity	Electrical conductivity between tip and electrode base using gel phantom
(V2) Color fastness and ruggedness	Sturdiness of silver thin film against: washing, dry and wet abrasion [99,100]
(V3) Morphology	The uniformity of silver coating on the micro and nanostructures using SEM scans; grain size of the coating using XRD [101]
(V4) Micro and Nanostructure integrity	SEM scans to validate the integrity of the micro and nanostructures after color fastness testing

3.1.2.1 Electrical characterization

The electrical conductivity of the sensor electrode measured to assess the consistency of silver thin film at the base of the electrode and on the flock micro/nano filaments. The silver thin film on the base of the electrode is characterized by measuring its sheet resistance using the Van der Pauw method. The silver thin film on the flock filament stricture is important for achieving electrical contact with the skin, therefore, it is characterized by measuring the contact impedance.

3.1.2.1.1 Van der Pauw method: Sheet resistance measurement

Van der Pauw method (by L.J. van der Pauw [102]) is used for measuring specific resistance of a flat lamella of random shape. For the measurement, four small electrical contacts (A, B, C and D in Figure 20 (a)) were made along the circumference of the flat sample. If the sample thickness is d, the resistance $R_{AB,CD}$ (the potential difference V_D-V_C per unit current flowing through contacts A and B) and $R_{BC,DA}$ (the potential difference V_A-V_D per unit current flowing through contacts B and C) are used to estimate of the specific resistivity of the lamella.

$$R_{AB,CD} = \frac{(V_D - V_C)}{I_{AB}} \; and \; R_{BC,DA} = \frac{V_A - V_D}{I_{BC}}$$

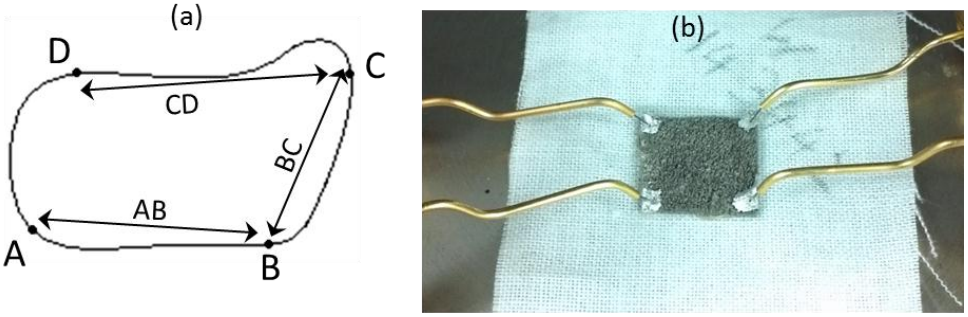

Figure 20: (a) Model schematic for Van der Pauw method for measuring sheet resistance of a flat lamella of random shape (b) Electrode sample (1cm x 1cm) characterized by Van der Pauw method using a 4 probe station

The flat lamella was assumed to be free of holes (consistent). The resistivity of the sample was denoted by ρ and the distance between points A and B was denoted by AB etc.

$$i.e. \quad \exp\left(-\frac{\pi d}{\rho} R_{AB,CD}\right) + \exp\left(-\frac{\pi d}{\rho} R_{BC,DA}\right) = 1 \tag{11}$$

By reciprocity theorem for passive four-poles, $R_{AB,CD} = R_{BC,DA}$. To compute the potential difference across D and C the following expression is used

$$V_D - V_C = \int_D^C E dr = \frac{\rho I_{AB}}{\pi d} \int_D^C \frac{dr}{r} \quad , where \;\; E = \rho J_{AB} = \frac{\rho I_{AB}}{\pi r d} \;\; by\ Ohm's\ Law \tag{12}$$

The point of current injection is A and exit is B. Variable r is the distance from point of current injection A. The expression for $R_{AB,CD}$can be derived from equation (12) as follows

$$i.e. \quad R_{AB,CD} = \frac{V_D - V_C}{I_{AB}} = \frac{\rho}{\pi d} \ln \frac{(AB + BC)(BC + CD)}{(AB + BC + CD) \cdot BC}$$

Similar expression can be drawn for $R_{BC,DA}$. A detailed derivation of these expressions can be found in the original paper by L.J. van der Pauw [102]. Further simplification of the model was done as follows [102]

$\pi d R_{AB,CD} = x_1 \;\; and \;\; \pi d R_{BC,DA} = x_2$

$x_1 = 1/2 \{(x_1 + x_2) + (x_1 - x_2)\}$

$x_2 = 1/2 \{(x_1 + x_2) - (x_1 - x_2)\}$

$$i.e.\ equation\ (11)\ can\ be\ written\ as \qquad \exp\left(-\frac{x_1}{\rho}\right) + \exp\left(-\frac{x_2}{\rho}\right) = 1$$

$$i.e. \quad \exp\left(-\frac{x_1 + x_2}{2\rho}\right)\left(\frac{\exp\left(-\frac{x_1 - x_2}{2\rho}\right) + \exp\left(\frac{x_1 - x_2}{2\rho}\right)}{2}\right) = \frac{1}{2}$$

$$i.e.\ \exp\left(-\frac{x_1+x_2}{2\rho}\right)\cdot\cosh\left(\frac{x_1-x_2}{2\rho}\right)=\frac{1}{2}$$

$$because\ x_1=x_2 \quad \exp\left(-\frac{x_1+x_2}{2\rho}\right)=\frac{1}{2}$$

$$i.e.\ \frac{x_1+x_2}{2\rho}=\ln 2$$

$$i.e.\ R_{AB,CD}=\frac{V_D-V_C}{I_{AB}}=\frac{\rho}{\pi d}\ln 2$$

$$i.e.\quad R_S=\frac{\rho}{d}=\frac{\pi}{\ln 2}\frac{V_D-V_C}{I_{AB}} \tag{13}$$

The specific sheet resistances of the samples were measured with the 4 probe system (Figure 20 (b)) and the Agilent 4156C Semiconductor Parameter Analyzer. The input voltage sweep was performed from -1 to 1 V and the specific sheet resistance was calculated using the formula in equation (13).

3.1.2.1.2 Contact resistance measurement

The electrical conductivity was measured by measurement of impedance between silver flock electrode and a remote Ag/AgCl reference electrode placed across a tissue phantom made of agar gel. The agar gel phantom was made by dissolving 5% by weight of pure agar (Alfa Aesar, Ward Hill, MA) in DI water at 85°C. The agar was allowed to set at room temperature. The gel was saturated with phosphate buffer saline (PBS) 0.01M pH 7.4 (Sigma Aldrich, St. Louis, MO). The circuit layout for contact resistance measurement is shown in Figure 21.

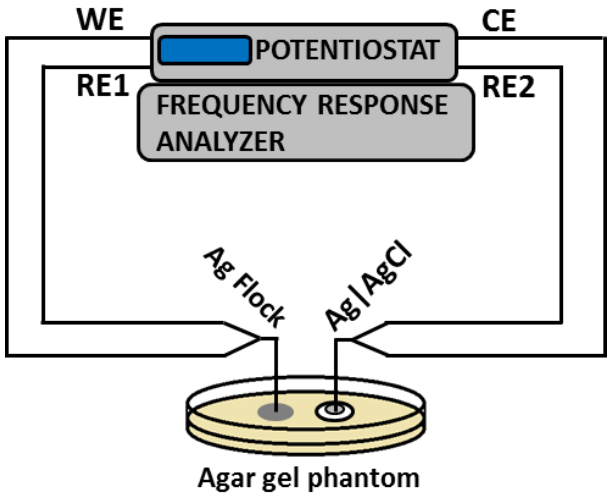

Figure 21: Experiment set up for Contact resistance measurement: 2-electrode configuration. The Potentiostat provides a sinusoidal input voltage of constant magnitude between Silver coated micro/nano structured (working) electrode (WE) and Silver|Silver Chloride gel (counter) electrode (CE). The resultant current between WE and CE is measured by the Frequency Response Analyzer. The reference electrodes (RE) 1 and 2 were shorted with the WE and CE respectively.

A potentiostat (Solartron 1287 SI Electrochemical Interface) was used to apply a sinusoidal input voltage of 10mV magnitude and frequency range of 0.1 Hz to 100 kHz between silver the micro/nano structured textile based electrode and standard silver-silver chloride (Ag|AgCl) ECG electrode. The resultant current was measured by a frequency response analyzer (Solartron 1255B). The Z-Plot software (Solartron) was used to control the voltage amplitude and frequency. The impedance and phase angle was calculated and plotted at Cole-Cole plot and Bode plot. A similar scan was done with Ag|AgCl electrode pair to estimate and subtract the impedance value of Ag|AgCl-gel interface from the experimental value.

Impedance data was fitted to equivalent circuit model discussed in section 2.2.2.2 with the Z-view software (Solartron) using least square fit method. The impedance cell was set up in a 2-electrode configuration (section 2.2.2.3), where leads for the reference electrodes were shorted with those of the working and the counter electrodes. The measurement setup was placed in that portion of the lab which was away from other electrical equipment and house air-conditioning was switched off. These precautions were taken to avoid electro-magnetic interference.

3.1.2.1.3 Electrode surface morphology

The electrode surface was characterized with Scanning Electron Microscopy (SEM) for coverage of the electrode surface by silver nanoparticles and silver nanoparticle film morphology. SEM was a Phillips XL30 ESEM field emission 15kV microscope at Institute for Nanoscience and Engineering in University of Arkansas. The scans were also observed for patterns of crystal growth.

X-ray diffraction (XRD) was used for quality and grain size of nanoparticles of silvercovering the surface of flock filaments and the base fabric. The XRD was a Miniflex (Rigaku Tokyo Japan) with a 30kV/15mA X-ray source. The flock fabric was cut into 20 x 20 mm square piece as a sample. The scan was done in a 2θ/θ mode from 35° to 80°. The x-ray diffraction pattern was used for estimation of grain boundary from Sherrer's formula [101], where: L is average particle size, $\lambda_{K\alpha 1}$ is X-ray wavelength (Cu source), θ_{max} is angle at the maximum peak and $B_{2\theta}$ is peak broadening at half the intensity of maximum peak.

$$L = \frac{0.9\,\lambda_{K\alpha 1}}{B_{2\theta}\cos\theta_{\max}} \tag{14}$$

The XRD spectrum shown in Figure 22 is a typical face centered cubic silver crystal structure. The second frame in the figure shows the relationship between the peak intensity I_0 and peak broadening $B_{2\theta}$.

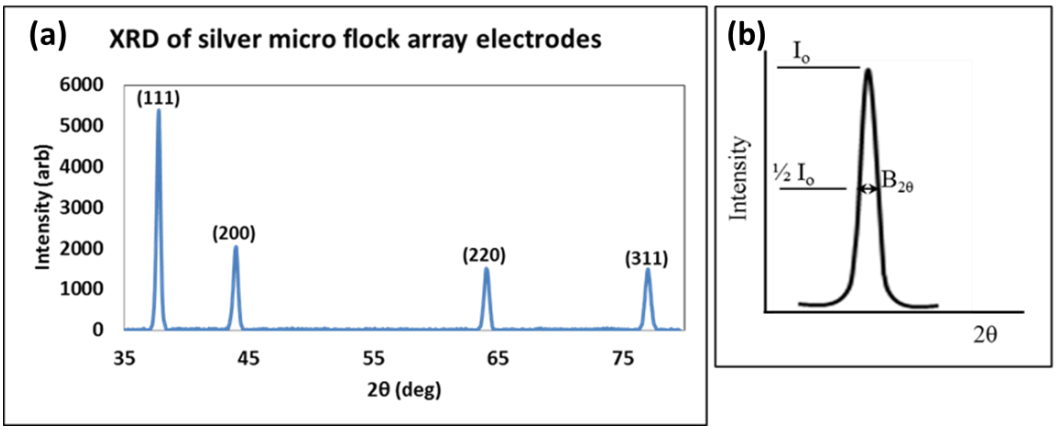

Figure 22: (a) XRD spectrum of silver nanoparticle coated micro flock array, (b) Interpretation of the XRD peak for measurement of silver nanoparticle size usingScherrer's formula

3.2. GOAL 2: Testing the electrical properties of nano-bio textile sensors under conditions: abrasion and washing

The conditions of abrasion and washing will be administered based on standard industrial protocols for color fastness as shown in TABLE 3. The electrical properties of the sensors will be tested by measuring sheet resistance of sensor electrode surface and contact resistance, using the protocols mentioned in sections 2.1.2.1.1 and 2.1.2.1.2 respectively.

Color fastness is tested based on the guidelines set by ISO 105-C6 2010 [99], ISO 105X12-2001 [100] (TABLE 3). Wash testing was done by using 4g/l standard detergent solution through 5 cycles at 50°C for 45 minutes and air drying followed by measurement of electrical properties. The detergent was compliant with the definition specified by American

Association of Textile Chemists and Colorists (AATCC) in 1993 [99]. Wash solution had 50 glass marbles to increase the intensity of wash cycle for high throughput testing.

The abrasion test was done in dry and wet conditions. Dry rubbing test was done with cotton rubbing cloth (10x10 mm) with applied force of 9N rubbing to and fro 10 times each followed by measurement of electrical properties. Wet rubbing test was done with water proof abrasive paper (10x10 mm, 680 grit)and the electrode samples were preconditioned by soaking in water to ensure 90-100% water uptake. The rubbing was done with applied force of 9N rubbing to and fro 10 times each followed by measurement of electrical properties.

TABLE 3: Color fastness test for determination of chemical and mechanical sturdiness of electrode silver coating (Ruggedness)

Testing	**Protocol**	**Description**
Silver layer fastness to domestic and commercial laundering	**ISO 105-C6:2010**	study electrical properties against temperature, alkalinity, bleaching and abrasive action [99]
Silver layer fastness to abrasion	**ISO 105-X12:2001**	study the electrical properties upon rubbing with dry rubbing cloth (abrasive paper) and wet rubbing cloth (abrasive paper) [100]

3.3 GOAL 3: Impedance mapping of nano-bio textile based sensors to study effects of conductive hybrid textile based nanostructures on signal flow through electrode-skin interface

To understand the effect of hybrid micro/nano structure on signal flow of electrical signal through interface between textiles based sensor electrode and skin, the impedance scan of the electrode was done on 5 healthy subjects. An approved protocol IRB# 11-09-093 (Appendix I) was followed for testing on human subjects.

3.3.1 Impedance measurement of electrode-skin interface

The micro/nano structured textile based electrodes were intended to be used as simple disc electrode for biopotential sensing and as concentric ring electrode pair for impedance measurement. Impedance scans were used to test the functionality of the electrode for the above mentioned applications. Impedance measurement was done using 2-electrode configuration for simple disc and 3-electrode configuration for concentric ring electrodes discussed in section 2.2.2.3, where the concentric ring electrode pairs forms the poles for input voltage. Standard Ag|AgCl electrode was used as the remote electrode as it can provide good electrical contact, thereby eliminating any skin preparation procedures.

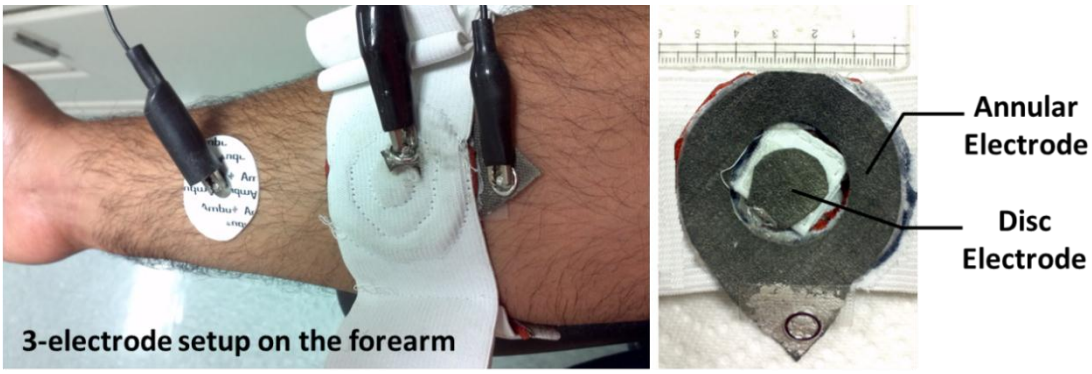

Figure 23: (a) 3-electrode setup on the fore arm with concentric ring electrode (CRE) pair and Ag-AgCl counter electrode, (b) CRE made with flock electrode

The impedance measurement setup was placed at the forearm of a healthy subject (Figure 23).Prior to this, skin moisture content of the subject was measured using skin moisture meter (portable Body Impedance Analyzer). The test electrode and the remote electrode were placed 2 cm apart to avoid any current leakage between the electrodes along the skin surface. The test electrodes were placed on the skin and pressure was applied on them with an elastic

band. This setup was kept in place for 5 minutes to allow the electrode-skin interface to stabilize.

A potentiostat (Solartron 1287 SI Electrochemical Interface) was used to apply a sinusoidal input voltage of 100mV magnitude and frequency range of 0.1 Hz to 100 kHz. The resultant current was measured by a frequency response analyzer (Solartron 1255B). The Z-Plot software (Solartron) was used to control the voltage amplitude and frequency. The impedance and phase angle was calculated and plotted at Cole-Cole plot and Bode plot. Impedance data was fitted to equivalent circuit model discussed in section 2.2.2.2 with the Z-view software (Solartron) using least square fit method. A similar scan was done with Ag|AgCl electrode pair (2-electrode configuration) to estimate and subtract the impedance value of Ag|AgCl-gel interface from the experimental value.

3.3.2 Finite Element Model to study effects of conductive hybrid textile based nanostructures on signal flow

The above experiments were used to measure the impedance of the electrode contact as a whole. To study the signal flow across the electrode and its contact with the substrate, the electrodes can be mapped for electrical current flow over its surface area. As mentioned in theory, the electrical properties of the substrate are important for current flow. For that reason, agar gel based tissue phantom was chosen as the substrate for consistency of result. The electrode-agar gel tissue phantom interface was modeled using finite element method to map the current flow through the interface. The agar gel has more consistent electrical conductivity and relative permittivity values as compared to the properties of skin that vary with moisture content.

The model was setup and simulation was executed on COMSOL Multiphysics 4.2 (COMSOL Inc., Burlington MA). The geometry of the electrode-agar gel phantom interface created on COMSOL is shown in Figure 24, where the array of 100 conductive microfibers separated from each other by 50μm were shown in contact with a block with electrical permittivity of agar gel.

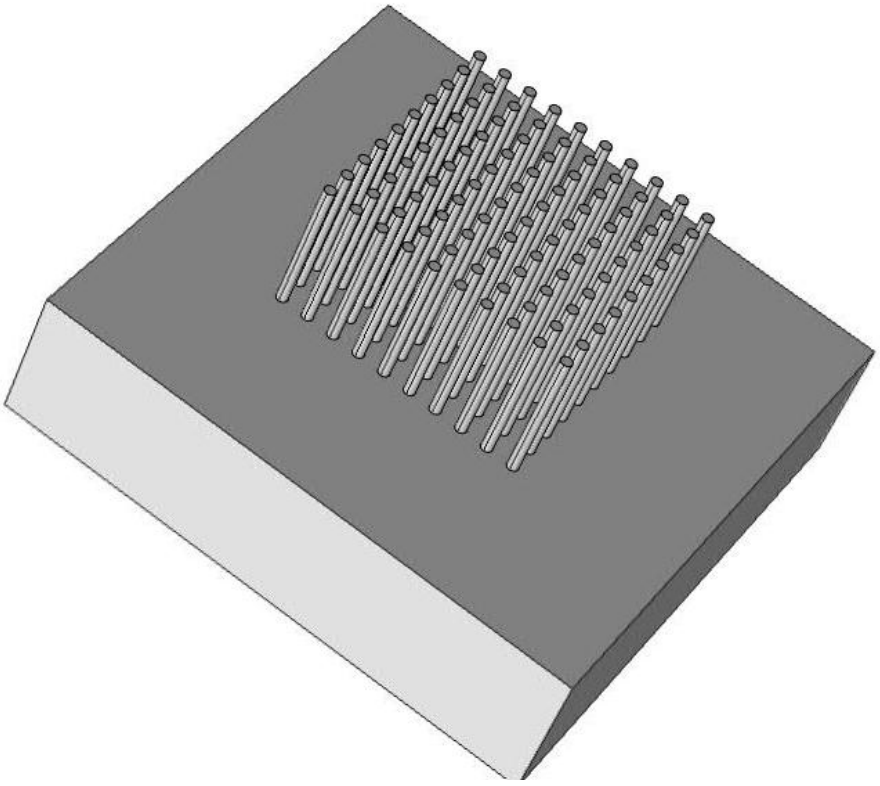

Figure 24: Model geometry of conductive microfiber array and agar gel phantom.

The model was based on harmonic form of Maxwell's equations (Section 2.3). The set equations (15-17) were implemented on the simulation geometry (domain).

$$\vec{\nabla} \cdot \vec{J} = Q_i \tag{15}$$

$$\vec{J} = \sigma\vec{E} + j\omega\vec{D} + \vec{J}_{external} \tag{16}$$

$$\vec{E} = -\vec{\nabla}V \tag{17}$$

The boundary of each element of the domain (microfibers and gel) was designated as electrically insulated (18).

$$-\vec{n} \cdot \vec{J} = 0 \tag{18}$$

The boundaries corresponding to the top face of all the pillars, faces of the micropillars that were in contact with the gel, face of the gel in contact with the micropillars and the bottom face of the gel were not subjected to this boundary condition. The top faces of the pillars were covered by boundary current source (19), where Q_i is the source and ***n*** is the normal vector. The faces of the micropillars and the face of gel that were in contact were put under the boundary condition Pair Contact Impedance (20). The values of σ and ε_r were that of the respective materials, d_s was the thickness of the film of impedance. The bottom face of the gel was designated as the current sink that was defined by the normal current density condition (21).

$$\vec{n} \cdot \left(\vec{J}_1 - \vec{J}_2\right) = Q_i \tag{19}$$

$$\begin{aligned} \vec{n} \cdot \vec{J}_1 &= \frac{1}{d_s}\left(\sigma + j\omega\varepsilon_0\varepsilon_r\right)\left(V_1 - V_2\right) \\ \vec{n} \cdot \vec{J}_2 &= \frac{1}{d_s}\left(\sigma + j\omega\varepsilon_0\varepsilon_r\right)\left(V_2 - V_1\right) \end{aligned} \tag{20}$$

$$-\vec{n} \cdot \vec{J} = J_n \tag{22}$$

Two types of materials were defined and their properties were as designated from literature (TABLE 4). The input voltage was 10mV, which was used to obtain the impedance

measurements from the agar gel phantom experiments. The mesh for this geometry was generated with finer mesh at the interface of the microfibers and the agar gel phantom (Figure 25). The simulation was run for frequency range of 0.1Hz to 100kHz to compute the current density in the domain.

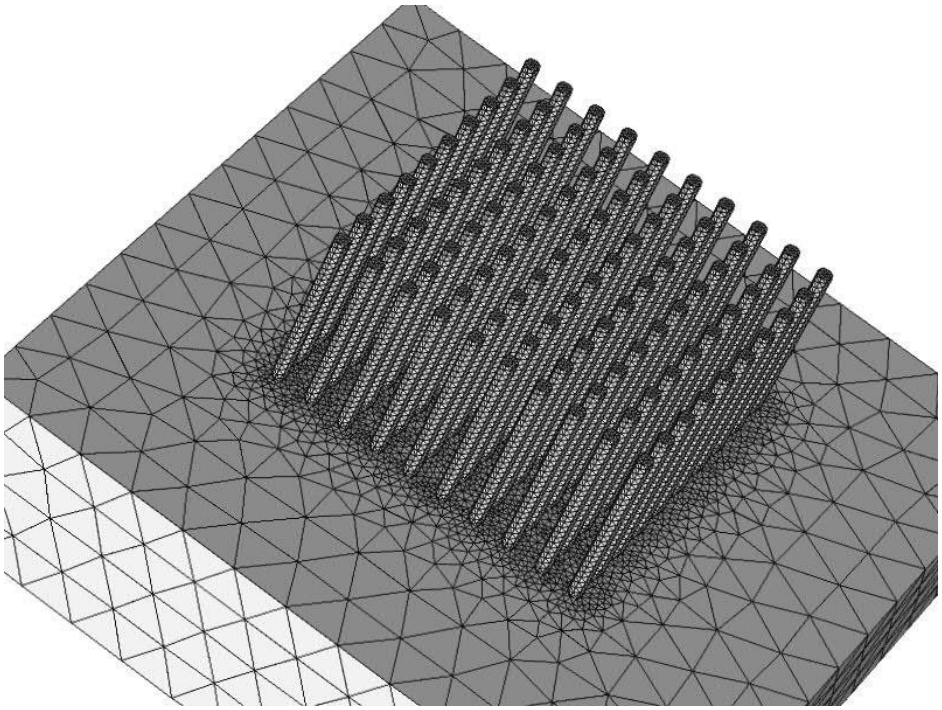

Figure 25: Physics controlled mesh generated for the model geometry. The mesh density was increased at the interface of the microfibers and the agar gel for higher resolution and accuracy in mapping of the electrical currents

TABLE 4: Properties of materials used for finite element simulation in COMSOL

	Name	Electrical Conductivity (σ)	Relative permitivity (ε_r)
Material 1	Silver nanoparticles	6.3×10^7 S/m	0.1
Material 2	5wt% agar gel phantom	8 S/m	80

Similar study was done for nanostructured microfibers with the geometry of the model modified to accommodate nanostructures on the face of microfibers that is in contact with the agar gel. The results were compared for the current distribution for the same input voltage and the direction of the current flow to determine any fringe effect.

3.4 GOAL 4: Nano-bio textile sensor performance in measurement of electrocardiogram (ECG) signals and electrode-skin interface electrical impedance under varying skin conditions

Human skin is a variable medium. It responds to changes in the ambient temperature and pressure applied on it. Especially when sweat appears, many low-resistance parallel pathways become active. It results in decrease in resistance of top layer of the skin called corneum. Its potential and resistance directly affect measurement of electrophysiological activity by electrodes on skin surface [103,104]. These effects are major challenges in the instrumentation of dry electrodes for ECG, EEG and impedance plethysmography.

The electrophysiological measurement experiments covered skin conditions: dry (relative humidity less than 40%), moist (relative humidity between 60% and 70%) and sweating (relative humidity more than 85%) [104]. Biopotential measurement and impedance scanning techniques are explained in the following subsections. A sample population of 5 subjects distributed across the age groups and with healthy skin was used for testing.

3.4.1 Biopotential measurement

The performance of micro/nano-bio textile based sensors in measurement of biopotential was assessed by recording ECG signals using a pair of these sensor electrodes. The differential ECG signal measured across the ventricular plane of heart i.e. lead II is shown in

Figure 26 and a standard for comparison. The scheme for validation of ECG signal was based on observing the basic ECG waveforms P, Q, R, S and T obtained from nano-bio textile based sensors to those obtained from standard Silver-Silver Chloride (||Ag|AgCl) electrodes.

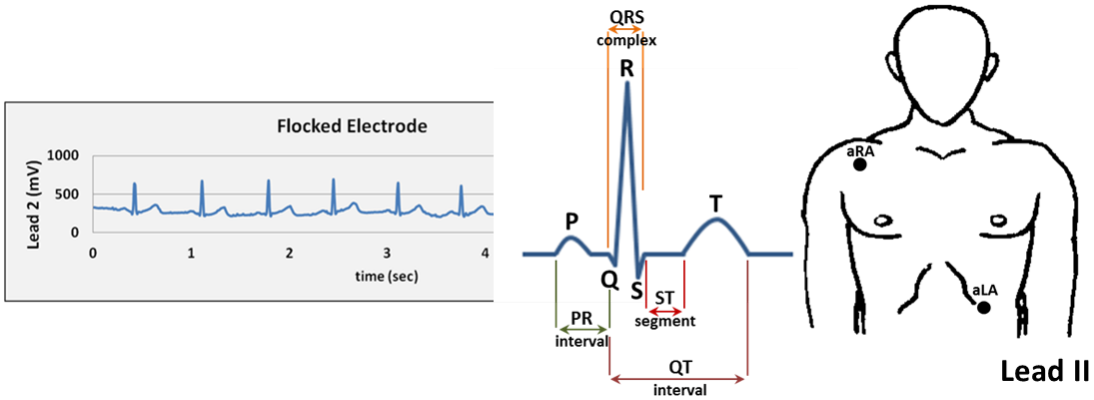

Figure 26: ECG Waveform comparison scheme: Constituent waveforms of ECG signal P, Q, R, S and T waves are observed for their quality and signal strength against the baseline noise.

The instrumentation of the, textile based or textile integrated, sensor systems was designed for seamless integration in the textile. The electronic connections, for relaying signals from the ECG sensor electrodes, were made out of conductive yarn (Sparkfun Electronics, Boulder, CO) with tribo-electric resistant insulation. The ECG electrodes were mounted on the positions shown in Figure 26.

The ECG signal was routed to a signal conditioning and wireless data transmission module. This module was fashioned like a small card so that it can be easily slipped into a pocket on the vest. The data was transmitted from the card to a remote laptop using ZigBee (MaxStream, Lindon, UT) wireless technology. Thus, allowing for the vest to be an autonomous sensing platform [105]. The block diagram of the card circuit is shown below in Figure 27. The laptop used a MATLAB (Mathworks, Natick, MA) based graphic user interface (GUI) for signal acquisition and recording.

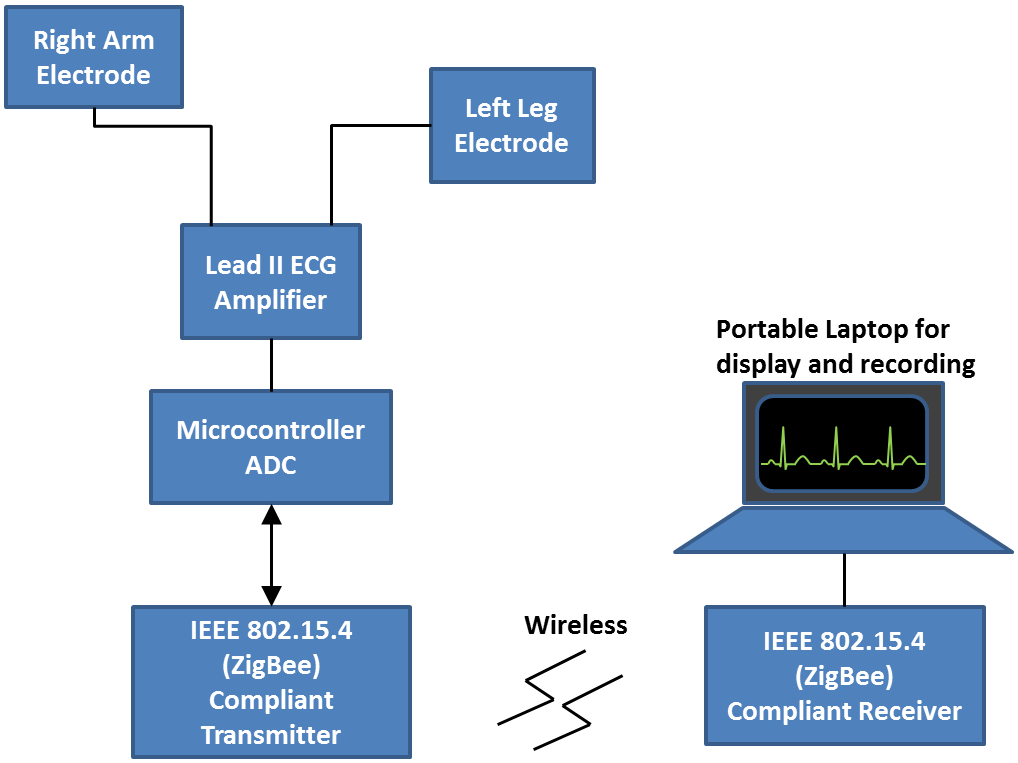

Figure 27: Block diagram of the transmission module for a portable ECG measurement system: ECG signal is amplifier by a differential analog amplifier, the analog to digital converter (ADC) and ZigBee module transmits the signal to a receiver connected to a laptop computer.

3.4.2 Impedance measurement of Skin-electrode interface

To assess the merit of a dry electrode based electrophysiological sensor system, the electrode-skin interface was characterized. The equivalent circuit model used for the electrode-skin interface in this study has been discussed in section 2.2.2.2. The impedance cell was set up in a 3-electrode configuration (section 2.2.2.3), where the working electrode is an annular ring of micro/nano structured textile. The voltage drop was measured between the working annular electrode and a reference concentric disc electrode made of same materials (a concentric ring electrode assembly). The current flow was measured between the working electrode and a remote silver-silver chloride counter electrode. The electrode materials compared were plane conductive textile, microstructured textile and nanostructured textile.

A potentiostat (Solartron 1287 SI Electrochemical Interface) was used to apply a sinusoidal input voltage of 100mV magnitude and frequency range of 0.1 Hz to 100 kHz. The resultant current was measured by a frequency response analyzer (Solartron 1255B). The Z-Plot software (Solartron) was used to control the voltage amplitude and frequency. Impedance data from Cole-Cole plot and Bode plots were fitted to equivalent circuit model discussed in section 2.2.2.2 with the Z-view software (Solartron) using least square fit method. A similar scan was done with Ag|AgCl electrode pair (2-electrode) to estimate and subtract the impedance value of Ag|AgCl-gel interface from the experimental value.

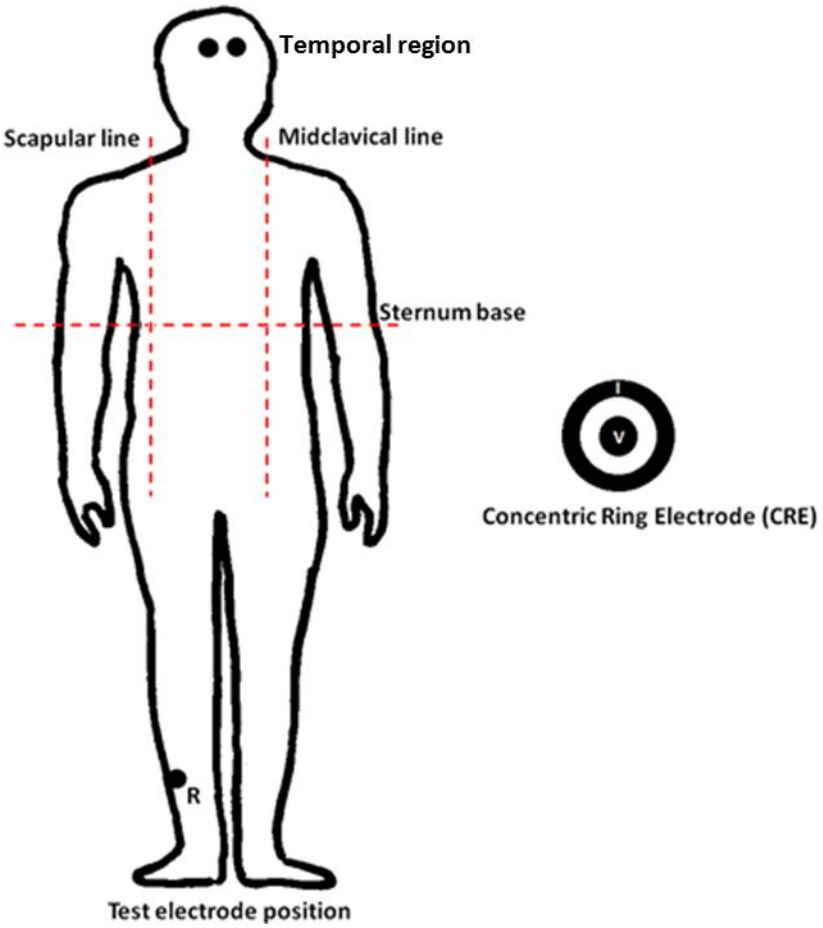

Figure 28: The electrode positions for impedance measurement: the sternum, midclavical line, scapular line, temporal region and right leg.

The electrodes were tested in regions that were identified as the positions for mounting micro/nano structured textile based sensor. Figure 28 shows the positions that were used for testing this sensor. These positions were identified as relevant to applications such as ECG, EEG and Impedance based plethysmography. The positions of interest were largely classified as sternum positions, midclavical line, scapular line, temporal region and the right leg.

4. Results

This section is a compilation of the results obtained from the experiments described in the chapter 3. The observations and outputs from data processing have been compiled in this section. Their discussion with respect to the 4 goals and the principle hypothesis has been included in the next chapter.

4.1 Morphology of Silver nanocrystal layer on flock fibers

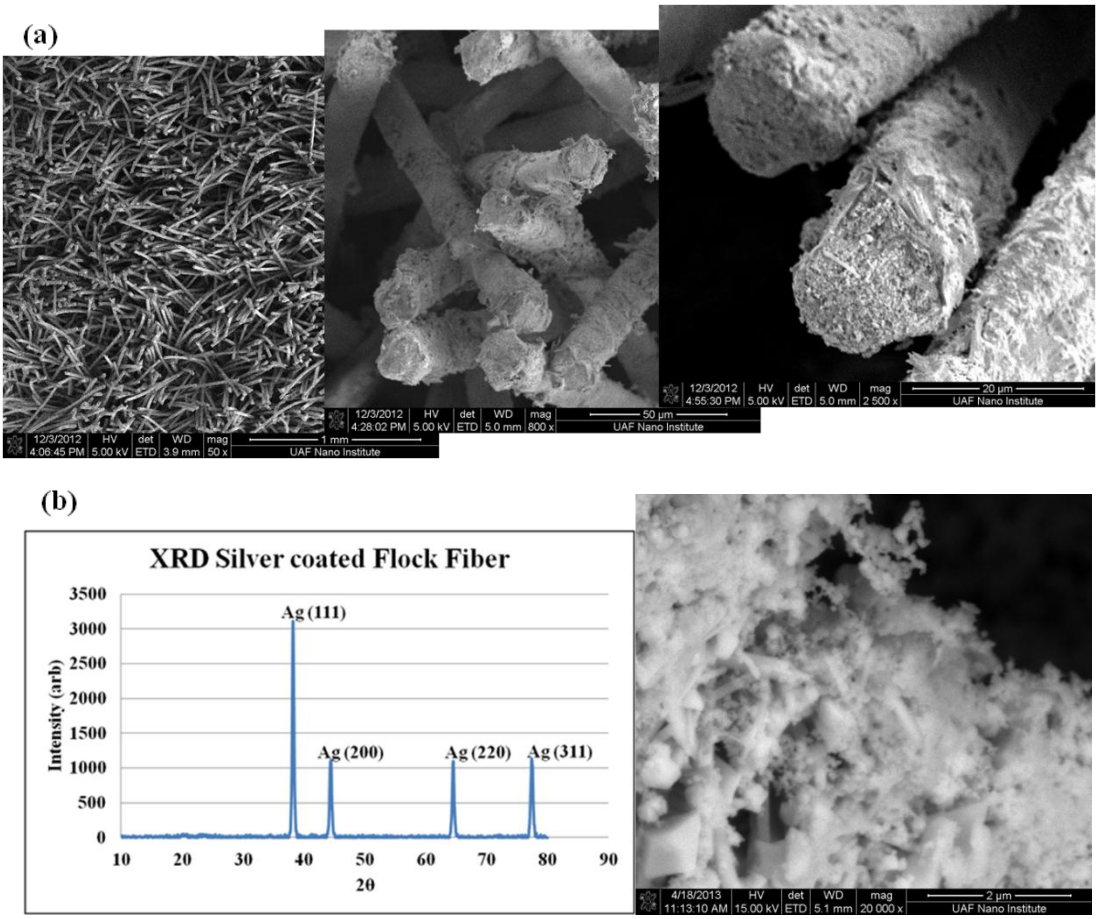

Figure 29: (a) SEM scans of silver flocked electrode with fiber dia. ~10µm. (b) XRD of silver coated flocked nylon fibers corresponding to face center cubic (fcc) silver

The silver film obtained from the electroless plating of the flocked fiber was analyzed for its morphology. The SEM scans in Figure 29(a) show flocked fibers (~10µm dia.) coated with silver nano-crystals. The XRD scan of metallized flocked fabric was identical to face

center cube (fcc) silver crystal structure. The crystal structures were also visible in the SEM scan of the flocked fabric (Figure 29(b)).

4.2 Optimization of fabrication process

The methodology for flocking of fibers on a fabric has been a well standardized industrial process, which was modified for flocking of the nanofibers. This study was aimed at rendering them electrically conductive towards application of these flocked fabrics as sensors. The process of electrical functionalization of the flocked fabric was optimized through different combinations of the process parameters (Section 3.1.2). The fabric samples were analyzed for electrical conductivity.

4.2.1 Conductive surface morphology

The experiment block for fabrication optimization was designed to accommodate for variation in parameters namely ink drying temperature, annealing temperature and annealing duration. The experiment blocks in Figure 30 (a and b) show a total of 32 combinations of the three design parameters. A sample from each combination was studied for grain size of silver nano-crystals that constitute the silver coated on the surface of the flock fibers. This is because the grain size is an important indicator of electrical conductivity of a thin film. The grain sizes were calculated form the peak values from XRD scan of respective samples using Sherrer's formula as shown in Figure 30.

(a)

Drying Temperature	Temperature for 30 minute annealing			
	25°C	120°C	160°C	200°C
25°C	24.2	24.65	27.15	27.4
45°C	25.94	26.51	27.54	30.26
65°C	28.89	31.04	29.37	**34.17**
100°C	30.32	27.35	27.36	30.05

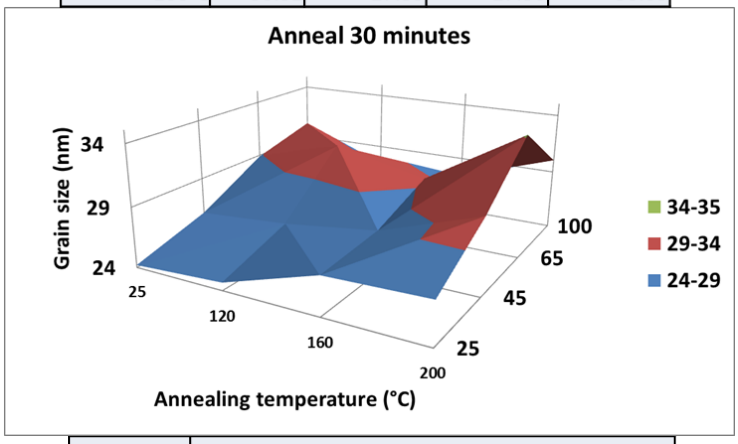

(b)

Drying temperature	Temperature for 1 hour annealing			
	25°C	120°C	160°C	200°C
25°C	24.2	24.17	31.85	33.22
45°C	25.94	27.92	29.59	30.86
65°C	28.89	29.67	29.4	**34.3**
100°C	30.32	29.95	30.43	30.44

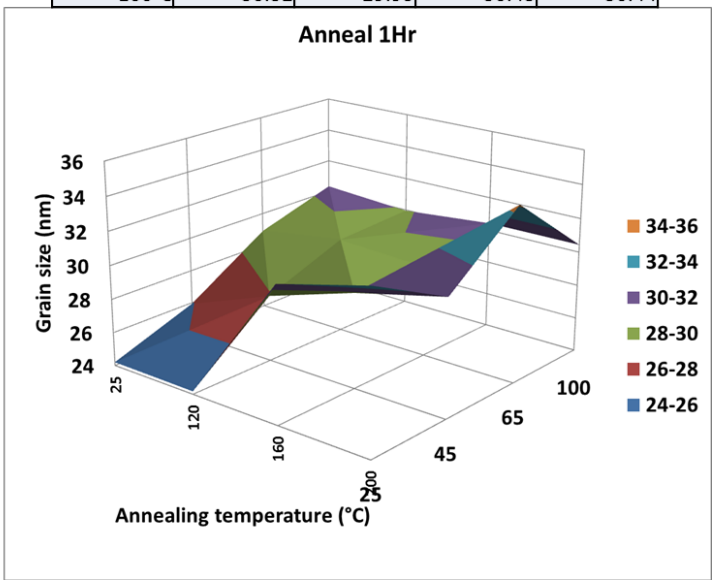

Figure 30: Grain sizes of silver nanoparticles obtained from processes with different drying temperature and annealing temperature for (a) 30 minutes annealing (b) 1hr annealing

Among the samples that were annealed for 30 minutes, the grain size increases with increase in ink drying temperature and annealing temperature (Figure 30 (a)). For samples that were not annealed the maximum grain size is achieved at drying temperature of 100°C. Upon introduction of the annealing step, the maximum grain sizes were observed at drying temperature of 65°C instead of 100°C. The maximum grain size was observed in the sample that was prepared by drying the silver ink at 65°C and annealing at 200°C.

The samples that were annealed for 60 minutes showed the same trend (Figure 30 (b)). The grain sizes for low drying temperatures (25°C and 45°C) increase as compared to the samples annealed at same temperatures for 30 minutes. However, the grain sizes did not increase significantly in case of high temperatures (65°C and 100°C).

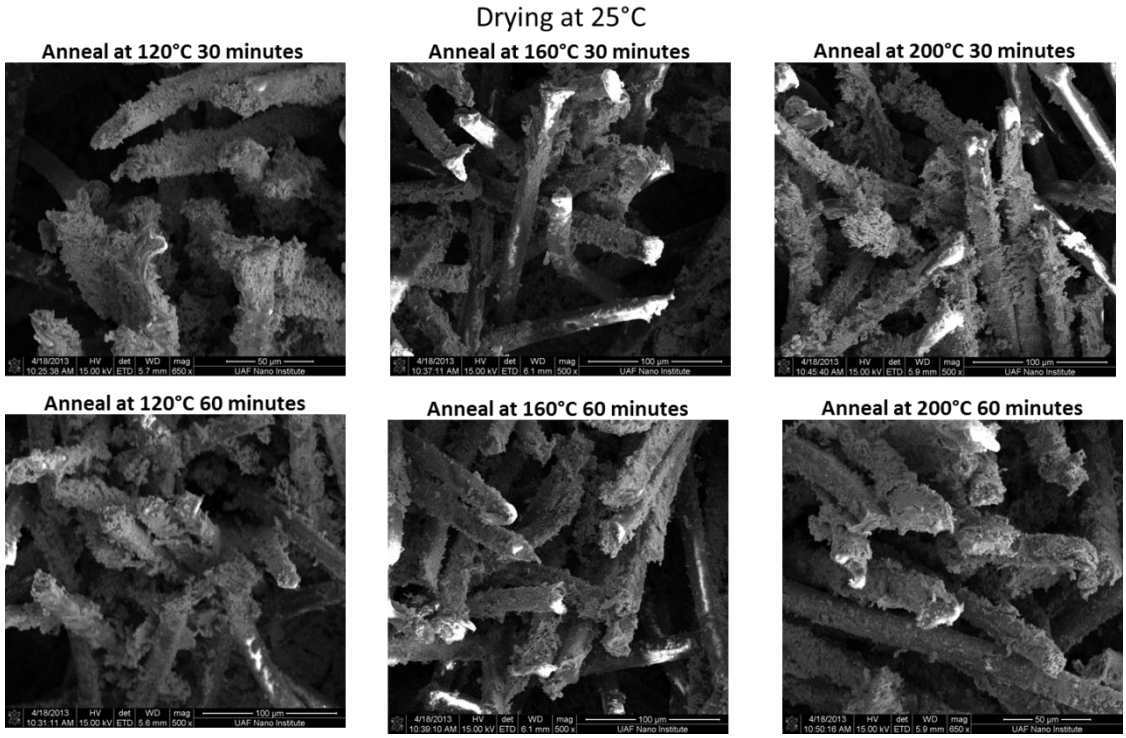

Figure 31: SEM scans of the samples dried at 25 °C and annealed at various temperatures and durations

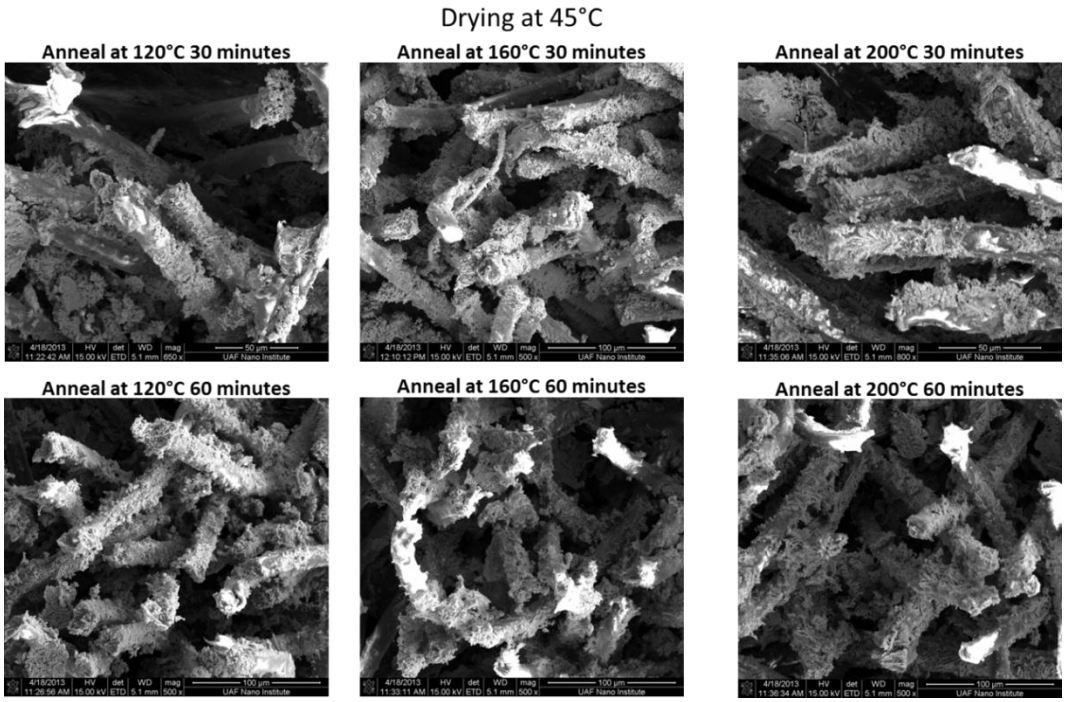

Figure 32: SEM scans of the samples dried at 45 °C and annealed at various temperatures and durations

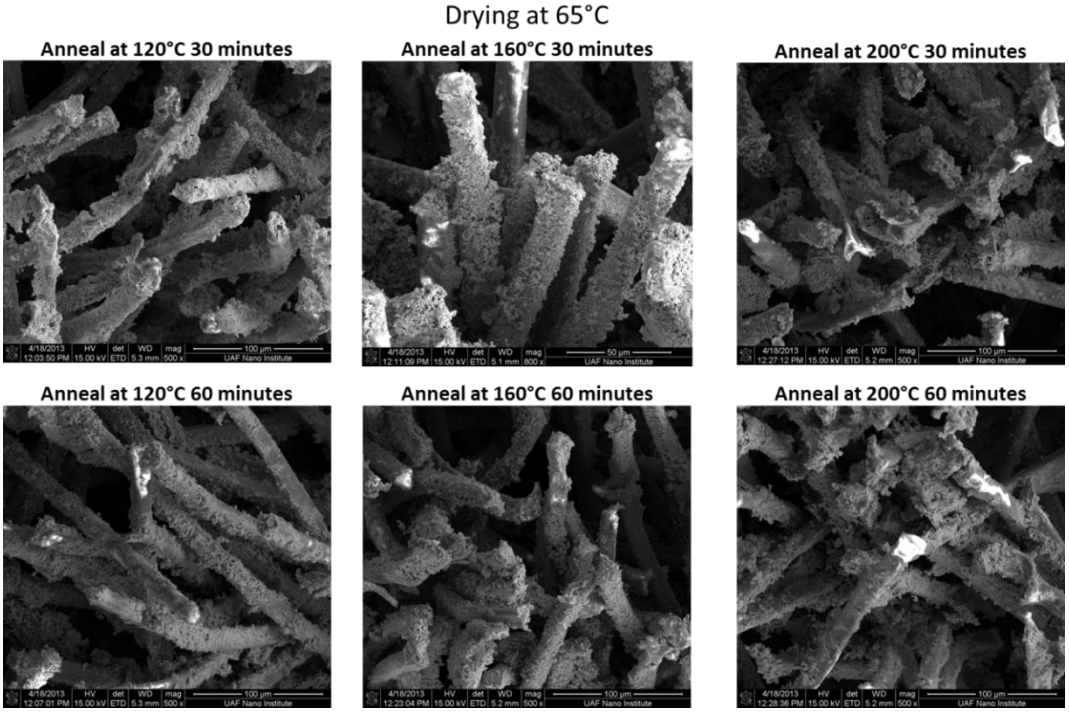

Figure 33: SEM scans of the samples dried at 65 °C and annealed at various temperatures and durations

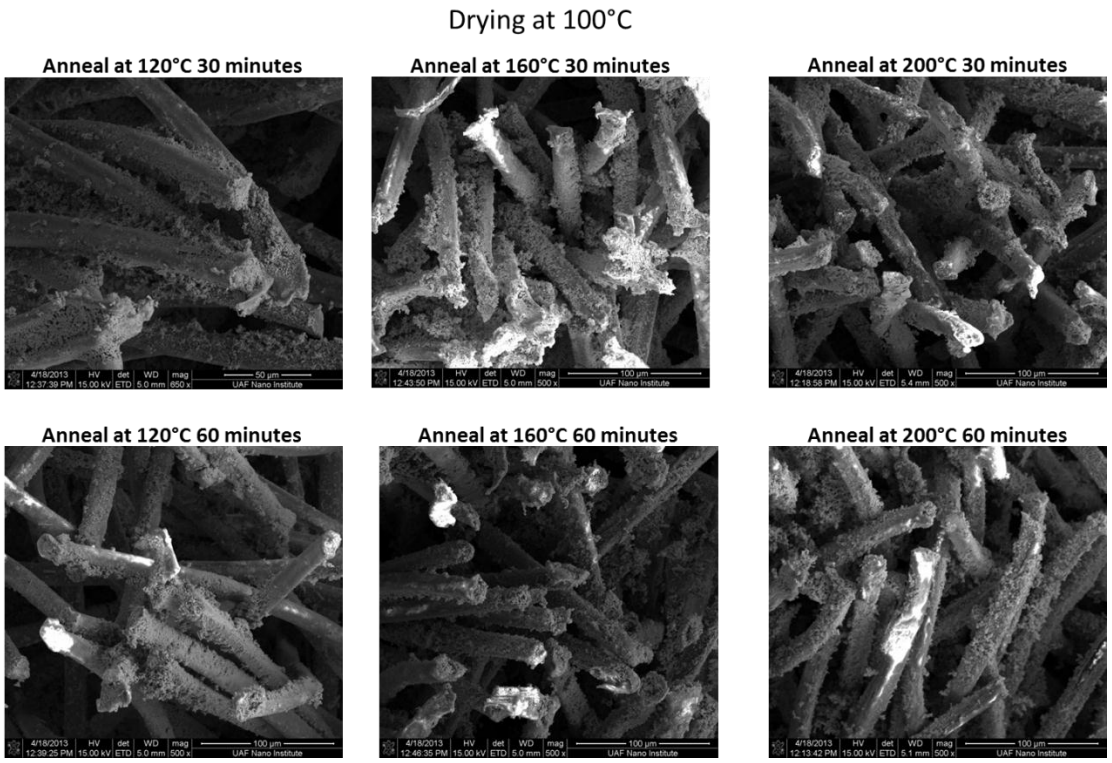

Figure 34: SEM scans of the samples dried at 100 °C and annealed at various temperatures and durations

The morphology of conductive layer of each sample was observed for thin film quality. The SEM scans in Figure 31 and32 show that the nano-silver crystal growth project away from the surface of the flock filament. This indicates that the drying was not complete at 25°C as well as 45°C, and crystal formation continued in the annealing stage. Such growth is mechanically weak (flaky).

The scans in Figures 33 and 34 show that the nano-silver crystal growth is concentrated on the surface of the flock filament. This indicates that at 65°C and 100°C the drying was complete. Since the annealing process is mainly for improving silver nano-crystal adhesion and grain size, there was no change in extent of silver nano-crystal coverage with change in

annealing temperature or duration. However, the scans in Figure 34 show that the extent of coverage reduces for samples dried at 100°C.

4.2.2 Electrical characterization of the conductive film

The electrical characterization of metallized sample was done to ensure complete coverage of the array of flock fibers as well as base of the fabric. This was done as two separate experiments by measurement of sheet resistance and the contact resistance of the sample. The sheet resistance is characteristic of the silver nano-crystal film covering the base fabric and the contact resistance is that of the silver nano-crystal film that covers the flock fibers.

Drying Temperature	Temperature for 30 minutes annealing Sheet resistance (mΩ/sq)			
	non	120°C	160°C	200°C
25°C	0.893 (1)	0.897 (2)	0.901 (3)	0.88 (4)
45°C	0.877 (5)	0.868 (6)	0.906 (7)	0.886 (8)
65°C	0.876 (9)	0.83 (10)	0.859 (11)	0.847 (12)
100°C	0.836 (13)	0.839 (14)	0.852 (15)	0.784 (16)

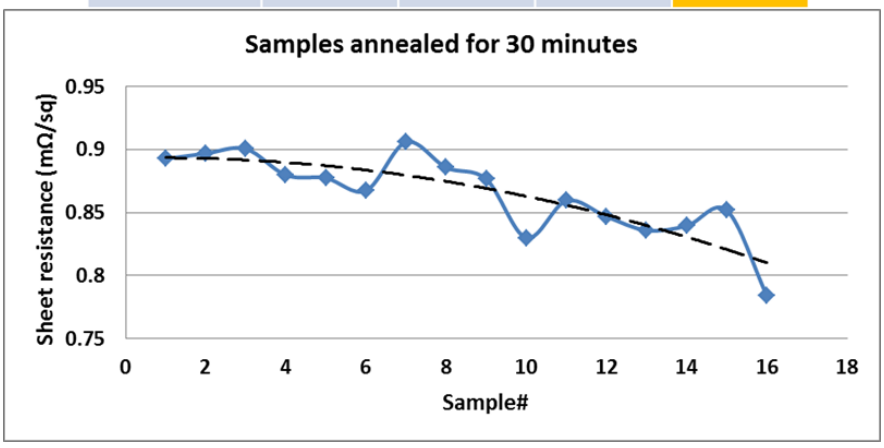

Figure 35: Variations in sheet resistance of flock electrode samples fabricated using different drying temperatures and different temperatures for 30 minute annealing process

The sheet resistance measurement of samples decreased with the increase in drying temperature and annealing temperature (Figure 35 and 36). The sheet resistance values show a general downward trend. There was no significant reduction in sheet resistance values due to increase in the duration of annealing.

Drying Temperature	Temperature for 1 hour annealing Sheet resistance (mΩ/sq)			
	non	120°C	160°C	200°C
25°C	0.946 (1)	0.918 (2)	0.834 (3)	0.858 (4)
45°C	0.877 (5)	0.896 (6)	0.861 (7)	0.768 (8)
65°C	0.876 (9)	0.856 (10)	0.883 (11)	0.747 (12)
100°C	0.836 (13)	0.794 (14)	0.831 (15)	0.792 (16)

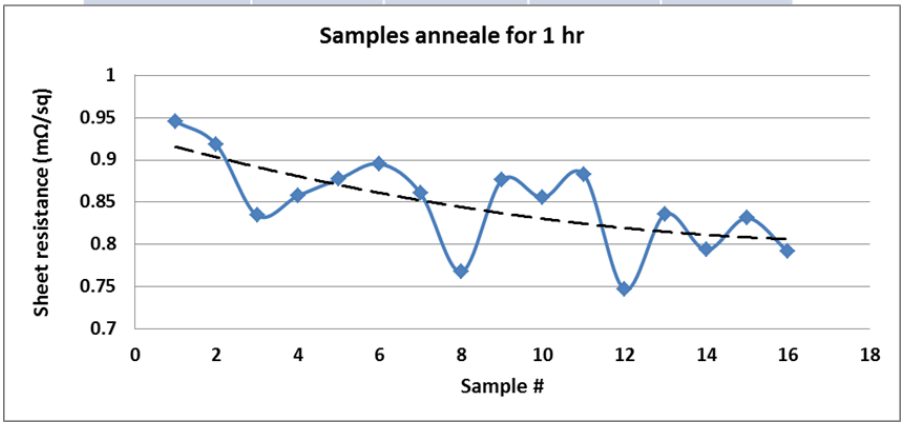

Figure 36: Variations in sheet resistance of flock electrode samples fabricated using different drying temperatures and different temperatures for 60 minute annealing process

TABLE 5: Parameters of the equivalent circuit fitted to contact impedance data for electrode-gel phantom interface. The samples were annealed for 30 minutes.

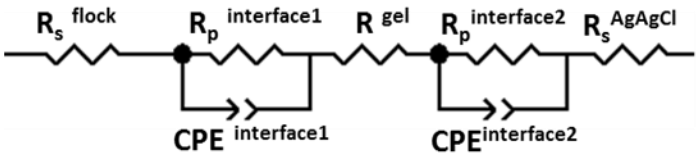

	Rs (Ω)	CPE-T (F)	CPE-P	Rp (Ω)
Dry at 25 °C				
No Annealing	1388	1.17E-05	0.51435	101310
Anneal at 120°C for 30 minutes	589.6	0.000127	0.73593	48565
Anneal at 160°C for 30 minutes	348.4	0.000136	0.79774	34711
Anneal at 200°C for 30 minutes	409.6	0.000121	0.71302	5490
Dry at 45 °C				
No Annealing	265.3	0.000164	0.76984	10974
Anneal at 120°C for 30 minutes	318.4	0.000859	0.58133	3091
Anneal at 160°C for 30 minutes	310.2	0.000905	0.65078	2699
Anneal at 200°C for 30 minutes	242.4	0.000937	0.80508	1599
Dry at 65 °C				
No Annealing	320.2	0.000441	0.70731	11097
Anneal at 120°C for 30 minutes	248.7	0.000658	0.82707	6663
Anneal at 160°C for 30 minutes	231	0.000289	0.70517	1453
Anneal at 200°C for 30 minutes	197.3	0.001433	0.66745	2177
Dry at 100 °C				
No Annealing	199.2	0.000315	0.76325	9331
Anneal at 120°C for 30 minutes	263	0.000506	0.64106	2492
Anneal at 160°C for 30 minutes	255.6	0.001091	0.64651	5123
Anneal at 200°C for 30 minutes	277	0.001704	0.47054	10228
AgAgCl –gel phantom	433	0.002082	0.51546	330.7

Contact resistance of the samples was considered as a combination of contact resistances of the flock electrode-gel phantom interface and the Ag/AgCl-gel phantom interface. The impedance data was fit to an equivalent electrical circuit with impedance elements accounting for the electrode R_s^{flock}, flock-gel interface $R_p^{interface1}$ and $CPE^{interface1}$, gel phantom R^{gel}, Ag/AgCl-gel interface $R_p^{interface2}$ and $CPE^{interface2}$, and Ag/AgCl electrode $R_s^{Ag/AgCl}$. The Ag/AgCl-gel phantom impedance was calculated separately and plugged in as fixed parameters. The parameters pertaining to the flock electrode were estimated by using the least square fit for

each sample (TABLE 5 and 6). The expression for polarizable capacitive element CPE impedance is $Z_{CPE} = \left(T(i\omega)^P\right)^{-1}$ where magnitude T and phase P are the relevant parameters. The resistive elements of the electrode and the electrode-gel phantom interface decrease with increase in drying and annealing temperature. The CPE parameter T increases with drying and annealing temperature. The CPE parameter P showed minimal variance and stayed between 0.6 and 0.8.

TABLE 6: Parameters of the equivalent circuit fitted to contact impedance data for electrode-gel phantom interface. The samples were annealed for 60 minutes.

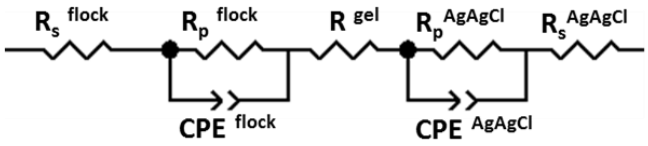

	Rs (Ω)	CPE-T (F)	CPE-P	Rp (Ω)
Dry at 25 °C				
No Annealing	1388	1.17E-05	0.51435	101310
Anneal at 120°C for 60 minutes	461	0.000169	0.75182	8223
Anneal at 160°C for 60 minutes	356.7	0.000511	0.70896	6338
Anneal at 200°C for 60 minutes	477.4	0.000214	0.690033	5453
Dry at 45 °C				
No Annealing	265.3	0.000164	0.76984	10974
Anneal at 120°C for 60 minutes	303.3	0.000676	0.64149	1417
Anneal at 160°C for 60 minutes	323.7	0.000495	0.68882	1325
Anneal at 200°C for 60 minutes	295	0.000854	0.63071	1495
Dry at 65 °C				
No Annealing	320.2	0.000441	0.70731	11097
Anneal at 120°C for 60 minutes	276.8	0.000564	0.58215	2373
Anneal at 160°C for 60 minutes	289.2	0.000321	0.7023	1505
Anneal at 200°C for 60 minutes	209.8	0.003601	0.56101	2525
Dry at 100 °C				
No Annealing	199.2	0.000315	0.76325	9331
Anneal at 120°C for 60 minutes	213.9	0.000418	0.64693	2155
Anneal at 160°C for 60 minutes	261.4	0.001414	0.61632	6284
Anneal at 200°C for 60 minutes	260.5	0.001416	0.60226	7053
AgAgCl –gel phantom	755.2	0.000591	0.59396	427.7

4.3 Conductive film sturdiness against abrasion and washing

The samples were tested for endurance to abrasion under wet and dry conditions to assess the effects of process parameters on sturdiness of the conductive films. Sheet resistance and contact resistance were measured from the samples after conducting the prescribed abrasion (Section 3.2). The sheet resistance showed no significant variations due to abrasion and remained close to a mean value of 0.8mΩ/sq (Figure 37-40). The observation was consistent for samples annealed for 30 minutes and 60 minutes.

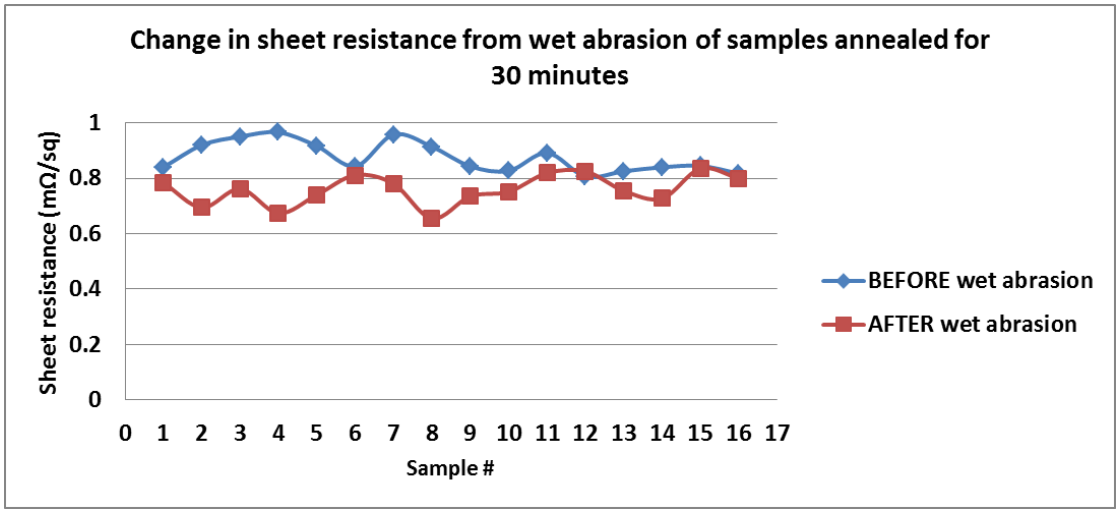

Figure 37: Sheet resistance before and after abrasion under wet conditions of samples fabricated through various temperatures for drying and 30 minutes annealing cycle. The numbering corresponds to the table shown in Figure 35.

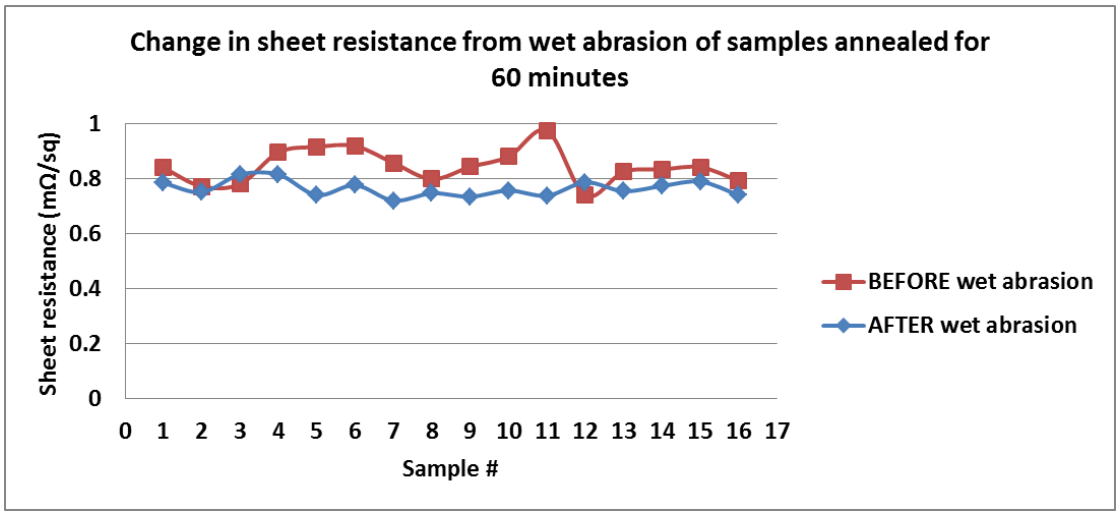

Figure 38: Sheet resistance before and after abrasion under wet conditions of samples fabricated through various temperatures for drying and 60 minutes annealing cycle. The numbering corresponds to the table shown in Figure 36.

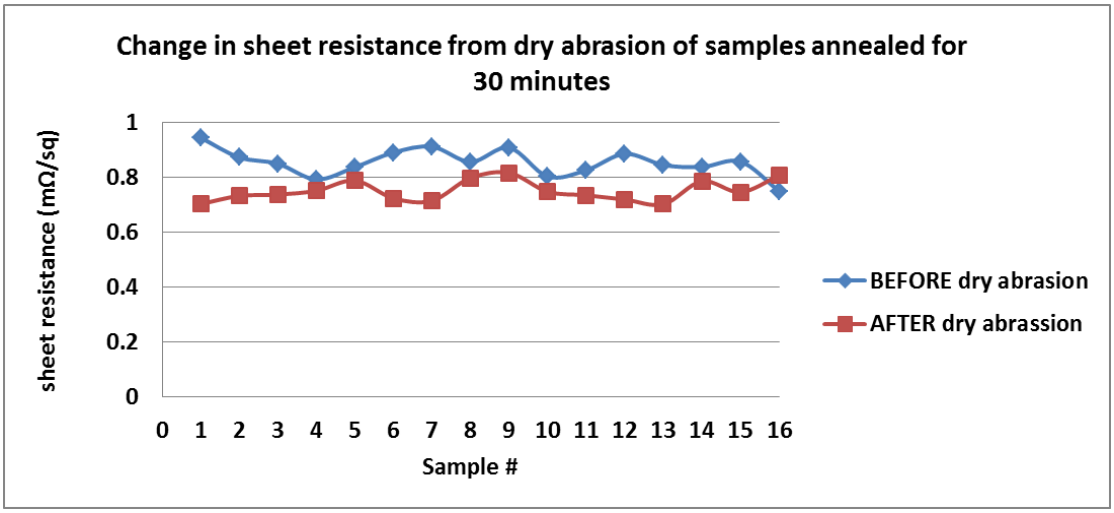

Figure 39: Sheet resistance before and after abrasion under dry conditions of samples fabricated through various temperatures for drying and 30 minutes annealing cycle. The numbering corresponds to the table shown in Figure 35.

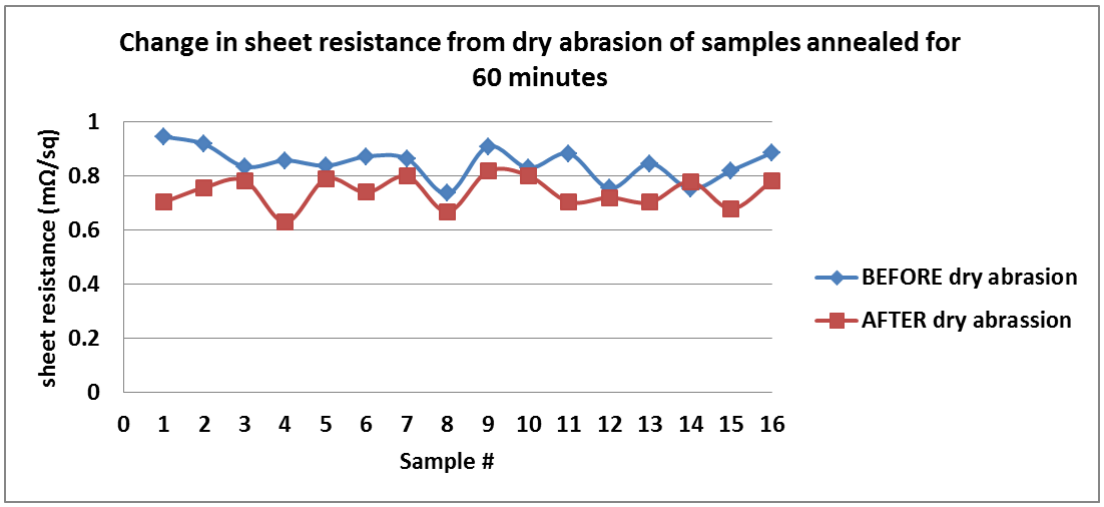

Figure 40: Sheet resistance before and after abrasion under dry conditions of samples fabricated through various temperatures for drying and 60 minutes annealing cycle. The numbering corresponds to the table shown in Figure 36.

Contact impedance measurements of samples were observed for change in characteristics of the equivalent circuit for the impedance data. It was observed that the impedance values increased after abrasion. It increase more for samples subjected to dry abrasion (Figure 42) as compared to those subject to wet abrasion (Figure 41). The characteristics of the equivalent (model) circuit changed in both cases. A parallel RC component was added to the equivalent (model) circuit for impedance after abrasion. This element was assigned to the flock electrode. The addition of the new RC couple in the circuit is also concurrent with shift in the phase curve (theta vs. Frequency) of the impedance data after abrasion.

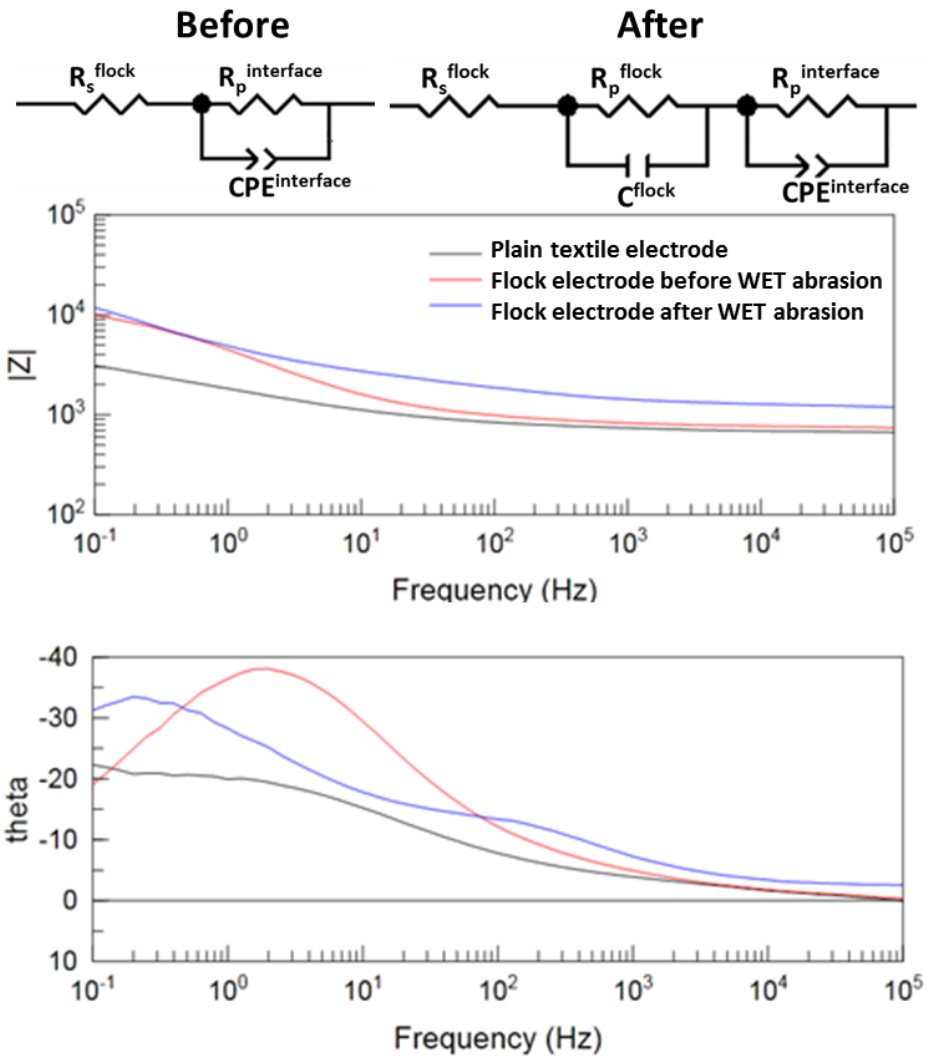

Figure 41: Contact impedance measurement before and after wet abrasion along with the equivalent (model) circuit for both cases.

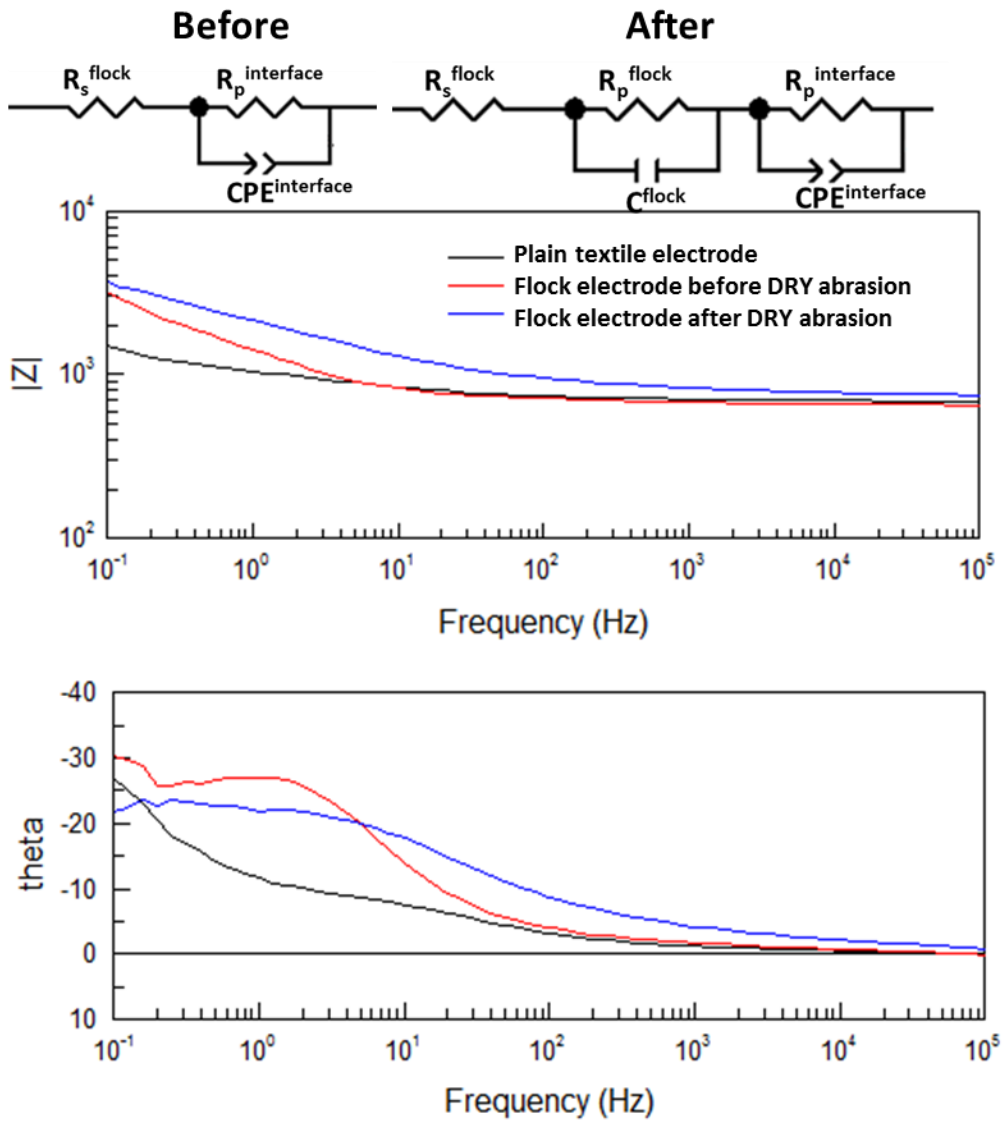

Figure 42: Contact impedance measurement before and after dry abrasion along with the equivalent (model) circuit for both cases.

The impedance data obtained from wash testing showed that the impedance rose steadily over successive wash cycles. The sheet resistance rose from 0.7-0.8mΩ/sq. to 50Ω/sq. and above (Figure 43). This observation indicates that the electrodes have lost the conductive film.

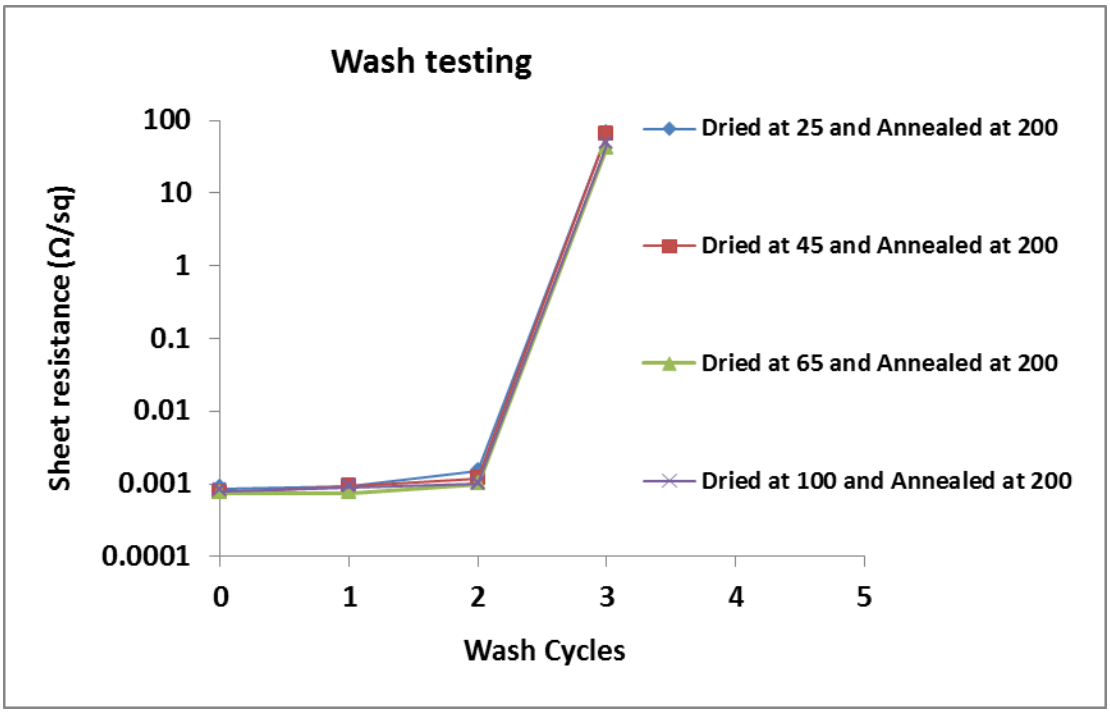

Figure 43: Impedance data from wash testing: (a) sheet resistance (b) contact resistance

4.4 Hierarchically structured textile based electrodes: Nanostructured flock and metallization

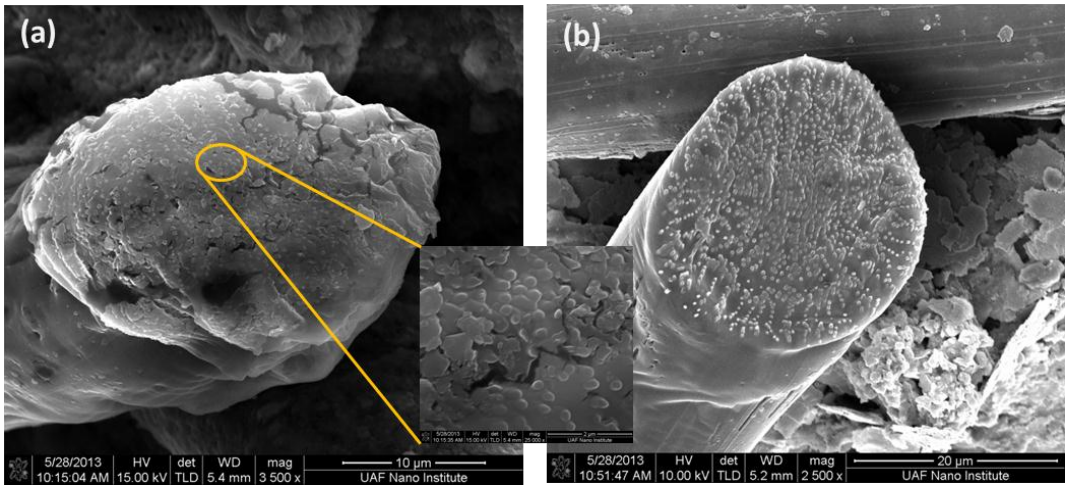

Figure 44: Polylactic acid nanocomposite fiber made of 1500 polypropylene nanofibers (dia. <200nm) in a matrix (sea) of polylactic acid: (a) nanocomposite fiber cross-section with nanofibers visible in the inset (b) polylactic acid dissolved to release the embedded nanofibers

The fibers of [polypropylene island in polylactic acid sea] nanocomposite yarn were flocked on the base fabric. The process was similar to that of microflock because the fibers were still of micrometer scale. A flock of these fibers was obtained on fabric. The embedded polypropylene nanofibers (Figure 44 (a)) were released by dissolving the polylactic acid matrix in warm 5% NaOH. The micro pillar was rendered nanostructured (Figure 44 (b)), which forms the basic element of the hierarchically structured textile based electrode.

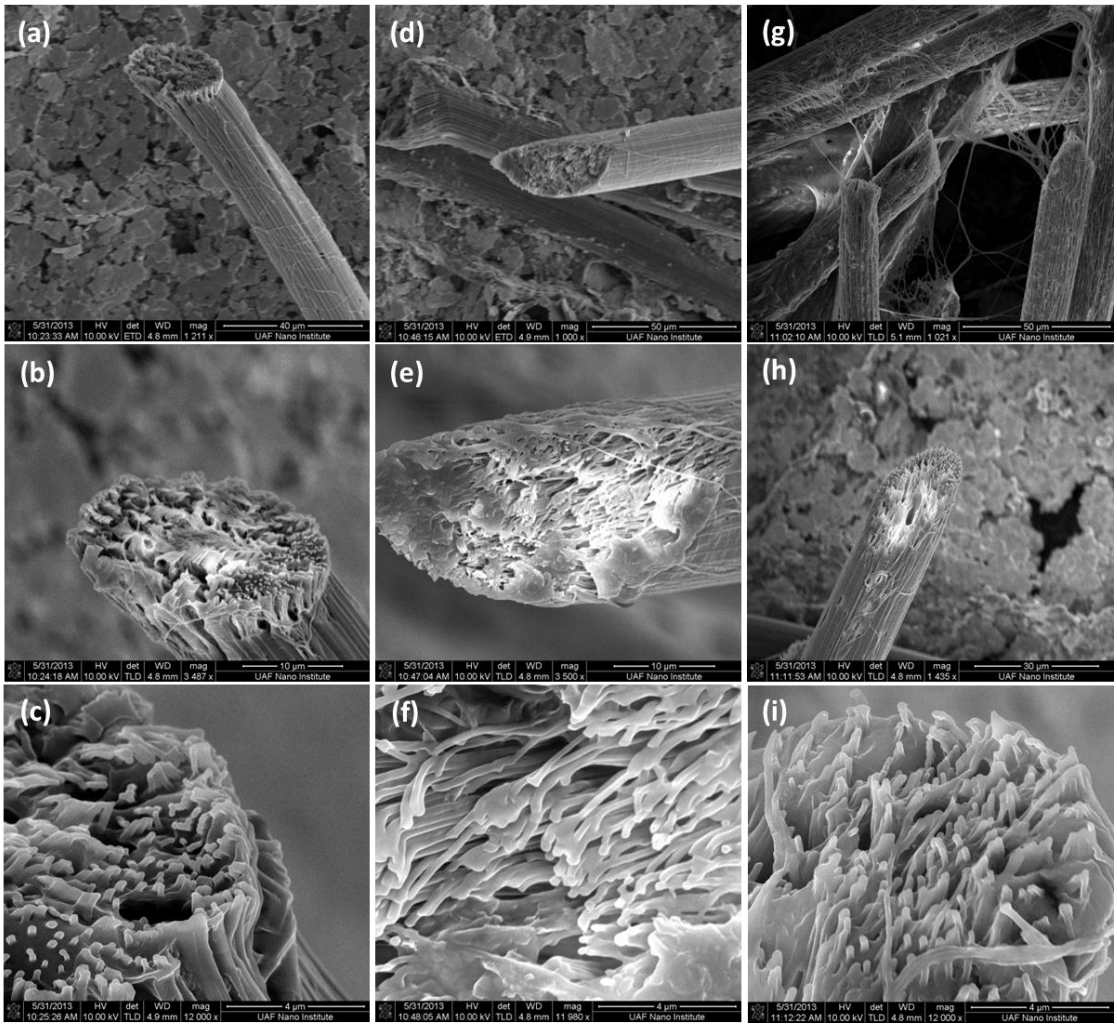

Figure 45: Etching off the polylactic acid to release nanofibers using warm 5% NaOH solution: (a)-(c) etching for 5 minutes, (d)-(f) etching for 10 minutes, (g)-(i) etching for 30 minutes

Nanotextured structures with free standing nanofibers at the crown were obtained by optimizing the NaOH assisted etching process. Samples with [polypropylene island in polylactic acid sea] nanocomposite flock were treated with 5% NaOH at 50°C for duration of 5, 10 and 30 minutes. The SEM scans of these samples showed the extent of dissolution of polylactic acid and release of nanofibers (Figure 45). After 5 minutes of treatment with NaOH, the nanofibers started to appear but were still clumped together (Figure 45 (a)-(c)). After 10 minutes, free standing nanofibers appear (Figure 45 (d)-(f)). After treatment for 30 minutes the polylactic acid matrix was dissolved to the extent that the nanofibers at the circumference were completely released and were seen collapsed on the fabric base because of their inherent tension (Figure 45 (g)-(i)).

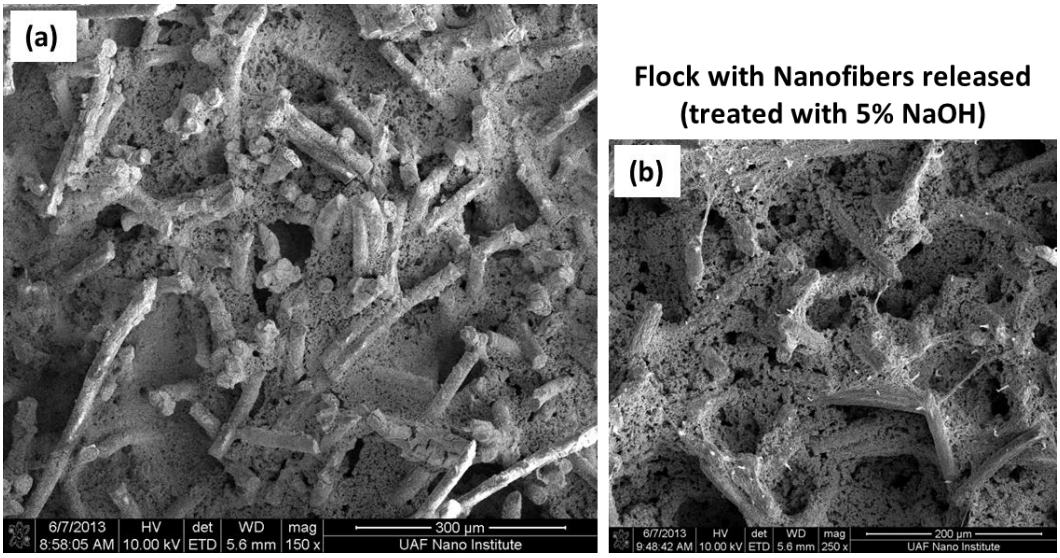

Figure 46: Evolution of the hierarchical structure: The micro pillars (a) treated with 5% NaOH to etch off the polylactic acid matrix polymer to expose embedded nanofibers rendering the micro pillars nanotextured (b)

The flock samples treated for more than 10 minutes, resulted in micro pillars of [polypropylene island in polylactic acid sea] nanocomposite microfibers with free standing nanofibers on their crown and flattened nanofibers on the based fabric (Figure 46). Hence, the flock samples were rendered nanostructured. The samples, metallized with silver, were observed under SEM to confirm uniform coverage of free standing nanofibers with silver nano-crystal layer (Figure 47).

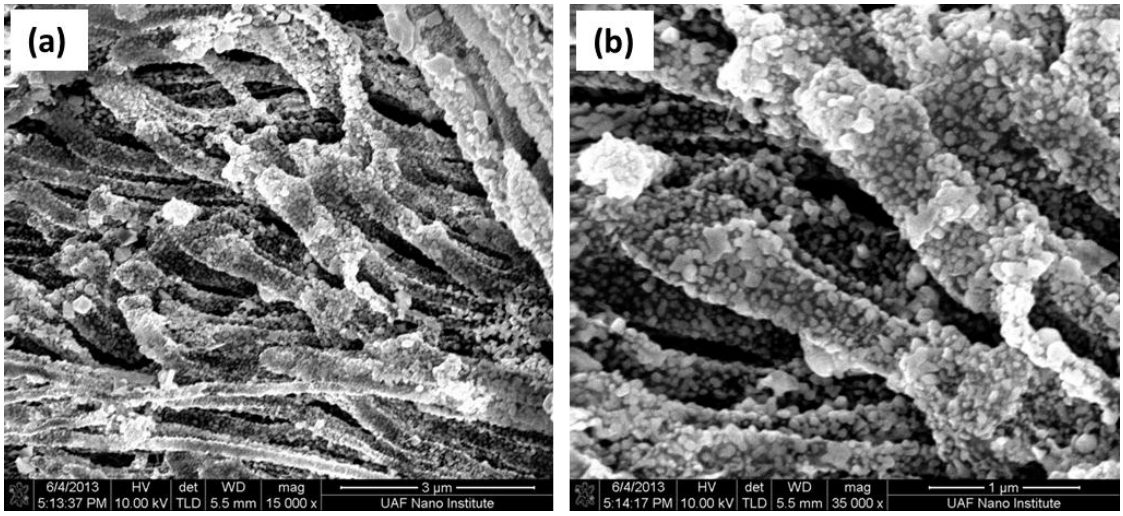

Figure 47: Nanofibers coated with silver nanoparticles

The metallized hierarchically structured fabric was tested as an electrode for contact resistance with agar gel based tissue phantom. The impedance data shows that magnitude of impedance of electrode with nanotextured flock was better than that with Microflock. Both the electrodes were better than plain electrode (Figure 48). The impedance data was fitted to equivalent (model) circuit depicted in TABLE 5 and 6. The circuit parameters obtained from model fitting indicate that the resistive element of the electrode (R_s) and resistive element of the electrode-gel interface (R_p) confirm with the trend. The polarizable capacitive element of the

interface (CPE-T, CPE-P) shows a higher P value for both flocked electrodes as compared to plain textile electrode.

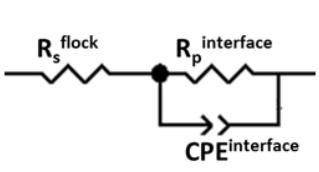

Electrode Type	Rs (Ω)	Rp (Ω)	CPE-T (F)	CPE-P
Plain textile	114.5	6828	0.000157	0.51148
Microflock	208	5618	0.000517	0.82861
Nanoflock	70	3572	0.000294	0.70538

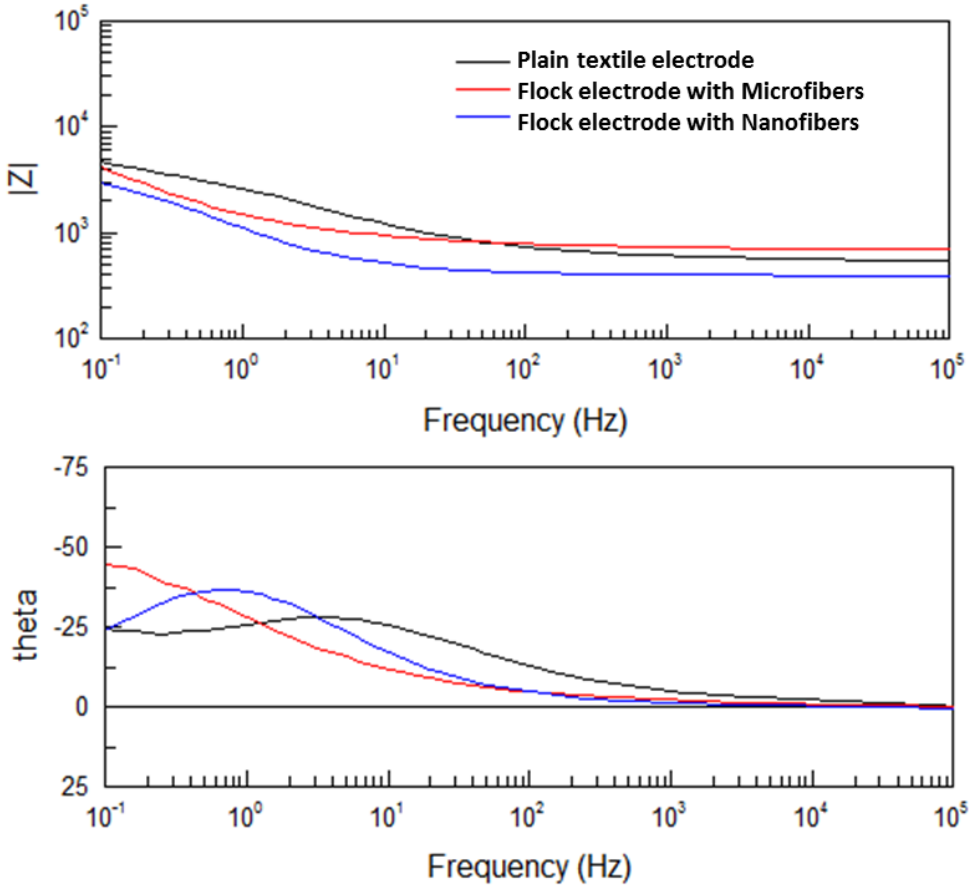

Figure 48: Comparison of contact impedance of textile based electrodes with different surface characteristics: nanotextured flock, micro flock and plain textile electrodes

4.5 Effects of conductive hybrid textile based nanostructures on signal flow through electrode-gel tissue phantom interface

The simulation was set up as described in section 3.3.2. The boundary shared by agar gel based phantom and the electrode was defined with continuity of normal current density and

contact impedance condition. The parameters electrical conductivity (σ) and relative permittivity (ε_r), current density and applied voltage were used from the contact impedance experiments done for each type of textile based electrode. The current vector distribution over the face of textile electrodes has been shown for plain textile electrode in Figure 49, microflock electrode in Figure 50 and nanostructured electrode in Figure 51. The results were visually examined for a qualitative evaluation of current vector. The current vector over the face of plain textile electrode was directed at angle instead of pointing downwards, which indicated that the current vector had comparable vertical as well as horizontal components. The current vector over the face of microflock electrode was pointing down with a slight tilt, which indicated that the current had a predominantly vertical component.

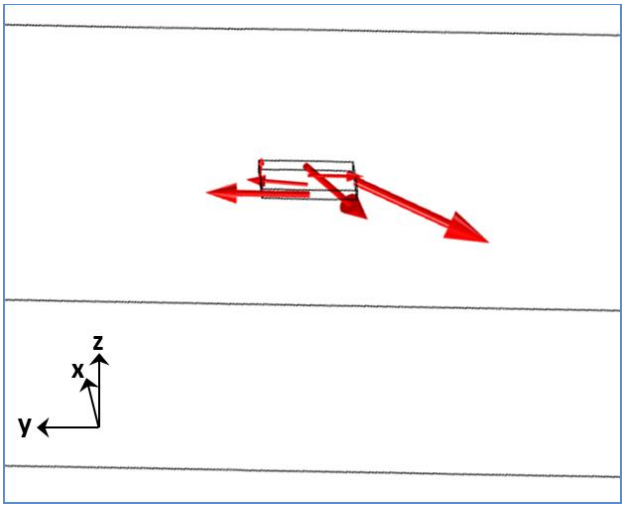

Figure 49: Current vector for plain textile electrode in contact with agar gel based tissue phantom with applied voltage of 10mV and current density obtained from the contact impedance experiments

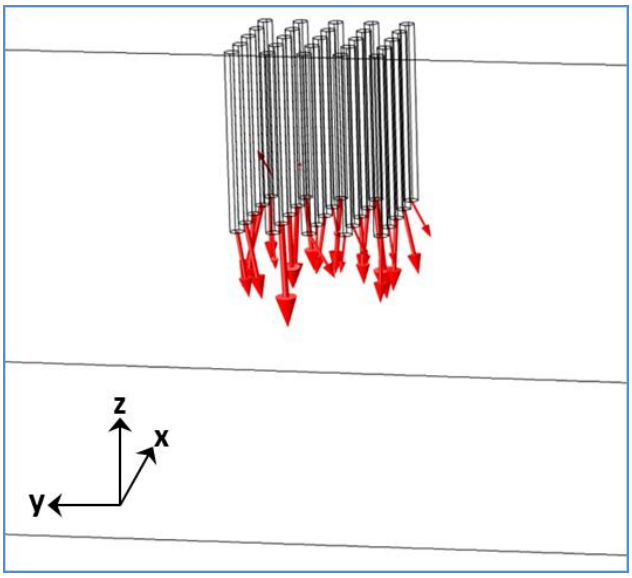

Figure 50: Current vector for microstructure textile electrode in contact with agar gel based tissue phantom with applied voltage of 10mV and current density obtained from the contact impedance experiments

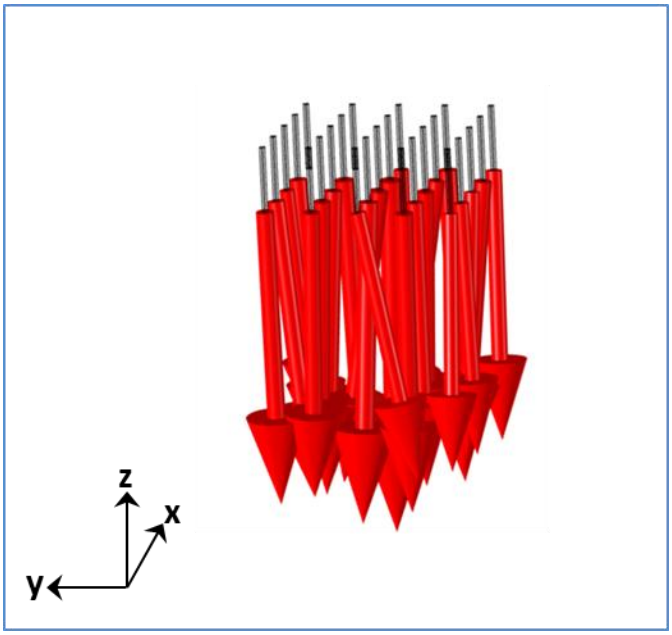

Figure 51: Current vector for plain textile electrode in contact with an agar gel based tissue phantom with applied voltage of 10mV and current density obtained from the contact impedance experiments

4.6 Characterization of electrical contact made between electrode and skin

All three types of textile electrodes- plain, micro Flock and nano Flock- were tested in a 2 electrode configuration on forearm of 5 subjects. The impedance data was fitted to the equivalent (model) circuit shown in Figure 48. TABLE 7-9 shows the circuit parameters for plain, micro Flock and nano Flock textile electrode respectively. TABLE 10 shows the circuit parameters for Ag/AgCl gel electrode, which were considered gold standard for this study.

The circuit elements, of dry textile based electrodes, corresponding to the electrode-skin interface (Rp, CPE-T and CPE-P) showed a greater dependence on the moisture level of the skin. For dry skin, the resistance Rp of micro and nano Flock electrodes was more than that of the plain textile electrode. For moist skin, Rp of micro and nano Flock electrodes was less than that of the plain textile electrode. The T parameter of polarizable capacitive element CPE for dry textile electrodes was greater than that of the Ag/AgCl gel electrode. Among the dry electrodes, the T parameter values were almost similar for all three types when the measurement was done on subjects with moist skin. In case of subjects with dry skin the T parameter for the micro and nano Flock textile electrodes was greater than the plain textile electrode. The P parameter of all three types of dry electrodes increased in case of dry skin. In comparison the P parameter for Ag/AgCl gel electrodes was unchanged.

TABLE 7: Contact impedance of plain electrode and forearm skin interface of 5 test subjects

			Plain			
Subject	Age	Skin moisture	Rs (Ω)	Rp (Ω)	CPE-T (F)	CPE-P
1	26	very dry	350.8	3.45E+07	1.10E-09	0.93248
2	35	moist	124.7	437800	7.01E-08	0.84311
3	30	dry	353	3.11E+07	1.18E-09	0.93087
4	35	moist	107.6	152600	2.54E-07	0.75163
5	65	moist	170.3	781500	1.62E-07	0.73637

TABLE 8: Contact impedance of micro flock electrode and forearm skin interface of 5 test subjects

			micro Flock			
Subject	Age	Skin moisture	Rs (Ω)	Rp (Ω)	CPE-T (F)	CPE-P
1	26	very dry	350.8	5.68E+07	5.11E-10	0.91782
2	35	moist	29.45	943750	6.28E-08	0.6695
3	30	dry	353	4.94E+07	5.51E-10	0.91301
4	35	moist	127	105970	4.85E-07	0.74831
5	65	moist	310	738850	1.45E-07	0.74995

TABLE 9: Contact impedance of interface between nano flock electrode and forearm skin of 5 test subjects

			nano Flock			
Subject	Age	Skin moisture	Rs (Ω)	Rp (Ω)	CPE-T (F)	CPE-P
1	26	very dry	13.23	6.96E+07	4.38E-10	0.93976
2	35	moist	30.45	814510	4.82E-08	0.70059
3	30	dry	13.23	6.96E+07	4.38E-10	0.93976
4	35	moist	79.34	119140	3.84E-07	0.80253
5	65	moist	245.9	383880	1.41E-07	0.75271

TABLE 10: Contact impedance of silver-silver chloride electrode and forearm skin interface of 5 test subjects

			AgAgCl			
Subject	Age	Skin moisture	Rs (Ω)	Rp (Ω)	CPE-T (F)	CPE-P
1	26	very dry	428.4	2.81E+06	4.49E-08	0.87934
2	35	moist	372.9	2.73E+06	9.46E-08	0.86065
3	30	dry	428.4	2.81E+06	4.49E-08	0.87934
4	35	moist	469.8	121210	4.90E-08	0.86218
5	65	moist	317	3.93E+05	4.49E-08	0.86308

Figure 52 shows a comparison between the magnitudes of impedance of Ag/AgCl gel electrode and various textile based electrodes as a function of frequency. Although the

magnitudes were similar at higher frequencies, a discernible difference between the magnitudes could be seen at lower frequencies.

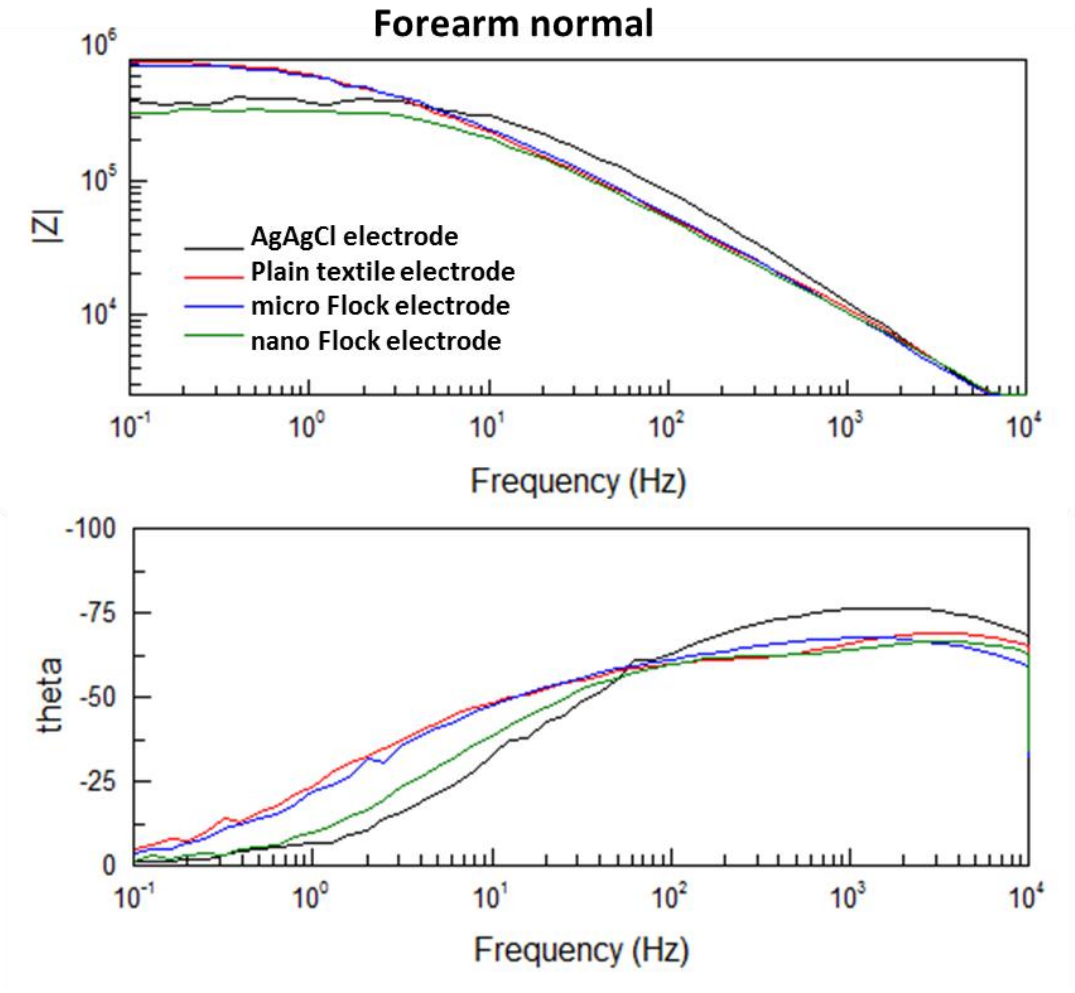

Figure 52: Impedance scan of textile based electrodes placed on forearm in a 2-electrode configuration.

The impedance data of concentric ring electrodes in 3-electrode configuration were obtained at forearm, leg, forehead and sternum of the subjects. The impedance scans covered the frequency range that includes electrophysiological signals encountered in medical diagnostics. The frequency range of 0.1Hz to 10kHz was set to include Electrocardiography signal (0.1 to

250Hz) [106], Electroencephalography signal (0.1 to 100Hz) [107], Electrooculography signal (0.1 to 10Hz) [108], Electromyography signal (50 to 3000Hz) [109], Electronic Impedance based Tomography and Plethysmography (10Hz to 5kHz) [110]. The impedance data were compared based on the magnitude of impedance and phase as functions of frequency. The analysis of impedance data from all the 5 subjects was done and only general trends have been mentioned here. The following figures are examples of the variation in the impedance for all the types of textile electrodes at different position on the body.

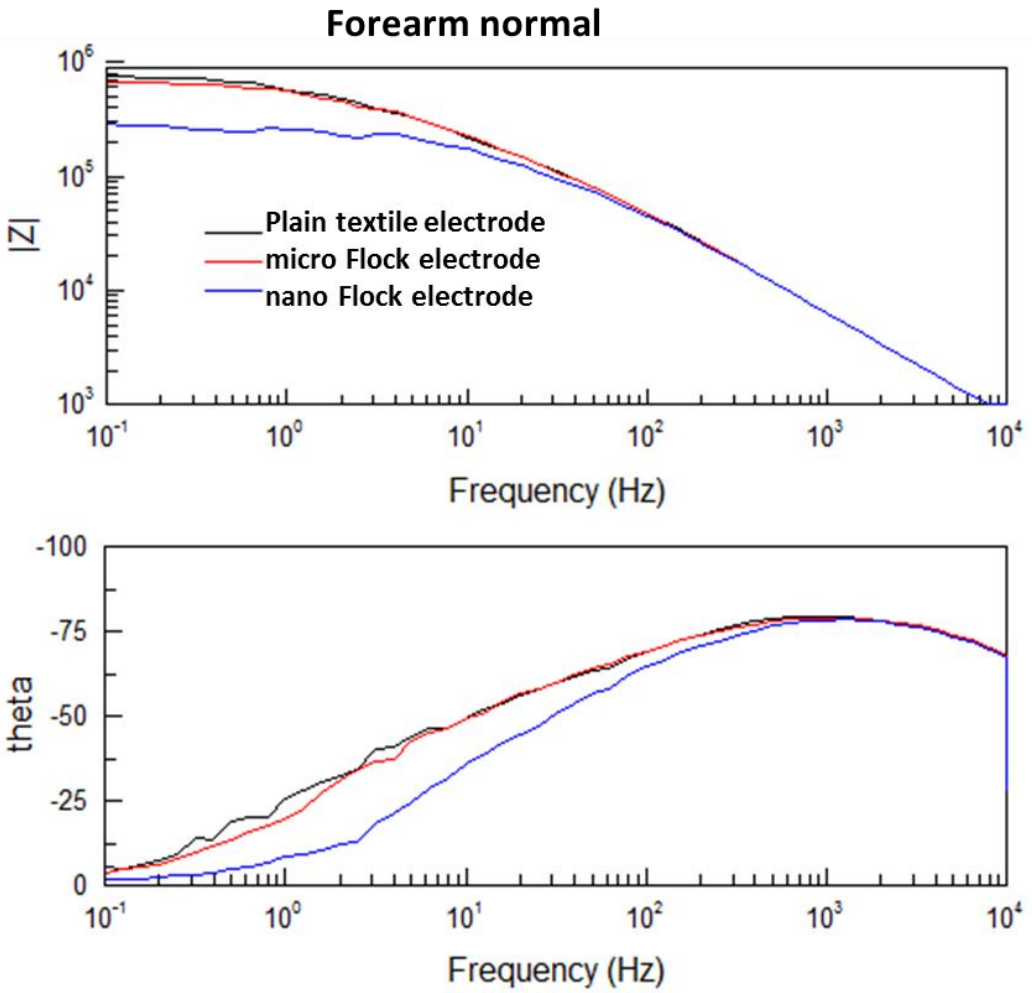

Figure 53: Impedance data from various types of textile based Concentric Ring Electrodes placed on forearm in 3-electrode configuration when subjects were in normal (non-sweaty) condition

The comparison of between the impedance data of the textile based concentric ring electrodes placed on the forearm showed that the nano Flock textile electrode had the least contact impedance (Figure 53). The phase curves of plain and micro Flock textile electrodes were same. The phase curve of nano Flock textile electrode was different except for the peak around 1kHz (Figure 53).

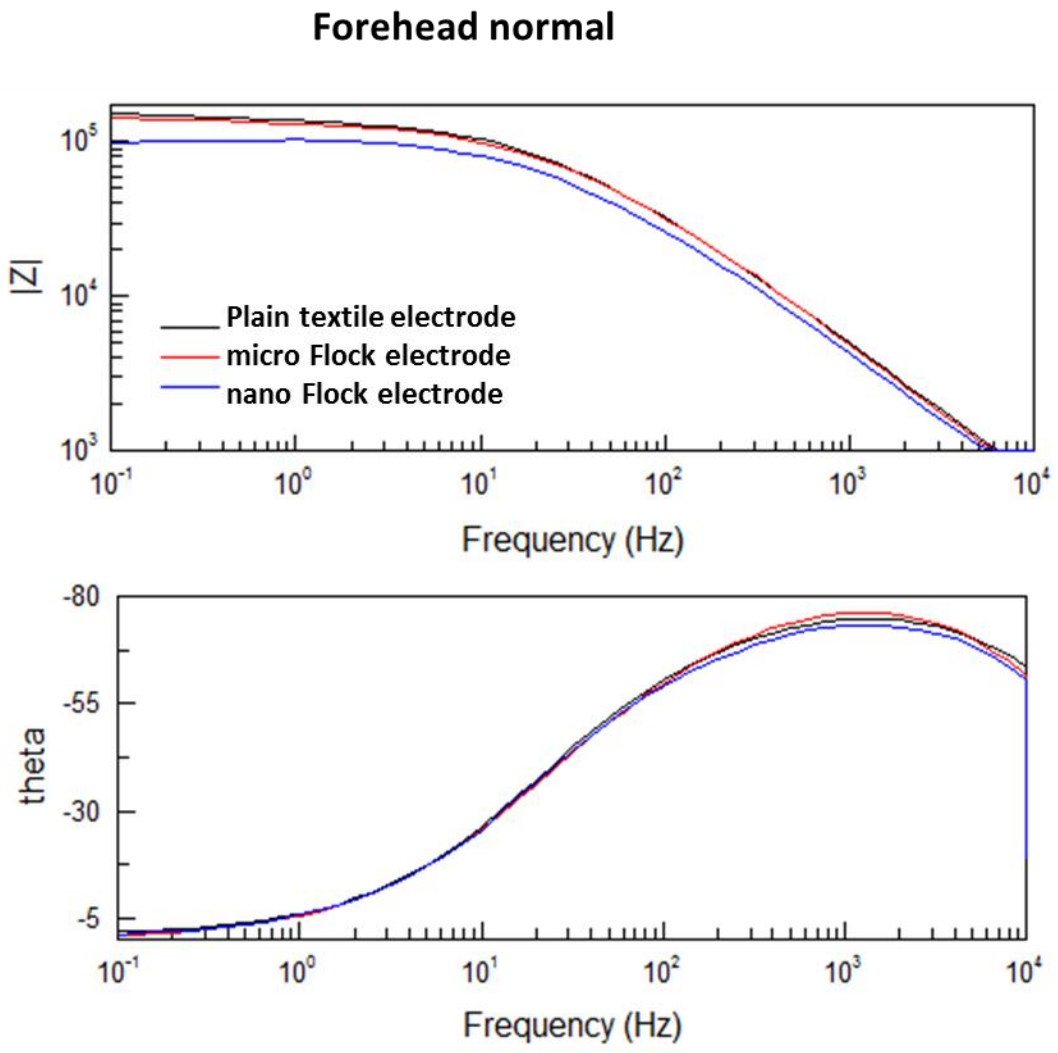

Figure 54: Impedance data from various types of textile based Concentric Ring Electrodes placed on forehead in 3-electrode configuration when subjects were in normal (non-sweaty) condition

The comparison of between the impedance data of the textile based concentric ring electrodes placed on the forehead showed that the nano Flock textile electrode had the least contact impedance (Figure 54). The phase curves of plain, micro Flock textile and nano Flock textile electrodes were same with the peak around 1kHz (Figure 54).

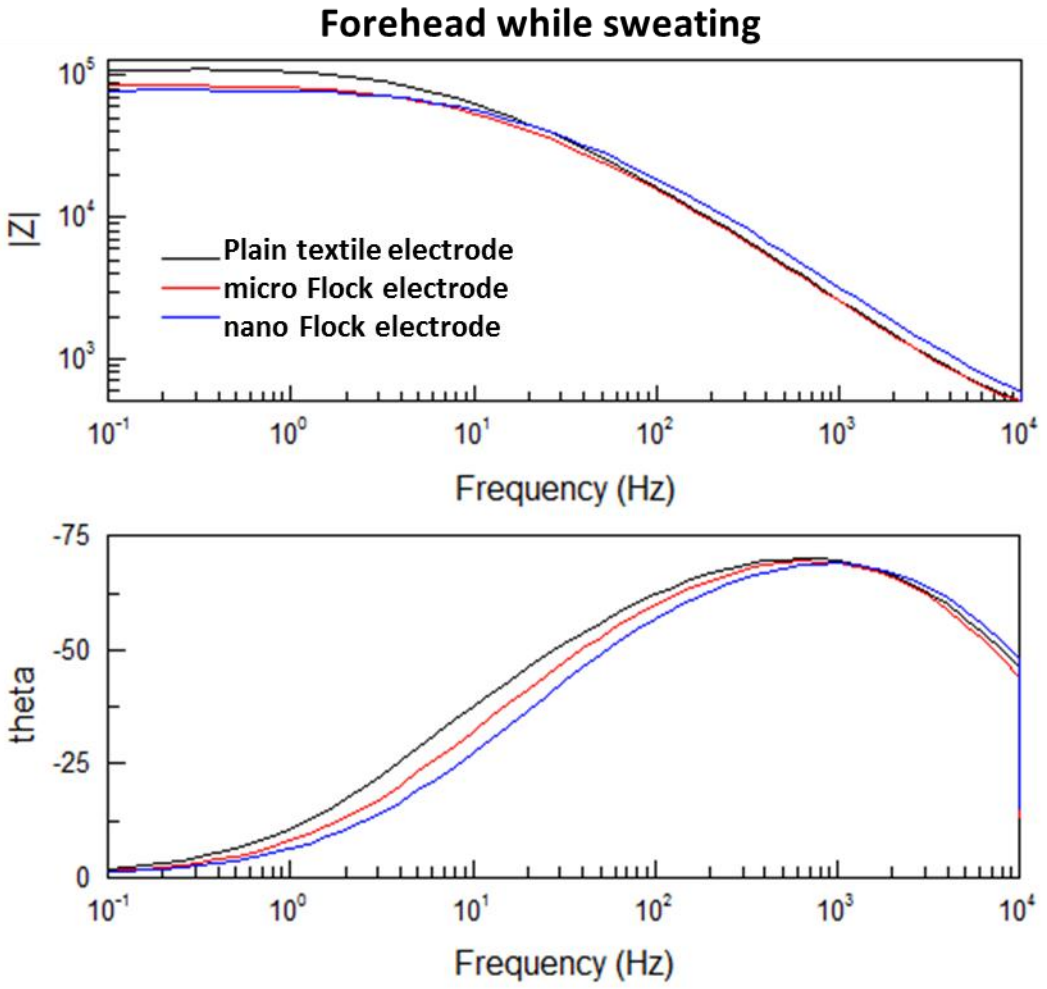

Figure 55: Impedance data from various types of textile based Concentric Ring Electrodes placed on forehead in 3-electrode configuration when subjects were in sweaty condition

The comparison of between the impedance data of the textile based concentric ring electrodes placed on the forehead showed that the nano Flock textile electrode had the least

contact impedance (Figure 55). The impedance of all the electrodes were less when subject was sweating than when in normal condition. The peaks of phase curves for plain and micro Flock textile electrodes shifted from 1kHz, whereas, the peak in phase curve for nano Flock textile electrode remained around 1kHz (Figure 55).

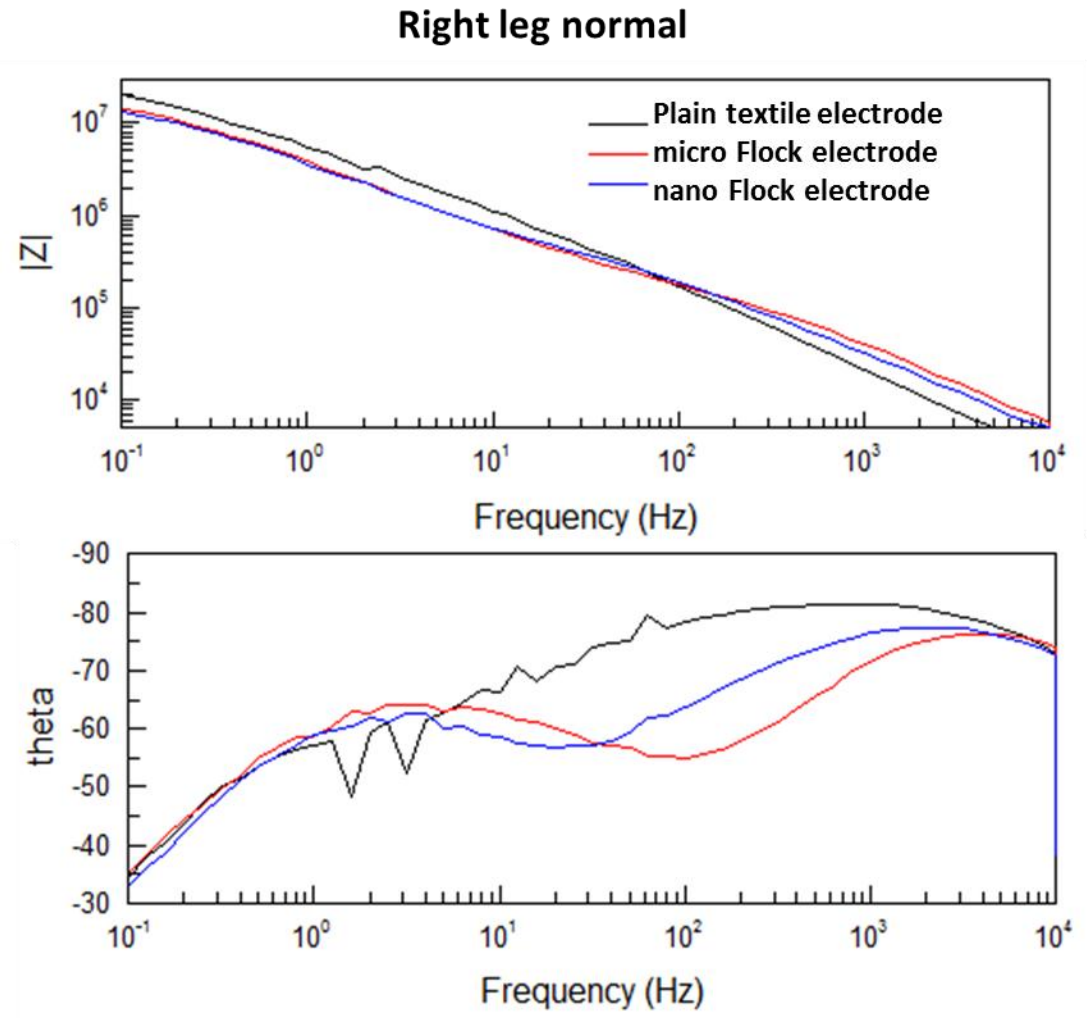

Figure 56: Impedance data from various types of textile based Concentric Ring Electrodes placed on right leg in 3-electrode configuration when subjects were in normal (non-sweaty) condition

The comparison of between the impedance data of the textile based concentric ring electrodes placed on the right leg showed that the micro and nano Flock textile electrode had the lower contact impedance than plain textile electrode (Figure 56). The phase curves for plain and micro Flock textile electrodes showed two separate peaks at around 3Hz and 3 kHz. The phase curve for plain textile electrode showed a plateau spanning from 1Hz to 1 kHz (Figure 56).

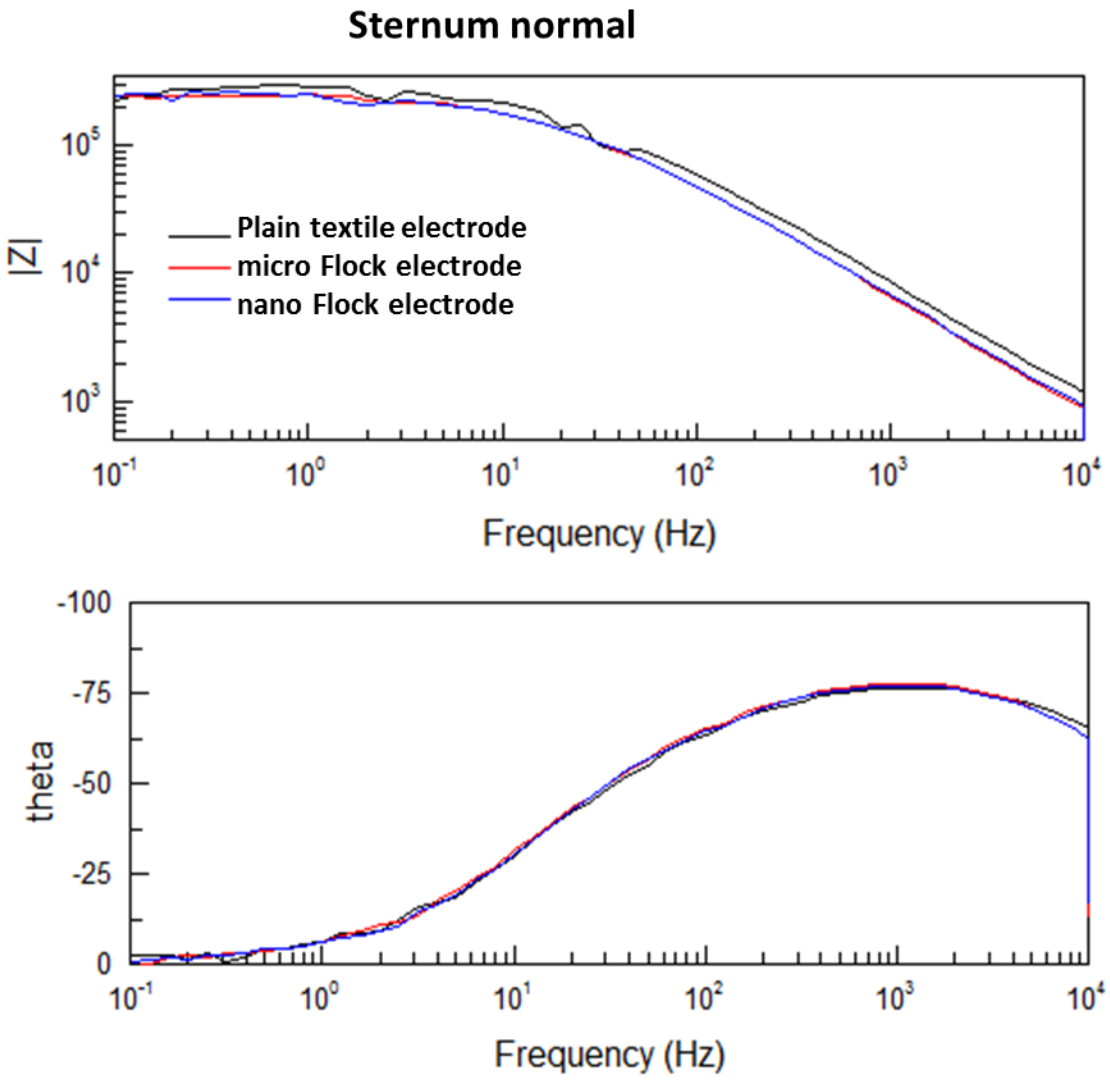

Figure 57: Impedance data from various types of textile based Concentric Ring Electrodes placed on sternum in 3-electrode configuration when subjects were in normal (non-sweaty) condition.

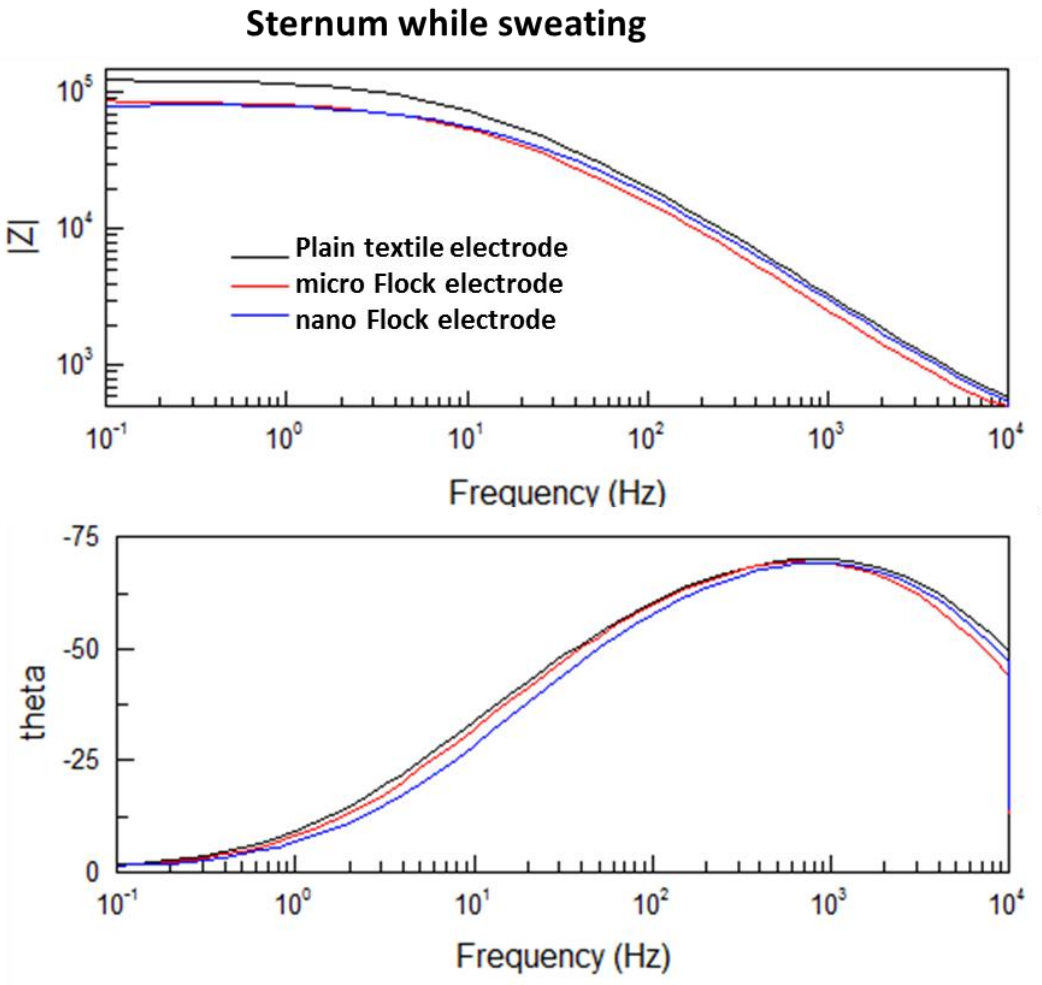

Figure 58: Impedance data from various types of textile based Concentric Ring Electrodes placed on sternum in 3-electrode configuration when subjects were in normal (sweaty) condition

The comparison of between the impedance data of the textile based concentric ring electrodes placed on the forehead showed that the micro and nano Flock textile electrode had the lower contact impedance than plain textile electrode (Figure 57). Phase curves of plain, micro Flock textile and nano Flock textile electrodes were same with the peak around 1kHz (Figure 57).

4.7 Biopotential signal acquisition from textile based electrodes

A pair of flocked textile electrodes was implemented on 5 healthy subjects as Electrocardiograph (ECG) sensors for obtaining Lead II ECG signal. The signal was compared with the Lead II signal obtained from a pair of standard Ag/AgCl gel electrodes. Signals were observed to identify the standard waveforms found in an ECG scan: P, Q, R, S and T waves and a check list was made for each subject (TABLE 11).

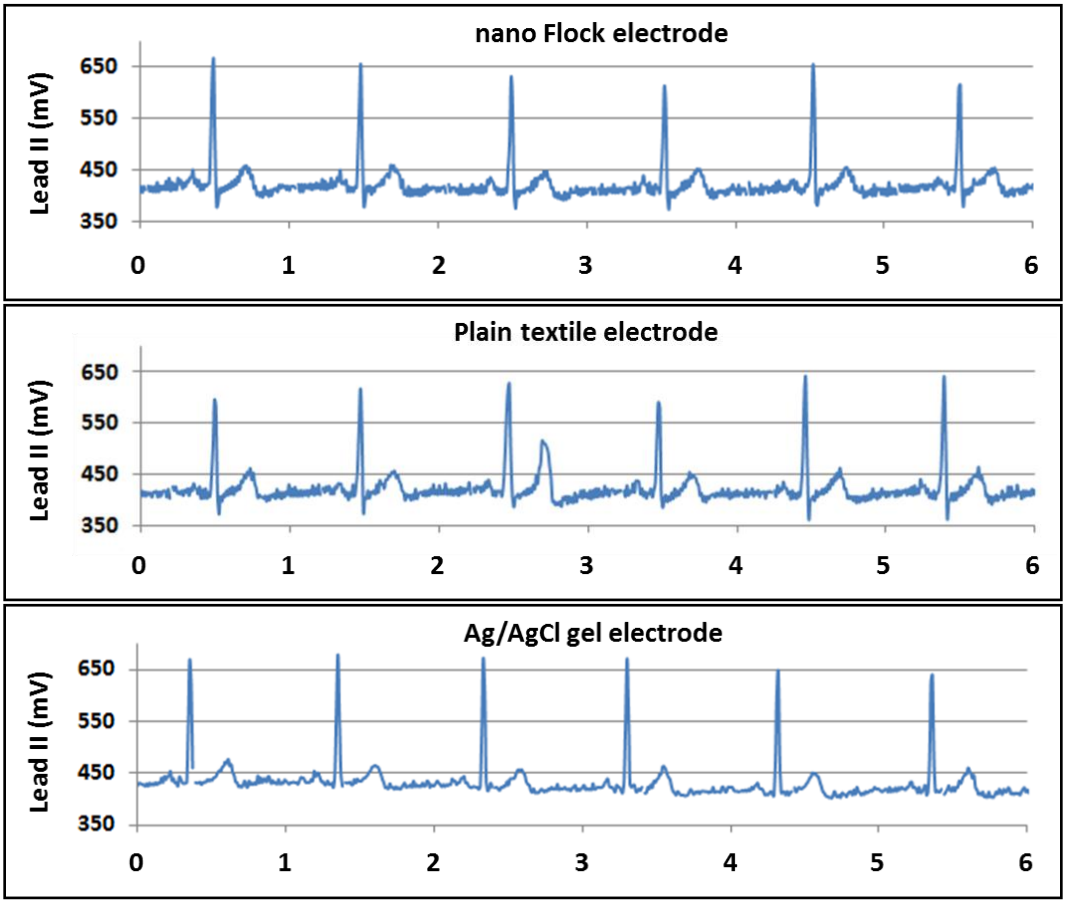

Figure 59: Electrocardiograph from nano Flock electrode, Plain textile electrode and Ag/AgCl gel electrode

It was found that the waveforms were visible in the signals from all 5 subjects. The R wave for textile based electrodes was slightly less profound that that for Ag/AgCl gel electrode. The S wave for textile based electrodes was more profound than that for Ag/AgCl gel electrode.

Among the textile based electrodes, R and S waves for nano Flock textile based electrode was higher than plain textile based electrode (Figure 59).

TABLE 11: Electrocardiograph checklist for ECG signals obtained from plain, micro Flock and nano flock textile electrodes

		Waveform comparison				
Subject	Electrode	P wave	Q wave	R wave	S wave	T wave
1	plain	✓	✓	✓	✓	✓
	micro Flock	✓	✓	✓	✓	✓
	nano Flock	✓	✓	✓	✓	✓
2	plain	✓	✓	✓	✓	✓
	micro Flock	✓	✓	✓	✓	✓
	nano Flock	✓	✓	✓	✓	✓
3	plain	✓	✓	✓	✓	✓
	micro Flock	✓	✓	✓	✓	✓
	nano Flock	✓	✓	✓	✓	✓
4	plain	✓	✓	✓	✓	✓
	micro Flock	✓	✓	✓	✓	✓
	nano Flock	✓	✓	✓	✓	✓
5	plain	✓	✓	✓	✓	✓
	micro Flock	✓	✓	✓	✓	✓
	nano Flock	✓	✓	✓	✓	✓

5. Discussion

The results in chapter 4 show the development and evaluation process of a novel hybrid nanostructured textile based electrode for biosensing applications. The process started with optimizing the conformal electroless plating process of the silver nano-crystal thin film. It was followed by assessment of sturdiness of the hybrid nanostructured electrodes with conductive thin film under physical abrasion and alkaline conditions. Then the hybrid nanostructured textile based electrode was compared with plane and microstructured textile based electrodes for its characteristics as biosensor. This chapter will discuss those results from the perspective of the 4 goals set in the beginning of chapter 3 and answer 4 questions posted at the beginning chapter 3. It will examine the hypothesis **"Nano-Bio Textile electrode improves bio-potential sensing"** based on the answers given to those questions.

5.1 GOAL 1: Design and fabricate nano-bio textile sensors with vertically free standing textile based nanostructures

The fabrication process used to get vertically free standing textile based structures was electrodeposition of electrostatically charged fibers under the influence of a strong external electric field. The process is prevalent in industry for microfibers but scaling to down for nanofibers imposes limitation such as insufficiently charged fibers. The resultant displacement force is not sufficient to drive the nanofibers trough the meniscus of the thin adhesive film on the base fabric. Hence, the process was modified to achieve the desired result inform of nano flock electrode. The use of [polypropylene island in polylactic acid sea] nanocomposite fibers ensured the deposition of micro scaled fibers as vertically free standing structures on the fabric with the help of the standard electrodeposition process. The polypropylene nanofibers were

released by etching off polylactic acid matrix. The process was aimed at partially exposing the polypropylene fibers at the crown, while keeping the lower nanocomposite fiber stock intact (Figure 44, 45). During process optimization, it was observed that the nanofibers that were released completely fell down on the base fabric or curled in to themselves (Figure 45 (g)). Since the NaOH uniformly etches polylactic acid at the tip and the side walls of the composite fiber, the nanofibers at the circumference were completely released by the time the nanofibers at the center were exposed. Hence, the textile sample had vertically free standing nanostructures as well as nanotextured base fabric (Figure 46).

The free standing structures were coated with conformal silver nano-crystal film to make them conductive. The resultant electrode has free standing structures that are a hybrid of polymeric textile material and its silver coating (Figure 29 and 47). The conformal coating was the product of a process derived from the standard silver coating techniques for non-metallic surfaces [111] and silver printing ink technology [112]. Thus, allowing silver coating on non-conductive soft/flexible substrates.

The silver coating process described in the section 3.1.1 was optimized for process parameters to obtain a uniform conformal coating of silver nano-crystals on the surface of hierarchically structured textiles. The optimization of the process was done to ensure formation of larger silver nano-crystals and improve their adhesion to the polymer fiber surface. The optimum process of drying at 65°C and annealing at 200°C for 1 hour resulted in large crystal or grain size, which resulted in better electrical conductivity [113]. This was evident from the optimization results shown in Figures 30, 35, 36 and TABLES 5 and 6. The variation in contact impedance, especially the resistive element of the textile electrode-agar gel tissue

phantom interface, shows a decrease with increase in drying and annealing temperature. This was confirmed by the SEM scans of the sample which showed increase in silver nano-crystal coverage of the tips with increase in drying and annealing temperature (Figures 31-34).

5.2 GOAL 2: Testing the electrical properties of nano-bio textile sensors under conditions: abrasion and washing

The electrical properties of nanostructured textile based electrode are due to the conformal silver nano-crystal coating. For the textile based electrode to be applicable for daily use as normal items of textile such as apparels or drapes, the silver nano-crystal coating should be able to withstand physical abrasion and washing. The sheet resistance results from physical abrasion testing in wet (Figure 37 and 38) and dry (Figure 39 and 40) conditions showed that the silver nano-crystal coating on base fabric could withstand these effects. The contact impedance data showed that after both wet (Figure 41) and dry (Figure 42) abrasion the electrodes develop a capacitive bilayer based impedance barrier. The abrasive action led to loss of silver coating at the tips of the free standing nanostructures, which introduces capacitive impedance (reactance) in the signal (current) flow.

The wash test setup for the textile electrodes was designed to simulate the wear and tear of 50 wash cycles in 5. After the first two wash cycles, the electrodes showed sheet resistance values that were less than 1 mΩ/sq. The sheet resistance of the textile based electrodes rose significantly after 3rd wash cycle. The textile based electrodes lost their electrical property after the 3rd wash cycle. A conservative estimation can be made that the textile electrodes can withstand 20 wash cycles.

The loss silver coating due to abrasion and washing is due to the fact that the silver nano-crystals were attached to the surface of the polymer fiber by weak Van der Waals force of attraction. For better adhesion of the silver nano-crystals to the fiber surface, binding agents or polymer based composite film may be helpful [114].

5.3 GOAL 3: Impedance mapping of nano-bio textile based sensors to study effects of conductive hybrid textile based nanostructures on signal flow through electrode-skin interface

The intended use of vertically free standing nanostructures was to improve the electrical contact made by textile based electrodes with the skin. Nanostructures increase the effective surface area of the electrode that decreases the contact impedance. Contact impedance scan was run in 2-electrode configuration on agar gel based tissue phantom. Impedance scans in Figure 48 show that magnitude of microflock textile electrode was less than that of plain textile electrode and the magnitude of impedance was the least for nanoflock electrode.

Phase angle curves (Figure 48) of the textile based electrodes shows that constant phase element (CPE) [R-CPE] interface changes from diffusive nature in plain textile electrode to capacitive nature in micro and nano flocked textile electrodes. This was also confirmed by the values of the P parameter of the equivalent (model) circuit for plain textile electrode (0.51148) and mico/nano flock textile electrode (0.7 to 0.83). For P = 0.5 the CPE shows charge diffusion through the impedance layer, whereas, P = 0.9 corresponds to a double layer capacitance [115].

The hybrid nanostructured textile based electrode has being developed here for detection of biopotential and bio-impedance. In both cases, the signals are generated on the basis of current flow towards and away from the electrodes. To study the effect of conductive

hybrid textile based nanostructures on signal flow through electrode-skin interface, the current flow through electro-gel tissue phantom interface was observed. Unlike human skin, the moisture level of an agar gel based tissue phantom does not show variability and has a smooth surface. The gel tissue phantom was used in order to have consistency in electrical property of the medium.

The experimental conditions of the above mentioned contact impedance scans were used to simulate the current flow through textile based electrode-agar gel based phantom interface. The electrical current vectors across the plain textile based electrode-gel phantom interface (Figure 49) were tilted at an angle from the normal vector, which indicated that it has a sizable component along the surface of the gel. This represented the fringe effect, i.e. current leaking at the edges of the electrode [116]. The electrical current vectors across the micro flock textile based electrode-gel phantom interface (Figure 50) were pointing straight down with a slight tilt with respect to the normal vector. This indicated a dominant downward current flow and a very small fringe effect. The electrical current vectors across the nano flock textile based electrode-gel phantom interface (Figure 51) showed the same directionality as the current vector of micro flock electrode. In this case, the electrical current now flows through discrete channels (nanoflock) at the tip of those micropillars, thereby reducing the fringe effect of the electrode.

The simulation clearly showed that the use of micro and nano flock electrodes improved the efficiency of current flow through the electrode-gel phantom interface. This simulation was performed for electrode placed on 5% agar gel based tissue phantom. It accounted for variation in electrical current flow with change in the morphology of the electrode. Simulations with textile based electrode-skin interface should be performed to

understand variations in electrical current with changes in the electrical property of the skin due to moisture, surface roughness and oils.

5.4 GOAL 4: Nano-bio textile sensor performance in measurement of biopotential signal and bioimpedance

The nano-bio textile based electrodes developed in this study were intended to be used for biopotential and bioimpedance measurement. As a proof of concept, the electrodes were implemented as sensors for measurement of electrocardiogram and as concentric ring electrode pair for measurement of impedance.

5.4.1 Measurement of electrocardiogram (ECG) signals

The ECG signals were measured in Lead II configuration. The ECG signals acquired from nano Flock and micro Flock textile based electrodes had all the constituent waves. This makes the ECG signal obtained from flock electrode relevant for monitoring of the heart condition. The R peak is used for detection of heart beat and for measurement of QRS broadening towards detection of tachycardia [117]. The S wave is useful for the QRS broadening and ST segment elevation in detection of myocardial infarction, angina, pericarditis, myocarditis and ventricular aneurysm, or ST depression in detection of ischemia, tachycardia, hypokalaemia and hypothermia, which is used for a score of cardiac conditions [117]. Both the waveforms are used for time-stamp and not their amplitude. Hence, profoundness of R and S waves should not be detrimental to their relevance for monitoring of the heart condition.

5.4.2 Electrode-skin interface electrical impedance under varying skin conditions

The plain, micro flock and nano flock textile based electrodes were tested for measurement of their contact impedance with human skin. The electrodes were tested on 5

subjects on their forearm, which is a standard site for skin impedance measurement [118]. The skin condition of those 5 subjects covered skin type very dry to moist. The electrode was arranged in 2-electrode configuration with Ag/AgCl gel electrode on subjects forearm. The parameters of the equivalent (model) circuit were tabulated for comparison (TABLE 7-10).

In comparison to Ag/AgCl gel electrode, the contact impedance of textile based electrodes was very dependent on skin moisture level. For moist skin, the textile electrodes had contact impedance that show charge diffusion through the impedance layer ($P<0.9$). For dry skin, the textile electrodes had contact impedance that show double layer capacitance ($P > 0.9$) [115]. The impedance magnitude of nano flock textile electrode is lower than micro flock textile electrode, which is lower than plain textile electrode. It is largely because the interface resistance and capacitance followed the same pattern. In case of moist skin, the nano flock textile electrode had impedance even lower than that of Ag/AgCl gel electrode (Figure 52).

The novel nanotextured flock textile based electrode was tested in as Concentric Ring Electrode (CRE) pair for bioimpedance sensing application. The CRE configuration was designed for measurement of contact impedance of the electrode-skin interface [119] and impedance based tomography and plethysmography when used with another CRE pair [120]. The nano flock textile electrode was compared with the micro flock and plain textile electrodes set up as CRE pair against an Ag/AgCl gel electrode as counter electrode.

The impedance scans were conducted by placing the electrodes on skin of forearm, leg, forehead and sternum. The data was compared among the textile electrodes between 0.1 Hz and 10 kHz to cover all the signal frequencies encountered during health monitoring (Figure 53-58). The nano flock electrode had the least impedance magnitude at all the sites. Impedance

magnitudes of micro flock and nano flock electrode are comparable on the skin of leg and sternum. The impedance magnitudes were the least at the forehead and the most at the leg, while those at forearm and sternum were in between. This was as reported in literature by Rosell et.al. (1988) [119]. The phase curves of the textile electrodes showed that peak of the curve for nano flock textile electrode was at 1 kHz for all the sites except for the skin of leg. For the sites where textile electrodes showed lower impedance, the phase angle curves for the plain and micro flock textile electrodes were similar to that of the nano flock textile electrode. For the sites where textile electrodes showed higher impedance, the phase angle curve showed either two peaks or a single broad plateau. This was due to an additional bilayer capacitance introduced due to very dry or rough skin. Under sweaty conditions, the impedance magnitudes of textile electrodes reduced but the trend remained the same. This is in agreement with a previous observation about dependence of impedance on skin moisture level.

5.5 Examination of the principle hypothesis

The aim of this study was to be able to provide answers for 4 questions posted at the beginning of the Research and Methodology section. In answer to the first question is that it is possible to fabricate chemically and mechanically sturdy conductive textile based nanostructures on fabric. The mechanical stability can be improved by use of silver nanocrystal-polymer nanocomposite. The second question can be answered in affirmative based on the comparison of nano flock textile electrode, micro flock textile electrode and plain textile electrode. Increase in surface area of the electrode from plain to micro flock to nano flock textile electrode led to increase in overall quality electrical contact.

The contact impedance measurements of textile electrode-agar gel based tissue phantom interface showed improvement in quality of electrical contact between textile electrode and agar gel by introduction of micro flock and then nano flock to the electrode surface. The simulation of textile electrode-gel based tissue phantom interface presented a map of electrical current flow through the interface. It showed that micro and then nano flock help improve the efficiency of electrical current flow through the interface. The capability of the textile electrodes to sense biopotential was found to be at par with that of Ag/AgCl gel based electrode. Impedance scan of textile electrode-skin in CRE pair was shown to improve with introduction of micro and then nano flock. But the contact impedance of the textile electrodes was very dependent on the moisture level of the skin.

These nanotextured flock textile based electrodes were glue less, dry and flexible sensors. This allowed for them to be reused and seamless integration into apparels and drapes of daily use for ubiquitous health monitoring. Hence, the hypothesis is validated. These novel hybrid nanostructured textile based electrodes form an electrically superior interface with the skin as compared to the plain textile electrodes, thereby ensuring better signal strength.

6. Conclusion

Returning to the hypothesis posed at the beginning of this study, it is now possible to state that nano-bio textile electrodes help to improve the sensitivity of biopotential and bioimpedance sensing systems by increasing the surface area in contact with the skin. The novelty of the research was development of vertically free standing array of electrically conducting nanostructures on textile which brought the performance of textile based dry electrode sensors close to or made them better than Ag/AgCl gel electrodes.

Taken together, the results suggested that: it is possible to fabricate chemically and mechanically sturdy electrically conductive textile based nanostructures on fabric. Vertically free standing nanostructures on textile electrode contribute to signal flow at the electrode-skin contact interface by improving the efficiency of signal (electrical current) flow across the interface and reducing fringe effects. The performance of hybrid nanostructured textile based bioelectrode was at par or better than Ag/AgCl gel electrodes, with the concession of dependence on skin moisture content.

These findings enhanced our understanding of the effect of electrically conducting nanostructures on the performance of textile based biopotential and bioimpedance sensors. The findings will help in fine tuning the performance of textile based electrodes to make them highly selective for a wide range of applications. Inclusion of these enhanced functionalities on smart textiles will assist in implementation of sensor systems embedded apparels and drapes for ubiquitous and unobtrusive health monitoring.

The nanotextured flock textile based electrode’s contact impedance varied with skin moisture content. This change in property impacts sensing mechanism of the textile electrode

for applications such as bioimpedance. A sample set of 5 test subjects was not big enough to completely understand the effect of skin moisture content on contact resistance of the textile electrodes. Bigger sample size will ensure a better understanding of this effect, which can then be compensated for in sensors instrumentation circuitry.

7. Future work

The hybrid nanostructured textile based electrodes have been demonstrated as bioimpedance sensors in a concentric ring electrode (CRE) pair configuration. The design can be explored as electronic impedance based tomography and plethysmography by coupling two CRE pairs. The CRE configuration also allows simultaneous detection of ECG signals by disc electrode and contact impedance by the CRE pair. A combination of the two signals, in real time, can facilitate in implementation of motion artifact rectification schemes in aiding ambulatory health monitoring.

The unique hybrid nanostructured textile based electrode has the potential for sensing application for detection of biomarkers such as pathogens and chemicals with high sensitivity and specificity. The fabrication process described in this research allows scope for patterned flocking of hybrid nanostructures, which can be made as an array of sensors with different selectivity. Future research might explore these sensor applications for medical diagnostics, public health, biosafety, contraband detection and many similar applications.

8. References

1. Jorg, H., “My Heart,” European Community 6th Framework Programme, 2003-2008. www.cordis.europa.eu and www.research.phillips.com

2. "10 Leading Causes of Death by Age Group, United States 2005-2010," National Vital Statistics System, National Centre for Health Statistics, Centres for Disease Control (CDC). (2005-2010)

3. Ectopic heartbeat definition, A.D.A.M Medical Encyclopedia http://www.ncbi.nlm.nih.gov/pubmedhealth/PMH0002090/

4. “International Statistical Classification of Diseases and Related Health Problems,” 10th Revision (ICD 10), Chapter IX, pp. I00-I99. (2010)

5. Fuster, V., Hurst, J.W., O’Rourke, R., “The Heart,” McGraw-Hill Professional. (2004)

6. American Heart Association, “Heart Disease and Stroke Statistics-2005,” Update. Dallas Texas American Heart Association. (2005)

7. Rawles, J., “Magnitude of benefit from earlier thrombolytic treatment in acute myocardial infarction: new evidence from Grampian region early anistreplase trial (GREAT),” BMJ, Vol. 312, pp. 212-215. (1996)

8. Led, S., Martinez-Espronceda, M., Redondo, J., Baquero, A., Serrano, L., Cabezas, L., Niegowski, M., “Wearable electrocardiogram (ECG) recorder for a Mobile Point-of-Care based on recent interoperability standards,” Point-of-Care Healthcare Technologies (PHT), 2013 IEEE , pp.287-290. (2013)

9. Garcia, T.B., Holtz, N.E., “12-lead ECG: The art of interpretation,” Jones and Bartlett, Sudbury, M.A. (2001)

10. Brosche, T.A.M., “EKG Handbook,” Jones and Bartlett, Sudbury, M.A., Section 10, pp.87-98. (2010)

11. Jahrsdeorfer, M., Guiliano, K., Stephens, D., “Clinical usefulness of the EASI 12-lead continuous electrocardiographic monitoring system,” Critical Care Nurse, Vol. 25(5), pp. 28-37. (2005)

12. “How are arrhythmias diagnosed?” National Heart Lung and Blood Institute. (n.d.) Retrieved February 5, 2013 from http://www.nhlbi.nih.gov/health/dci/Diseases/arr/diagnosis.html

13. Ariyarajah, V., Mercado, K., Apiyasawat, S., Puri, P., Spodick, D.H., “Correlation of left atrial size with p-wave duration in interatrial block,” Chest, Vol. 128(4), pp. 2615-2618. (2005)

14. Brosche, T.A.M., “EKG Handbook,” Jones and Bartlett, Sudbury, M.A., Section 9, pp.51-85. (2010)

15. “Electrical Impedance Tomography: Methods, History and Applications,” Ed. Holder D.S., Institute of Physics, Series in medical Physics and Biomedical Engineering, London. (2005)

16. Rai, P., Kumar, P.S., Oh, S., Kwon, H., Mathur, G.N., Varadan, V.K., Agarwal, M.P., “Smart healthcare textile sensor system for unhindered-pervasive health monitoring,” Proc. SPIE Nano., Bio. & Info-Tech. Sensors and Systems 2012, Vol. 8344, 83440E. (2012)

17. Luepker, R.V., Raczynski, J.M., Osganian, S., Goldberg, R.J., Finnegan, Jr, J.R., Hedges, J.R., Goff, Jr, D.C, Eisenberg, M.S., Zapka, J.G., Feldman, H.A., Labarthe, D.R., McGovern, P.G., Cornell, C.E., Proschan, M.A., Simons-Morton, D.G., “Effect of a Community Intervention on Patient Delay and Emergency Medical Service Use in Acute Coronary Heart Disease. The REACT trial,” J. American Medical Association, Vol. 284 (1), pp. 60-67. (2000)

18. Kannel, W.B., Belanger, A.J., “Epidemiology of heart failure,” American Heart Journal, Vol. 121 (3), pp. 951-957. (1991)

19. Bhattacharyya, K., “Revolution in the Marketing,” RSA Journal (Feb. 2006), pp. 50-54. (2006)

20. Bergey, G.E., Squires, R.D., Sipple, W.C., "Electrocardiogram Recording with Pasteless Electrodes," IEEE Transactions on Bio-medical Engineering, Vol, BME-18 (3), pp. 206-211. (1971)

21. David, R.M., Portnoy, W.M., "Insulated Electrocardiogram Electrodes," Med. &Biol. Eng., Vol. 10, pp. 742-751. (1972)

22. Tao, X., “Smart Fibers, Fabrics and Clothing,” Cambridge, Woodhead. (2001)

23. Zhang, X., Tao, X., “Smart textiles: Passive smart,” June 2001 pp. 45-49; “Smart textile: Active smart,” July 2001, pp. 49-52; “Smart textiles: Very smart,” August 2001, pp. 35-37, Textile Asia.

24. Pejis, T., Chairman Smart Textiles Symposium (in call for papers), Plastic Electronics Conference, September 2005, Frankfurt, www.plastictronics.org. (2005)

25. Park, S, Gopalsamy, C., Rajamanickam, R., Jayaraman, S., “The Wearable MotherboardTM : An Information Infrastructure or Sensate Liner for Medical Applications,” Studies in Health Technology and Informatics, IOS Press, Vol. 62, pp. 252-258. (1999)

26. Park, S., Jayaraman, S., “Wearable Biomedical Systems: Research to Reality,” Proc. IEEE Int. Conf. Portable Information Devices PORTABLE07, pp. 1-7. (2007)

27. Coosemans, J., Hermans, B., Peurs, R., “Intergrating wireless ECG in textiles,” Sensors and Actuators A, 130-131, 48-53 (2006).

28. Lee, Y., D., Chung, W., Y., “Wireless sensor network based wearable smart shirt for ubiquitous health and activity monitoring,” Sensors and Actuators B, 140, 390-395 (2009).

29. Alzadi, A., Zhang, L., Bajwa, H., “Smart Textile Based Wireless ECG System,” Proc. IEEE Systems, Applications and Technology Conference (LISAT) 2012, pp. 1-5. (2012)

30. Rattfalt, L.; Chedid, M.; Hult, P.; Linden, M.; Ask, P., "Electrical Properties of Textile Electrodes," Engineering in Medicine and Biology Society, 2007. EMBS 2007. 29th Annual International Conference of the IEEE , vol., no., pp.5735-5738, 22-26 Aug. 2007

31. Curone, D., Secco, E.L., Tognetti, A., Loriga, G., Dudnik, G., Risatti, M., Whyte, R., Bonfiglio, A., Magenes, G., “Smart Garments for Emergency Operators: The ProeTEX Project,” IEEE Trans. Info. Tech. Biomed., Vol. 14 (3), pp. 694-701. (2010)

32. Aarts, E., Marzano, S., “The New Everyday-Visions on Ambient Intelligence,” 101 Publishers, Rotterdam, The Netherlands. (2003)

33. Mazzoldi, A., De Rossi, D., Lorussi, F., Scilingo, E.P., and Paradiso, R., “Smart Textiles for Washable Motion Capture Systems,” AUTEX Research Journal, Vol. 2(4), pp. 199-203. (2002)

34. De Rossi, D., Carpi, F., Lorussi, F., Mazzoldi, A., Paradiso, R., Scilingo, E.P., Tognetti, A., “Electroactive Fabrics and Washable Biomonitoring Devices,” AUTEX Research Journal, Vol. 3(4), pp. 180-185. (2003)

35. Clemens, F., et.al., “Computing Fibers: A Novel for intelligent Fabrics?” Advanced Engineering Materials, Vol. 5 (9), pp. 692-687. (2003)

36. Gimpel, S., et.al., “Textile-based Electronics Substrate Technology,” Journal of Industrial Textiles, Vol. 33(3), pp. 179-189. (2004)

37. Post, E.R, Orth, M., “Smart Fabric, or Washable Computing,” Proc. IEEE Int. Symposium on Wearable Computers, Cambridge (MA), USA, Oct. 1997, pp. 167-168. (1997)

38. Catrysse, M., “Wireless power and data transmission for implantable and wearable monitoing systems,” PhD Thesis, K. U. Leuven. (2004)

39. Rai, P., Kumar, P.S., Oh, S., Kwon, H., Mathur, G.N., Varadan, V.K., Agarwal, M.P., “Smart healthcare textile sensor system for unhindered-pervasive health monitoring,” SPIE Smart Structures+NDE, Nano., Bio. & Info-Tech. Sensors and Systems 2012, Vol. 8344, 83440E. (2012)

40. Pantelopoulos, A., Bourbakis, N., “A survey on wearable biosensor systems for health monitoring,”30th Annual Int. Conf. of the IEEE, EMBS 2008, pp. 4887-4890. (2008)

41. Pacelli, M., Caldani, L., Paradiso, R., "Textile Piezoresistive Sensors for Biomechanical Variables Monitoring," Proc. 28th Ann. Int. Conf. IEEE EMBS 2006, pp. 5358-5361. (2006)

42. Jorg, H., "My Heart," European Community 6th Framework Programme, 2003-2008. www.cordis.europa.eu and www.research.phillips.com

43. Numetrex® Heart Monitoring Apparel. www.numetrex.com

44. Smart T-shirt by GOW Trainer. www.gowtrainer.com

45. Wearable Wellness System from Smartex s.r.l. Pissa Italy. www.smartex.it

46. Lim, Z., H., Chia, Z., X., Kevin, M., Wong, A., S., W., Ho, G., W., "A facile approach towards ZnO nanorods conductive textile for room temperature multifunctional sensors," Sensors and Actuators B: Chemical, 151 (1), 121-126. (2010)

47. Vigneshwaran N., Kumar, S., Kathe, A., A., Varadarajan, P., V., Prasad, V., "Functional finishing of cotton fabric using zinc oxide-soluble starch nanocomposites," Nanotechnology, 17 (20), 5087-5095. (2006)

48. Dhawan, A., Muth, J., F., Kekas, D., J., Ghosh, T., K., "Optical nano-textile sensors based on the incorporation of semiconducting and metallic nanoparticles into optical fibers," Smart Nanotextiles. Symposium (Materials Research Society Symposium Proceedings, 920, 121-126. (2006)

49. Varadan, V., K., Oh, S., Kwon, H., and Hankins, P., "Wireless Point-of-Care Diagnosis for Sleep Disorder With Dry Nanowire Electrodes," J. Nanotechnol. Eng. Med., 1 (3), 031012 (11 pages). (2010)

50. Varadan, V., K., Kumar, P., S., Oh, S., Kwon, H., Rai, P., Banerjee, N., and Harbaugh R., E., "e-Nanoflex Sensor Systems: Smartphone-Based Roaming Health Monitor," L. Nanotechnol. Eng. Med., 2 (1), 011016 (11 pages). (2011)

51. Maharani, D., K., Kartini, I., Aprilita, N., H., "Nanosilica-Chitosan Composite Coating on Cotton Fabrics," Third Nanoscience and Nanotechnology Symposium 2010, 1284, 87-91. (2010)

52. Rai, P., Ho, T., Xie, J., Hestekin, J., A., and Varadan, V., K., "Glucose Driven Nanobiopower Cells for Biomedical Applications," J. Nanotechnol. Eng. Med. 1, 021009 (2010) (7 pages)

53. Locher, I., Klemm, M., Kirstein, T., Troster, G., "Design and Characterization of Purely Textile Patch Antennas," Vol. 29 (4), pp. 777-788. (2006)

54. Dhawan, A., Ghosh, T.K., Seyam, A.M., Muth, J., "Woven Fabric-based Electrical Circuits, Part II: Yarn and Fabric Structures to Reduce Crosstalk Noise in Woven Fabric-based Circuits," Textile Research Journal, Vol. 74, pp. 955-960. (2004)

55. Xue, P., Tao, X.M., "Morphological and Electromechanical Studies of Fibers Coated with Electrically Conductive Polymer," Vol. 98 (4), pp. 1844-1854. (2005)

56. Jiang, S.Q., Newton, E., Yuen, C.W.M., Kan, C.W., "Chemical silver plating on polyester/cotton blended fabric," J. App. Polymer Science, Vol. 100(6), pp. 4383-43878. (2006)

57. Jiang, S.Q., Newton, E., Yuen, C.W.M., Kan, C.W., "Chemical Silver Plating on Cotton and Polyester Fabrics and its Application on Fabric Design," Textile Research Journal, Vol. 76 (1), pp. 57-65. (2006)

58. Brevnov, D.A., "Electrodeposition of Porous Silver Films on Blanket and Patterned Aluminum-Copper Films," L. Electrochem. Soc., Vol. 153 (4), pp. C249-C253. (2006)

59. Wang, H., Wang, J, Hong, J., Wei, Q., Gao, W, Zhu, Z., "Preparation and characterization of silver nanocomposite textile," J. Coat. Technol. Res., Vol. 4 (1), pp. 101-106. (2007)

60. Yeon, S.J., "Study on texture evolution and properties of silver thin film prepared by sputtering deposition," Appl. Surf. Sci., Vol. 221, pp. 281-287. (2004)

61. Holme, I., "Nanotechnologies for Textiles, Clothing, and Footwear," Textile Magazine, Vol. 32 (1), pp. 7-11. (2005)

62. Tonezzer, M., Lacerda, R.G., "Zinc oxide on carbon microfiber as flexible gas sensor," Physica E: Low-dimensional Systems and Nanostructures, Vol. 44 (6), pp. 1098-1102. (2012)

63. Naik, A., "Future impact of nanotechnology in textile research," Proc. II Int. Symposium in Textile Engineering Natal Brazil, pp. 7-11. (2004)

64. Munirathinam, V., Anandhan, G., Paramasivam, M., "Enhanced sensing of anthraquinone dye using multiwalled carbon nanotubes modified electrode," Int. J. Environmental Analytical Chem., Vol. 93 (3), pp. 349-363. (2013)

65. Sahoo, S., Ouyang, H., Goh, J.C.H., Tay, T.E., Toh, S.L., "Characterization of a novel polymeric scaffold application in tendon/ligament tissue engineering," Tissue Engineering, Vol. 12, pp. 91-99. (2006)

66. Barhate, R.S., Ramakrishna, S., "Nanofibrous filtering media: Filtration problems and solutions from tiny materials," J. Membrane Science, Vol. 296, pp. 1-8. (2007)

67. Oh, T.I., Yoon, S., Kim, T.E., Wi, H., Kim, K.J., Woo, E.J., Sadleir, R.J., "Nanofiber Web Textile Dry Electrodes for Long-Term Biopotential Recording," IEEE Trans. Biomedical, Circuits and Systems, Vol. 7(2), pp. 204-211. (2013)

68. Yoon, H., Deshpande, D.C., Ramachandran, V., Varadan V.K., "Aligned nanowires growth using lithography-assisted bonding of a polycarbonate template for neural probe electrodes," Nanotechnology, Vol. 19, 025304 (8pp). (2008)

69. Eichhorn, S.J., Hearle, J.W.S., Jaffe, M., Kikutani, T., "Handbook of Textile Fibre Structure, Volume 2- Natural, Regenerated, Inorganic and Specialist Fibres," Woodhead Publishing Limited, Oxford. (2009)

70. Reneker, D.H., Chun, I., "Nanometer diameter fibers of polymer, produced by electrospining," Nanotechnology, Vol. 7, pp. 216-223. (1996)

71. Baker, W.R., "Microdenier spinning," Int. Fiber J., April 1992, pp. 7-15. (1992)

72. Montazer, M., Alimohammadi, Shamei, A., Rahimi, M.R., "In situ synthesis of nano silver on cotton using Tollen's reagent," Carbohydrate Polymers, Vol. 87, pp. 1706-1712. (2012)

73. Son, W.K., Youk, J.H., Park, W.H., "Antimicrobial cellulose acetate nanofibers containing silver nanoparticles," Carbohydrate Polymers, Vol. 65, pp. 430-434. (2006)

74. Sanchez, L.R., Blanco, M.C., Quintela, M.A.L., "Electrochemical synthesis of silver nanoparticles," J. Physical Chemistry B, Vol. 104, pp. 9683-9688. (2000)

75. Vimala, K., Sivudu, K.S., Mohan, Y.M., Sreedhar, B., Raju, K.M., "Controlled silver nanoparticles synthesis in semi-hydrogel networks of poly(acrylamide) and carbohydrates: A rational methodology for antibacterial application," Carbohydrate Polymers, Vol. 75, pp. 463-471. (2009)

76. Capek, I., "Preparation of metal nanoparticles in water-in-oil (w/o) microemulsions," Advances in Colloid andInterface Science, Vol. 110, pp. 49-74. (2004)

77. Sharma, V.K., Yngard, R.A., Lin, Y., "Silver nanoparticles: Green synthesis and their antimicrobial activities," Advances in Colloid and Interface Science, Vol. 45, p.. 83-96. (2009)

78. Walker, S.B., Lewis, J.A., "Reactive Silver Inks for Patterning High-Conductivity Features at Mild Temperatures," J. American Chem. Soc., Vol. 134, pp. 1419-1421. (2012)

79. Banerjee, K., Srivastava, N., Xu, C., Li, H., "Carbon nanomaterials for next-generation interconnects and passives: physics, status, and prospects," IEEE Trans. Electron Devices, 56 (9), 1799-1821. (2009)

80. Sanjines, R., Abad, M., D., Vaju, Cr., Smajda, R., Mionic, M., and Magrez, A., "Electrical properties and applications of carbon based nanocomposite materials: An overview," Surface & Coatings Technology, article in press. (2011)

81. Kang, M., G., Park, H., J., Ahn, S., H., and Guo, L., J., "Transparent Cu nanowire mesh electrode on flexible substrates fabricated by transfer printing and its application in organic solar cells," Solar Energy Materials and Solar Cells, 94 (6), 1179-1184. (2010)

82. Rattfalt, L.; Chedid, M.; Hult, P.; Linden, M.; Ask, P., "Electrical Properties of Textile Electrodes," Engineering in Medicine and Biology Society, 2007. EMBS 2007. 29th Annual International Conference of the IEEE , vol., no., pp.5735-5738, 22-26 Aug. 2007

83. Tregear, R.T., "Physical Functions of Skin," Chapter 2, Academic Press, New York. (1966)

84. Fricke, H., "The theory of electrolytic polarization," Phil. Mag., Vol. 14, pp. 310-318. (1932)

85. Medrano, G., Ubl, A., Zimmermann, N., Gries, T., Leonhardt, S., "Skin Electrode Impedance of Textile Electrodes for Bioimpedance Spectroscopy," Proc. IFMBE, Vol. 17, pp. 260-263. (2007)

86. Neuman, M.R., "Biopotential Electrodes," Medical Instrumentation Application and Design, 3rd Edition, Editor: Webster J.G., John Wiley and Sons, New York, pp. 183-232. (1998)

87. Dozio, R., Baba, A., Assambo, C., Burke, M.J., "Time Based Measurement of the Impedance of the Skin-Electrode Interface for Dry Electrode ECG Recording," Proc. 29th Annual Int. Conf. IEEE EMB8, pp. 5001-5004. (2007)

88. Besio, W., Prasad, A., "Analysis of Skin-Electrode Impedance Using Concentric Ring Electrode," Proc. 28th IEEE EMBS Annual Int. Conf., SuB05.4. (2006)

89. Tregear, R.T., "Physical functions of skin," Academic Press, London and New York, pp. 53-72. (1966)

90. Barnett, A., "The phase angle of normal human skin," j. Physiol, Vol. 93. Pp. 349-366. (1938)

91. Hua, P., Woo, E.J., Webster, J.G., Tompkins, W.J., "Finite Element Modelling of Electrode-Skin Contact Impedance in Electrical Impedance Tomography," IEEE Trans. Biomed. Engg., Vol. 40 (4), pp. 335-343. (1993)

92. Cardu, R., Leong, P.H., Jin, C.T., McEwan, A., "Electrode contact impedance sensitivity to variations in geometry," Physiological Measurement, Vol. 33, pp. 817-830. (2012)

93. Wang, W., Eisenberg, S.R., "A three-dimensional finite element method for computing magnetically induced currents in tissues," IEEE Trans. Magn., Vol. 30, pp. 5015-5023. (1994)

94. Bowtell, R., Bowley, R., "Analytic calculations of the E-fields induced by time-varying magnetic fields generated by cylindrical gradient coils," Magn. Reson. Med., Vol. 44, pp. 782-790. (2000)

95. Huang, J.J., Cheng, K.S., "The Effect of Electrode-Skin Interface Model in Electrical Impedance Imaging," Proc. Int. Conf. Image Processing (ICIP 98), pp. 837-840. (1998)

96. Hua, P., Woo, E.J., Webster, J.G., Tompkins, W.J., "Finite Element Modelling of Electrode-Skin Contact Impedance in Electrical Impedance Tomography," IEEE Trans. Biomed. Engg., Vol. 40 (4), pp. 335-343. (1993)

97. Jian, S.Q., Newton, E., Yuen, C.W.M., Kan, C.W., "Chemical Silver Plating on Cotton and Polyester Fabrics and its Application on Fabric Design," Textile Research Journal, Vol. 76 (1), pp. 57-65. (2006)

98. Walker, S.B., Lewis, J.A., "Reactive Silver Inks for Patterning High-Conductivity Features at Mild Temperatures," J. American Chem. Soc., Vol. 134, pp. 1419-1421. (2012)

99. "Textiles-Tests for color fastness- Part C06: Color fastness to domestic and commercial laundering," ISO 105-C06:2010, International Standard 4th edition. (2010)

100. "Testiles – Tests for color fastness Part X12: Color fastness to rubbing," ISO 105X12-2001, International Standard 5th Edition. (2001)

101. Patterson, A.L., "The Scherrer Formula for X-Ray Particle Size Determination," Physical Review, Vol. 56, pp. 978-982. (1939)

102. Van der Pauw, L., J., "A method of measuring specific resistivity and Hall effect of discs of arbitrary shape," Phillips Research Report, Vol. 13, pp. 1-9. (1958)

103. Tagami, H., Ohi, M., Iwatsuki, K., Kanamaru, Y., Yamada, M., Binjiro, I., "Evaluation of the Skin Surface Hydration in Vivo by Electrical Measurement," J. Investigative Dermatology, Vol. 75, pp. 500-507. (1980)

104. Fowles, D.C., Christie, M.J., Edelberg, R., Grings, W.W., Lykken, D.T., Venables, P.H., "Committee report: Publication recommendations for electrodermal measurements," Psychophysiol. Vol. 18, pp. 232-239. (1981)

105. Rai, P., Kumar P.S., Oh, S., Kwon, H., Mathur, G.N., Varadan, V.K., Agarwal, M.P., "Smart healthcare textile sensor system for unhindered-pervasive health monitoring," in Nanosensors, Biosensors, and Info-Tech Sensors and Systems 2011, Proceedings of SPIE Vol. 8344 (SPIE, Bellingham, WA 2011) 83440E.

106. Szczepanik, Z., Rucki, Z., "Frequency analysis of electrical impedance tomography system," IEEE Trans. Instrumentation and Measurement, Vol.49 (4), pp. 844-851. (2000)

107. da Silva, F.L., Niedermeyer, E., "Electroencephalography: Basic Principles, Clinical Applications, and Related Fields," 5th Edition, Lippincott Williams & Wilkins. (2004)

108. Saritha, C., Sukanya, V., Narasimha Murthy, Y., "ECG Signal Analysis Using Wavelet Transforms," Bulg. J. Phys. Vol. 35, pp. 68-77. (2008)

109. Daud, W.M.B.W., Sudirman, R., Al Haddad, A., "Wavelet Frequency Energy Distribution of Electrooculogram Potential Towards Vertical and Horizontal Movement," Modelling and Simulation (CIMSiM), 2010 Second International Conference on Computational Intelligence, 28th-30th Sept. 2010, pp. 326-329. (2010)

110. Loeb, G.E., Gans, C., "Electromyography for Experimentalists," The University of Chicago Press, Chapter 17, pp. 244. (1986)

111. Zeng, H.L., "The Handbook of Electroplating Technology," Mechanical Industry Publisher, Beijing, pp. 563-606. (2002)

112. Walker, S.B., Lewis, J.A., "Reactive Silver Inks for Patterning High-Conductivity Features at Mild Temperatures," J. Am. Chem. Soc., Vol. 134, pp. 1419-1421. (2012)

113. K. Seal, M.A. Nelson, Z.C. Ying, D.A. Genov, A.K. Sarychev, V.M. Shalaev, "Growth, morphology, and optical and electrical properties of semicontinuous metallic films," Phys. Rev. B, Vol. 67, 035318. (2003)

114. Wasif, A.I., Laga, S.K., "Use of Nano Silver as an Antimicrobial Agent for Cotton," AUTEX Research Journl, Vol. 9 (1), pp. 5-15. (2009)

115. Jacquelin, J., "The Phasance concept: a review," Current Topics in Electrochem., Vol. 4, pp. 2-13.(1997)

116. Cardu, R., Leong, P.H.W., Jin, C.T., McEwan, A., "Electrode contact impedance sensitivity to variations in geometry," Physiol. Meas., Vol. 33, pp. 817-830. (2012)

117. Brosche, T.A.M., "EKG Handbook," Jones and Bartlett, Sudbury, M.A., Section 10, pp.87-98. (2010)

118. Clar, E.J., Her, C.P., Sturelle, C.G., "Skin impedance and moisturization," L. Soc. Cosmet. Chem., Vol. 26, pp. 337-353. (1975).

119. Rosell, J., Colominas, J., Riu, P., Pallas-Areny, R., Webster, J.G., "Skin Impedance From 1 Hz to 1MHz," IEEE Trans. Biomed. Engg., Vol. 35 (8), pp. 649-651. (1988)

120. Besio, W., Prasad, A., "Analysis of Skin-Electrode Impedance Using Concentric Ring Electrode," Proc. 28th IEEE EMBS Annual Int. Conf. New York, pp. 6414-6417. (2006)

9. Appendix

Letter of approval for protocol used for testing human subject in this study is as follows

UNIVERSITY OF ARKANSAS
THE TOUP OF A

210 Administration • Fayetteville, Arkansas 72701 • (479) 575-2208 • (479) 575-3846 (FAX)
Email: irb@uark.edu

Research Compliance
Institutional Review Board
September 25, 2012

MEMORANDUM

TO:	Vijay Varadan Pratyush Rai Prashanth Shyamkumar
FROM:	Ro Windwalker IRB Coordinator
RE:	PROJECT CONTINUATION
IRB Protocol #:	11-09-093
Protocol Title:	*Smart Textile Sensor System for Health Monitoring*
Review Type:	☐ EXEMPT ☒ EXPEDITED ☐ FULL IRB
Previous Approval Period:	Start Date: 09/28/2011 Expiration Date: 09/27/2012
New Expiration Date:	09/27/2013

Your request to extend the referenced protocol has been approved by the IRB. If at the end of this period you wish to continue the project, you must submit a request using the form *Continuing Review for IRB Approved Projects*, prior to the expiration date. Failure to obtain approval for a continuation on or prior to this new expiration date will result in termination of the protocol and you will be required to submit a new protocol to the IRB before continuing the project. Data collected past the protocol expiration date may need to be eliminated from the dataset should you wish to publish. Only data collected under a currently approved protocol can be certified by the IRB for any purpose.

This protocol has been approved for 100 total participants. If you wish to make *any* modifications in the approved protocol, including enrolling more than this number, you must seek approval *prior to* implementing those changes. All modifications should be requested in writing (email is acceptable) and must provide sufficient detail to assess the impact of the change.

If you have questions or need any assistance from the IRB, please contact me at 210 Administration Building, 5-2208, or irb@uark.edu.